TECHNICAL REPORT

A STUDY OF ROOM FIRE DEVELOPMENT: THE SECOND FULL-SCALE BEDROOM FIRE TEST OF THE HOME FIRE PROJECT (July 24, 1974)

VOLUME II - ANALYSIS OF TEST RESULTS

Edited By

Paul A. Croce
Factory Mutual Research Corporation

Contributions From Harvard University and
Factory Mutual Research Corporation

Prepared for:

THE HOME FIRE PROJECT (NSF/RANN)
through Harvard University
under Grant No. NSF-GI 34734X

FMRC Serial No. 21011.4
RC75-T-31

June 1975

Approved by

C. Yao, Manager
Applied Research

R. Friedman
Vice President and
Director of Research

Factory Mutual System
Factory Mutual Research
1151 Boston-Providence Turnpike
Norwood, Massachusetts 02062

ABSTRACT

The goal of this work was to analyze and observe, in a realistic home setting, fire development from ignition through full room involvement, and the subsequent extinguishment of the fire. A full-scale bedroom facility, similar to that used in the first Home Fire Project bedroom test, was selected and furnished in typical fashion with a resulting fuel load of 4.0 lb/sq ft of floor area. A simulated match ignition of the mattress was used to start the fire; ventilation was provided through a single open doorway. Measurements made during the burn (173 in total) included gas and surface temperatures, heat fluxes, gas velocities, gas species concentrations, optical densities, weight loss, differential pressure, and relative humidity. Following ignition, the fire was observed at first to grow slowly, but steadily, as the mattress became more involved, then more rapidly with full room involvement occurring at approximately 7 min after ignition. This test did not exhibit the change from a growing to a diminishing fire that occurred in the first test when the room became fully involved at approximately 17 1/2 min after ignition.

Several theoretical and empirical approaches were applied in analyzing the test results. Two theoretical analyses, a mechanistic model of the fire development process and a hydraulic model of the flow through the doorway, were successful in depicting the growth of the fire as well as the behavior of the depth of smoke layer inside the room. Burning rates obtained from 1) the doorway-flow theory, 2) an enclosure energy balance and 3) flame area measurements, were all compared with values derived from the measured weight loss. A careful investigation of the radiative fluxes within the room indicated that, in addition to direct flame radiation, an important source of radiant energy leading to fire spread was the dense, optically thick smoke layer present in this test. This smoke layer 1) tended to block radiation from hot upper walls and ceiling, 2) constituted a major source for radiant energy which is transferred to surfaces within the room and 3) provided even a significant portion

of the energy fed back to the burning bed. Two studies were made of the thermal response of the second major fuel element to become involved in the fire, i.e., the bureau; one study examined the ignition of the top surface, while the other yielded the temperature distribution within, the mass loss from, and the ignition of a frontal section as a function of time. Lastly, an evaluation is included of instrumentation that was newly applied or undergoing development.

On the day following the bedroom fire, a supplementary test was performed in the same facility; a paraffin oil pan fire (3 ft dia) in the emptied bedroom provided a less complex large-scale fire to test new instrumentation techniques.

Volume I of this report presents a detailed description of the facility and tests (bedroom and pan fires), and all data in tabulated form; Volume II presents an analysis of the test results.

ACKNOWLEDGEMENT

The editor gratefully acknowledges all contributors for their cooperation in preparing this volume. The comments of Prof. H.W. Emmons, Dr. R. Friedman and Dr. G. Heskestad were very helpful. The editorial assistance of Mr. L. Post and the typing of Mrs. H. Hurley are sincerely appreciated.

This work was sponsored by the National Science Foundation through a grant from its Research Applied to National Needs (RANN) program (NSF - GI34734X).

CONTRIBUTORS

R.L. Alpert - Senior Research Scientist, FMRC (Sections IX and XI)

P.A. Croce - Senior Research Scientist, FMRC (Sections VI and XIII)

J. deRis - Manager, Basic Research Dept., FMRC (Section IX)

H.W. Emmons - Abbott and James Lawrence Professor of Engineering and Gordon McKay Professor of Mechanical Engineering, Harvard University (Section IV)

N.D. Fowkes - Visiting Professor, Harvard University; now at University of Western Australia (Section III)

D. Kligler - Undergraduate, Harvard University (Sections IV and V)

R. Land - Research Associate, Harvard University (Section XII)

G.H. Markstein - Principal Research Scientist, FMRC (Section VIII)

A. Modak - Senior Research Scientist, FMRC (Section X)

J.S. Newman - Research Scientist, FMRC (Section XIII)

L. Orloff - Research Scientist (Advanced), FMRC (Section IX)

P.J. Pagni - Visiting Professor, Harvard University; now at University of California at Berkeley (Section III)

J. Prahl - Visiting Professor, Harvard University; now at Case Western Reserve University (Section V)

F. Tamanini - Senior Research Scientist, FMRC (Section VII)

TABLE OF CONTENTS

LIST OF FIGURES

LIST OF TABLES

I
INTRODUCTION

The Home Fire Project is a National Science Foundation-RANN sponsored investigation of the unwanted fire in the home being conducted jointly by Harvard University and Factory Mutual Research Corporation (FMRC). The overall research program is directed toward understanding ignition, growth and extinguishment of a residential fire. Basic mechanisms and useful modeling laws are being sought in a number of laboratory experiments and analyses. In addition, three full-scale, realistic test burns are presently included in the program. The purpose of the full-scale test program is to observe, monitor and analyze fire development up to, including, and slightly after full room involvement, and the subsequent extinguishment thereof, in a typical and realistic domestic setting. It also provides an opportunity to all project workers for making related measurements and observations under realistic home fire conditions and, hence, provides realistic information and direction to all project efforts. The first full-scale bedroom fire test was performed in the summer of 1973 and is reported elsewhere*. A description of the second test, including all data, is presented in Volume I of this report. Volume II contains several analyses of our bedroom fire data (mostly from the second test) performed by various members, both from Harvard and FMRC, of the Home Fire Project team.

The first (1973) bedroom fire test utilized a full-scale bedroom facility furnished in typical fashion with inexpensive, used furniture. Flaming ignition was initiated on the (polyurethane) mattress, and ventilation was provided through a single open doorway (windows were simulated). After ignition, the fire was observed to grow as the mattress became more involved, diminish

*Croce, P.A. and Emmons, H.W., "The Large-Scale Bedroom Fire Test, July 11, 1973," FMRC Technical Report RC74-T-31, Serial No. 21011.4, prepared for the Home Fire Project (NSF-RANN), July 1974, NTIS PB-235 731/AS.

considerably when available mattress material was consumed, resume growth when additional combustibles became involved (mattress foundation and carpet), and then suddenly spread through the entire room, with flames bursting out the doorway, at approximately 17 1/2 min after ignition.

The second (1974) test utilized a similar facility with all furnished items matching as closely as possible those in the first test*. Ignition and ventilation were the same as for the first test. In the second test, the fire was observed at first to grow slowly, but steadily, as the mattress became more involved, then more rapidly, with the bureau igniting just before full room involvement occurred at approximately 7 min after ignition. This fire did not exhibit the change from a growing to a diminishing fire that occurred in the first test.

The drastically different fire behavior was, to a certain degree, surprising. The facility for the second test was only slightly different from that of the first test, and, hence, a similar fire behavior was expected. It is possible that the mattress material may have been significantly different in the two tests. In addition, ambient conditions to the test room leading up to and on the day of the test were quite contrasting, with high relative humidity levels (~75 percent) for the first test and moderate levels (~50 percent) for the second test. Lastly, the external boundary conditions were slightly different for the two tests since the orientation of the second test room was changed from that of the first test to avoid interference with the doorway flow by external drafts; concomitant changes could have (inadvertently) influenced the flow into and out of the doorway in such a way as to affect fire development+. It is impossible to say at this time whether the mattress material, humidity or boundary conditions caused the observed difference in fire behavior, but all of these items will be better controlled (including a duplicate set of furnishings) in the third test, scheduled for July 1975.

*New, inexpensive items were purchased; material, geometry and weight were considered in trying to duplicate the furnishings from the first test.

+The 1974 fire plume was observed to "lean" or be drawn toward the bedside corner at approximately 4 1/2 min after ignition, which, no doubt, influenced subsequent fire growth; the 1973 fire plume remained fairly vertical on the mattress, even when pillow and headboard became involved.

There was another noticeable difference between the first two tests. In the first test, our expressed goal was to study fire growth to, and including, "flashover". Also in the first test, "flashover" was clearly discernible, being characterized by several well-defined events (e.g., flames across ceiling, fire spread to other major items, full room involvement, flames bursting out of doorway), all occurring quite suddenly and over a fairly short duration (5-10 sec). In the second test, "flashover" was not so easily recognized; in fact, even though the fire generally grew much more rapidly than in the first test, all of the usual identifying features of "flashover" were spread over a period of 40-70 sec (see Volume I for further details), and it was difficult for observers to say when "flashover" occurred. As a result, in order to avoid any confusion over the use of the word "flashover" in a technical sense, it was suggested* that the use of terms describing the various parts of the "flashover" process would reduce ambiguity in scientific discussion. The following terms were defined:

1. FLAMEOVER - The process in which flames first move out across a ceiling.
2. FULL ROOM INVOLVEMENT - The process by which most combustibles in an enclosure fire first become involved.
3. VENTILATION CONTROL - The process by which the rate of oxygen flow into a room, and hence the burning rate in the room, is controlled by the flow through the opening(s).
4. BURST - The process by which gases burst out of the room through the opening. This may be accompanied by a noise, often a "whoosh", and sometimes by an increase of flame and smoke outside.

These definitions should suffice until more of the room-fire development process is uncerstood. Nowhere in the analyses that follow is "flashover" mentioned technically without clear definition, and all references to fire behavior are consistent with the above definitions. The analyses include treatments of the fire spread process (theoretical), the flow through the doorway,

*H.W. Emmons, Harvard University

an energy balance for the enclosure, the response of a major fuel element in the room, the radiative heat fluxes and their sources, and instrumentation either newly applied or under development.

Thus far, only a minor portion of the analytical work has been devoted to extinguishment (more will be included for the third test). Sprinkler extinguishment of residential fires is not common. Some studies of this application are under way*. In the bedroom fire tests, the sprinkler has been manually activated only after the room has been totally involved. An automatic sprinkler would operate much sooner. It was estimated that, for the second bedroom fire, an automatic sprinkler would have activated no later than 5 min after ignition when the flames were still localized on the bed and conditions in the lower half of the room were still apparently non-lethal.

*For example, Kung, H.C., Residential Sprinkler-Protection Study, FMRC Technical Report, July 1975.

II
SUMMARY OF ANALYSES

A considerable, combined effort was expended by Home Fire Project members in analyzing the bedroom fire test data. There are three general areas of analysis: 1) theoretical and semi-empirical treatments of room fire development, including the mechanics of flow through the doorway; 2) the measurement of and response to various heat fluxes within the room; and 3) the evaluation of instrumentation under development or newly applied.

A mechanistic model for the fire development process in a room from flaming ignition to just after flame-over has been developed for the bedroom test (Section III). The model includes effects of: heat release rate, enhancement by radiative feedback, combustion-zone-induced flow (two approaches), plume entrainment, energy exchange in the ceiling gas layer, and flow through the doorway. With measured values of burning rate as input (theoretical values can be used when available), the model yielded predictions of flameover time, flame height as a function of time, ceiling-layer temperature and depth as functions of time, and a scaled species concentration/optical density history. Despite the simple approaches sometimes used (because of lack of anything better) in formulating the model, this first attempt appears to provide reasonably good results. This model, however, was developed a posteriori (after the fire test), and the general applicability remains to be tested.

A detailed study of the flow through the doorway was made (Section IV) based upon a general theory of fire-induced flow through a room opening. The buoyancy-driven flow is calculated from a hydraulic point of view, assuming the existence of a neutral plane in the room and doorway. The time-dependent, measured temperature distribution in the doorway is utilized to calculate the flow of gases (both inward and outward) through the doorway as a function of time; an experimentally-determined flow coefficient is applied to correct for vena contracta and other orifice-type effects. The fuel-air ratio, calculated from doorway temperatures and thermal properties of the fuel, is then used to determine the rate of burning in the room as a function of air flow, and hence, the burning rate history for the enclosure. Calculated values of flow and

burning rate show good agreement with experimental results. A measurement of pressure inside the room during the fire tends to support the neutral-plane assumption (Section V).

A concerted effort was made to measure total and radiative heat fluxes within the room and to isolate the major sources of radiative energy. In a novel experiment, measurements were made with a scanning, collimated-beam radiometer that was located below the bedroom floor and looked vertically upward toward the ceiling through a hole in the floor (Section VIII). The radiometer viewed the ceiling gas layer backed alternately by the hot ceiling and a water-cooled plate. The results show that practically all of the radiation seen by the radiometer in this test came from the hot, sooty smoke layer; the hot ceiling was obscured from the radiometer once the smoke layer achieved a thickness of approximately 200 mm. This conclusion was supported (Section X) by comparing the equivalent radiation temperature associated with the measured radiance with gas temperatures measured at the lower edge of the smoke layer (determined from optical density measurements). The conclusion was further corroborated (Sections IX and X) by the measurements of a wall-mounted, wide-angle radiometer which became obscured by the descending smoke layer shortly before room involvement and which subsequently indicated a radiant flux nearly completely accounted for by smoke radiation (determined from the scanning radiometer data). Consequently, the descending smoke layer constituted the major source of radiative energy contributing to fire spread throughout the room. The total radiant power lost by the smoke layer was approximately 20 percent of the combustion heat release rate of the fire, assuming 100 percent combustion efficiency (Section IX). It appears feasible that actual combustion efficiency (as a function of time) may be obtainable in future work from gas concentration measurements (Section VI).

It also appears that, prior to room involvement (when most of the heat flux incident on the bed was coming from the flames), radiation from the smoke layer still provided significant enhancement of the bed fire. After room involvement, the hot gas layer provided even a greater portion of the heat flux to the bed (Section XI).

Two studies were made of the thermal response of the bureau, the second major fuel item to be involved in the fire. In one of these studies (Section IX), it was assumed that only smoke radiation heated the top bureau surface. Calculation of the resulting temperature rise from ambient to ignition temperature yielded a predicted time of ignition in reasonable agreement with observation. In the second such study (Section VII), the responses of two thermocouples imbedded in the front panel of a drawer in the bureau were utilized to calculate the heat flux impinging on the panel surface and the mass loss rate due to pyrolysis as functions of time. Comparison of measured total weight loss agreed well with that predicted by the analysis. Furthermore, the ignition time of the drawer panel was calculated (based upon a critical flame temperature criterion) and also agreed well with observation.

Attempts to measure the flame radiance with a collimated-beam radiometer and the plume thermal energy flux with thermocouples met with difficulty because of the movement of the fire on the bed (Section IX). From measurements of flame area and height, the early-fire, burning-rate history was estimated (Section IX) and found to compare reasonably well with burning rates derived from measured weight loss data. Values of burning rate calculated from an energy balance for the enclosure also compared well with the measured data. (Section VI); the energy balance also revealed that the heat loss to the walls was quite significant, approaching 50 percent of the total heat release rate of the fire during flame-over and room involvement.

Two small, prototype fan anemometers demonstrated their capability of providing useful velocity data while withstanding a severe fire environment (Section XII). Some electrical noise problems were evident, but these appear to be correctable for future applications.

Several simply-constructed, and relatively inexpensive aspirated thermocouples were used in the bedroom fire test in an attempt to measure true gas temperatures. Results from laboratory tests and the bedroom test indicate that, under room fire conditions, the aspirated probe reliably registered gas temperatures, significantly better than a bare-bead thermocouple (Section XIII).

III

A MECHANISTIC MODEL OF THE 1973 AND 1974 BEDROOM TEST FIRES

N.D. Fowkes
Harvard University

3.1 INTRODUCTION

3.1.1 Objective

The objective was either

1) to predict theoretically the outcome of the 1973 and 1974 test fires[1] up to and including flame-over, or

2) to determine what aspects of fire development in the bedroom are insufficiently understood to make such predictions.

3.1.2 Background

There has been a great deal of theoretical and experimental work done on the post "flashover" behavior of fires in a building[2,3,4,5] and our understanding in this area is "reasonably" good. Our understanding of the conditions leading up to "flashover" is, however, not so complete, which is unfortunate from a practical point of view, because this problem is the more important one. In view of the fact that the required knowledge of important pieces of the problem has only just been obtained (and there are still important deficiencies in our understanding), this gap is understandable. The recent crib studies[6,7,8] and those on the natural convective flow through an opening[9,10,11], in particular, were absolutely necessary before one could even proceed with the room fire development problem. It was felt that an attempt to attack this problem should be made at this early stage, if only to identify the most serious deficiencies. In view of the known deficiencies, this first attempt has been surprisingly successful.

3.1.3 Summary

1) Our present understanding of the factors determining flame shape[10,12] is not good enough to enable us to determine the rapid buildup of fire (in a room) as assisted by local radiative enhancement.

2) If we use the (before "flame-over") fire burning rate as input, then our knowledge of the other room fire processes is sufficiently good so that we can predict most other major features of the room fire reasonably well. We can, for example, determine mass fluxes of gases into and out of the room, the temperature buildup in the room, the depth of the hot gas ceiling layer, etc. Most importantly, it appears that we can accurately predict the flame-over time.

3) Our present knowledge of smoke production and movement is not good enough for danger-to-life estimates.

3.1.4 The Approach Adopted In This Work

Our present knowledge of pyrolysis, combustion, and the geometric factors involved in burning is not good enough to enable us, for example, to predict the outcome of laboratory material tests. With this in mind, the following question seemed to be the appropriate one to ask at this stage: given the laboratory-determined burning rate of the materials used in the bedroom fire under open conditions (in particular for our case, the mattress which played a central role in both fires (see Figure 3.1)), can we determine what will happen under bedroom fire conditions? Pagni's observations[12] provide the necessary mattress burning rate data. This was the question initially considered. Subsequently, we decided to consider the less ambitious question: given the mattress burning rate actually recorded in the bedroom tests, can we determine everything else about the room fire? The answering of this question would at least enable us to test our understanding of the "non-local"* aspects of the room fire. In fact, as it turns out, the approach leads to a qualitative and quantitative understanding of "flame-over".

*"local" here means close to the fire

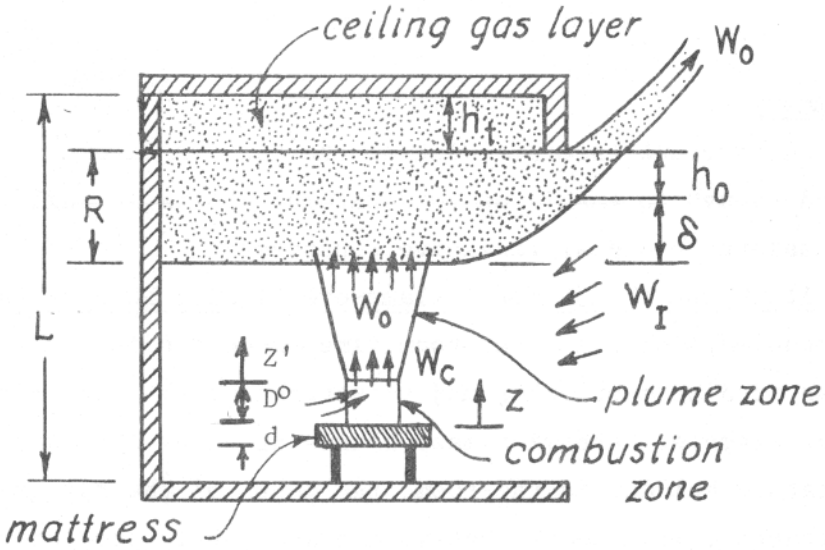

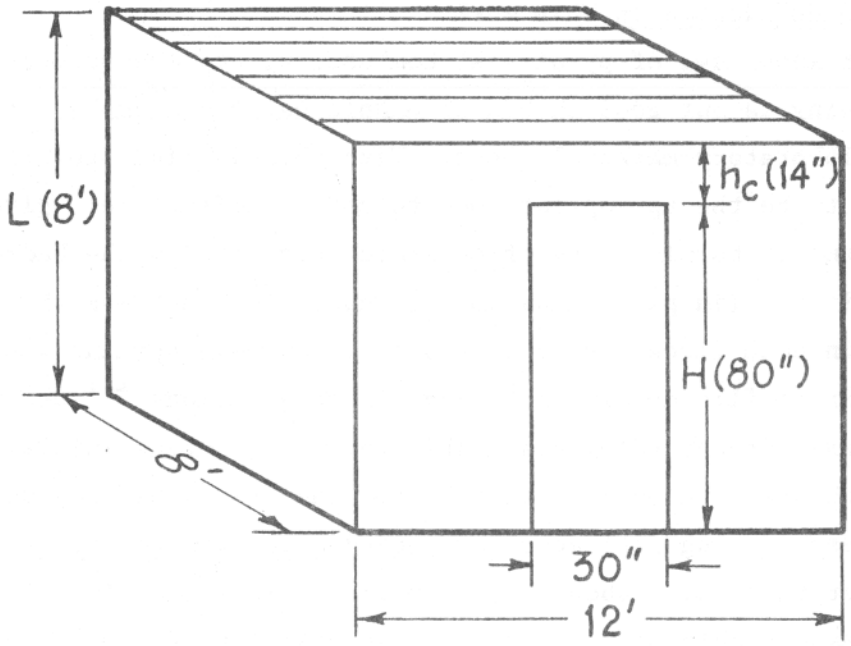

FIGURE 3.1 THE BEDROOM GEOMETRY AND MODEL

3.1.5 The Conceptual Model

Air, fuel, and heat are the necessary components for fire. Initially (Stage 1), fire growth on a mattress in a room is limited by local fuel availability and heat retention, and the fire behaves as if it were not contained in a room. Subsequently (Stage 2), additional heat retention (arising because the fire is enclosed) enhances fire growth. Finally, (Stage 3), if the fire grows sufficiently large, the inability of the fire to supply itself with sufficient air (through the available openings) to burn all the released fuel will limit its growth. The whole room may or may not be involved in burning at this stage. If, for example, the only openings are door cracks, etc., then only a small local fire may be sustained (under steady conditions) by air intake. For the door size openings of consideration here, complete room involvement occurs during Stage 3. The above stages seem to be relatively distinct (see, e.g., the crib in enclosure tests [7,8]) and will be treated as being completely distinct here. During Stages 1 and 2, the hot combustion gases rise and are replaced by cool air drawn into the combustion zone. Additional air is entrained in the hot gas plume, and the resulting mixture collects under the ceiling and subsequently flows out the opening (a door in our case). The flow of air into the room and the flow of products out of the room compete for the available opening space.* Most importantly, there exists a maximum possible air flux that can be drawn into the room through a certain size opening; once this stage is reached, the control of air flow into the room shifts from the plume to the door. The burning rate in the room may or may not be limited by this air intake.

Throughout this analysis, the following assumptions are made:

1) Fluid mechanic response to burning rate changes are instantaneous;

*The flows are weakly coupled before choked conditions are reached, and strongly thereafter.

2) The heated gases arriving at the ceiling mix completely and instantaneously with the hot gas already there, and the heat losses occur uniformly throughout this hot gas layer (thus, there are two layers of fluid in the room - a uniform temperature hot ceiling gas layer and a cool, atmospheric temperature, lower gas layer);

3) All reactions are stoichiometric, and the heat released is released inside the room.

During Stages 1 and 2, it is assumed:

1) The combustion zone draws in, and the plume entrains, as much air as it would under open conditions;

2) If the flux of air called for by the plume and combustion zone is less than the maximum (choked flow flux) that can be drawn through the opening, the air thus withdrawn from the room will be replaced by air coming in the door;

3) If the flux called for by the plume and combustion zone exceeds the choked flow flux, the complement will be removed from the room itself, thus drawing down the ceiling layer until steady conditions are again reached;

4) The released pyrolysis gases burn in the flame zone.

It is also assumed that (for our open door situation) that the transition from Stage 2 to Stage 3 occurs instantaneously when the ceiling gas layer reaches 450°C - the temperature at which most items in the room would normally pyrolyze. This event is referred to as "flame-over".

During Stage 3 (in our case), the room itself will become totally involved. It is assumed that the burning rate is then determined completely by choked flow air intake through the door.

These assumptions will be discussed as they are introduced into the following model. For convenience in presenting the model, particular reference is made to the 1974 test.

3.2 THE MODEL

3.2.1 Fuel Burning Rate in the Room

Pagni[12] has made laboratory burning rate observations on a mattress (with cover) under open conditions. The mattress was identical to that employed in the 1974 room test, and was supported on a metal sheet. The mattress support in the room fire appeared to be relatively non-porous, so Pagni's observations should be relevant to the early fire stages. He found that at the end of the first 2 min from ignition, a cylindrical hole (radius 5 cm) had been "drilled" by the fire through the mattress (of thickness d = 8 cm, and density $\rho_M = 0.02$ gm/cm^3). In the remaining minutes of the observation, the flame moved radially, uniformly with depth, at a slowly increasing velocity (velocity ≈ 0.1 cm/sec). During this time, the burnt region maintained a cylindrical geometry with its interior filled with a turbulent, luminous flame. Thus, during Stage 1 in the room fire tests, we would expect the mass loss rate ($\dot{m}$) to be given by

$$\underline{\text{Stage 1}}: \quad \dot{m} = 0.2\pi r \rho_M d, \text{ gms/sec} \qquad \text{for } 120<t<330 \text{ sec}, \tag{3.1}$$

where r is the radius of the burnt region in centimeters. Although mass loss rates were not calculable in the room fire test during the first 345 sec, the overall mass loss was measured at the end of the 345 sec and is consistent with calculations based on the above expression for 120<t<330 sec (this time span defines Stage 1).*

*Unfortunately, Stage 2 (in which a rapid increase in the weight loss rate occurs) had already been reached before the first weight loss measurements could be made in the room test, so that we have no direct Stage 1 data from the room fire test to compare with Pagni's result. If, however, we take eq (3.1) as describing Stage 1 and use an extrapolation of the recorded results to both define the end of Stage 1 (found to be 330 sec) and describe Stage 2, then we obtain for total weight loss up to the 345 sec mark the value .408 kg, which compares reasonably with the .454 kg actually recorded.

After about 330 sec from ignition, a rapid increase in the bed weight loss rate was observed (see Figure 3.2) due to a combination of events (pillow involvement, intense radiative feedback from the nearby headboard and wall, headboard involvement). The following least-squares exponential fit to the data points,

Stage 2: $\dot{m}(t) = 1000 \exp(.0363t - 17.5)$, gms/sec for $t > 330$ sec (3.2)

will be used to describe the burning rate during Stage 2. The cross-sectional flame area, A, (measured at the base of the flames) will be required for later combustion zone calculations. If we assume that cylindrical geometry persists (and ignore the geometric complications associated with headboard burning etc.), then

$$A(t) = \pi r^2(t), \tag{3.3}$$

with the conditions

$$\dot{r}(t) = \dot{m}(t)/(2\pi r \rho_M d) ,$$

and $r(t=120) = 5$ cm,

determining A(t).

Once gas temperatures in the room exceed the pyrolysis temperature of most articles of furniture etc. (taken as 450° C*), the expelled pyrolysis gases will collect under the ceiling, and we would expect burning to commence there (we call this event "flame-over") and quickly engulf the whole room. There was plenty of available fuel in the bedroom, so that the assumption that complete room involvement occurs immediately when the ceiling gas layer reaches 450°C, and the assumption that the burning rate jumps to the maximum burning rate

*The pyrolyzing temperatures of cellulose are 350°C - 450°C.

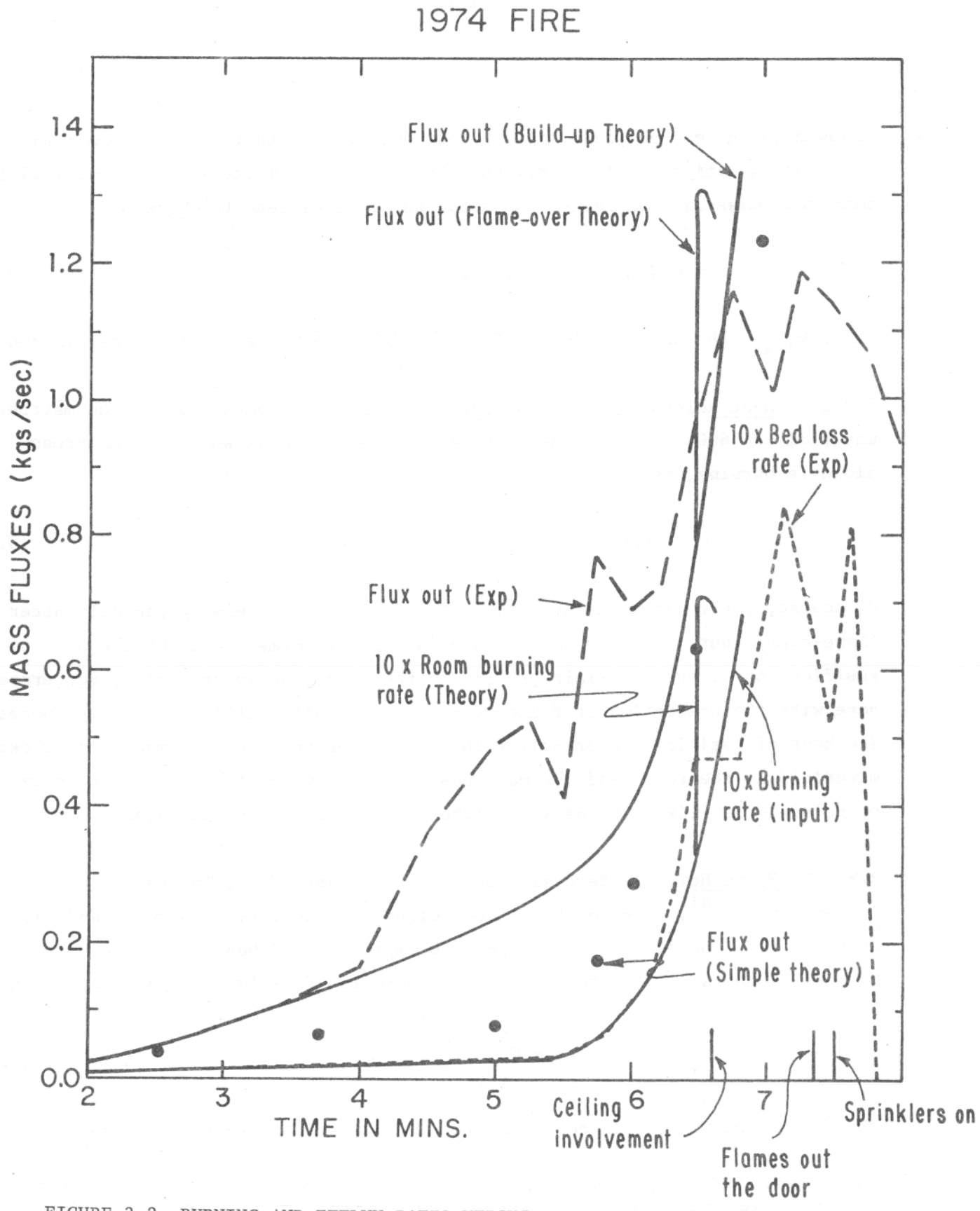

FIGURE 3.2 BURNING AND EFFLUX RATIO VERSUS TIME AFTER IGNITION

allowed (under choked conditions) by air intake through the door, seem reasonable approximations. Since 18.4 mass units of air combine (stoichiometrically) with each mass unit of fuel*, the above assumptions lead to Stage 3:

$$\dot{m} = W_{iMAX}/18.4, \text{ gms/sec}, \tag{3.4}$$

where W_{iMAX}, the choked flow air flux into the room, has yet to be determined.

3.2.1.1 Heat Release Rate in the Room - The heat of combustion of the mattress material is 6600 cal/gm so that the heat release rate Q, while the mattress alone is burning, is given by

$$Q = 6600\ \dot{m}\ , \quad \text{cal/sec}. \tag{3.5}$$

Of course, other materials are involved in the fire process (especially after flame-over), but, since we do not have detailed information about the heat of gasification of the materials present in the room, and we are mainly concerned here with the prediction of flame-over, eq (3.5) will suffice for our purposes. The heat of gasification of polyurethane is lower than that of most "cellulosic" materials in the room, and the mattress is the major heat source; so this expression is not likely to be inordinately in error for our purposes.

3.2.1.2 Flame Height - Several studies in the past, e.g., Thomas[13] and Kosdon, et al[14], have related flame heights to the rate of burning and size of the fire. The formulae developed are empirical and based on valid data. Emmons[15] has suggested the following compromise formula for flame height, L.F.,

$$\frac{L.F.}{2r} = 1.65 \left[10^6 \frac{\dot{m}^2}{(2r)^5} \right]^{.25}, \tag{3.6}$$

and this estimation of flame height will be used in the work to follow.

*This corresponds with a 4 to 1 oxygen/fuel ratio. (Editor's note: The editor was not able to determine how Prof. Fowkes obtained this ratio; the editor calculates the stoichiometric air-polyurethane ratio, on a mass basis, to be 7.5 rather than 18.4.)

Pagni's laboratory observations[12] on the mattress burning rate indicate that $\dot{m} \propto r$ (see eq 3.1) under open conditions, so that eq (3.6) would predict a flame height varying as $(\dot{m})^{.25}$ throughout his experiment. It will be interesting to see how this prediction checks with observation. I suspect that more (and important) physics is involved in determining flame shape and height than indicated by these simple formulae.

3.2.1.3 Radiation Enhancement of Fire Growth - Since we are using as input the bed weight loss data measured in the bedroom test, any determinations we make of the burning rate enhancement due to radiation feedback from the headboard, the walls, and the smoke hot gas ceiling layer, will not play a role in the mainstream calculations. Because of the uncertainty of present flame shape theories, and the geometric difficulties associated with the determination of local radiative enhancement of the fire, no attempt will be made here to determine this enhancement factor. We will, however, make an attempt to determine what effect radiation from the smoky, hot, ceiling gas layer can have on the fire burning rate throughout the duration of the test. In particular, it will be interesting to see if radiation from this layer can significantly affect the onset of flame-over.

Alpert's estimate[16] of radiative enhancement, RE, will be used here,

$$R.E. = \frac{\text{mass flux induced by thermal ceiling radiation}}{\text{mass flux caused by the free burning fire}} = \frac{\dot{q}_{rad}}{.4} \qquad (3.7)$$

where $\dot{q}_{rad} = \sigma T^4$, with $\sigma = 1.356 \times 10^{-12}$ cal/cm^{2}sec °K^4 and T = temperature in °K.

3.2.2 The Combustion Zone

Some of the energy generated by combustion is radiated away from the fire vicinity, and most of the remaining energy heats gas in the neighborhood of the fire. We will assume the quantity ϕ_2 is radiated, where

$$\phi_2 = \gamma Q \qquad (3.8)$$

with $\gamma = 1/4$, and the quantity ϕ_c is absorbed by the gases leaving the combustion zone, where

$$\phi_c = (1 - \gamma)Q. \tag{3.9}$$

We would now like to determine the flux of air drawn into the combustion zone by this heat source, so that eventually we can determine the flux and temperature of hot gas arriving at the ceiling via the plume. Plume theory gives the required result if the plume height is large compared with the source "size"*; however, in our case this is not true throughout the test, so we will attempt a combustion zone analysis.

3.2.2.1 Background - A satisfactory (even crude) analysis of the combustion zone of a fire has not yet been produced. Even the much simpler problem of determining the flow near a finite heat source** is not solved. Models based on entrainment laws fail to produce the relatively shallow but strong inflow over the fire perimeter (known as fire wind) that carries in most of the oxygen necessary for combustion and couples the fire to its environment. (Since the flame height theories are based on entrainment ideas, they are suspect). Numerical studies of this problem (using the full Navier-Stokes equations) have been made by Knight[17] and Smith, et al[18]. Smith has shown conclusively that the fire wind is driven by the dynamic pressure field generated by the strong buoyant acceleration close above the ground. Given the present lack of usefully simple models for the combustion zone, the following simple models are suggested, and will be used in the work to follow.

---

* so that the amount of air entrained << amount of air drawn into the combustion zone

**In this problem, we do not have to solve the coupled flame shape and induced gas motion problems.

3.2.2.2 A Simple Model - Here we simply assume that the flame draws into the combustion zone just sufficient air to combine with the released fuel. Under these conditions, the mass flux rising up out of the combustion zone, W_c gms/sec, (where W_c = air flow + fuel flow) is given by

$$W_c = 19.4\ \dot{m},\ \text{gms/sec}. \tag{3.10}$$

One might expect that more air will be drawn into the combustion zone than is necessary to burn up the fuel, so that the above estimate of flow is likely to be low. The above approach is somewhat naive. Gas movements are not directly influenced by chemical kinetics; it is the buoyancy-inducing heat flux that induces gas movements.

3.2.2.3 A Buoyancy Model - A simple buoyancy-driven motion is assumed here. The area of the flame at its base is taken as the "effective" area of the combustion zone and D^o (as yet undetermined) defines an effective height of this region (see Figure 3.1). We will assume the gas density throughout the combustion zone, ρ, is constant, so that particles of gas arriving from ∞ and passing through the sides of the combustion zone "box" are instantaneously raised in temperature to the combustion-zone gas temperature. Since the particles start at ∞ with the same energy content and receive the same heat input, then (assuming no losses) they will leave the combustion zone with the same kinetic energy. Thus, if w is the vertical velocity, then we would expect $w = w(z)$ (see Figure 3.1). If W_c is the flux out of the zone, then

$$W_c = \rho w(D^o)A, \tag{3.11}$$

and the vertical momentum flux out of the zone is*

$$W_c\, w(D^o) = Ag(\rho_a - \rho)D^o \ , \tag{3.12}$$

so that, using eq (3.11):

$$W_c^{\,2} = A^2 g\rho\ (\rho_a - \rho)D^o \ , \tag{3.13}$$

where ρ_a is atmospheric air density. (Over the length scale D^o, of the order of radius r, the amount of entrainment is small.) The vertical movement of gas out the zone creates a horizontal pressure gradient outside the zone dragging in the mass required. Mass conservation tells us how much air must be drawn into the zone as a function of vertical position z to be consistent with eq (3.13). This gives

$$2\pi r u(z)\rho_a D^o = W_{cz}(z) \ , \tag{3.14}$$

where u is the horizontal component of velocity into the zone.
Thus, using eq (3.13) we obtain

*There are inbuilt assumptions in the development of eq (3.12) that require careful theoretical and experimental evaluation and are of real physical interest. The problem is essentially the fireplace problem. We all know that if the fire sits on a grill it burns more rapidly than if it is located on the floor. This may be simply a heat source phenomenon, or it may be a phenomenon that is special to the fire situation. Thus, the location of a heat source may affect the mass flux of air dragged into the source zone, e.g., it may be easier for the air to come from underneath if the source is on a porous support. On the other hand, the accelerated burning of a fire on a grill may be caused by the fact that the oxygen meets the fuel closer to the fuel source in the grill fire case so that there would be enhanced fuel evaporation in this case. We will carry through with the above analysis in the hope that the physics is reasonably correct.

$$u = \frac{\sqrt{\rho(\rho_a - \rho)g}\, A}{2\pi r\, \rho_a} \frac{1}{\sqrt{D^o}} , \tag{3.15}$$

so that $\frac{u}{w} = O(1)$ when $D^o = O\left(\frac{r}{2}\right)$ Thus, little mass flux is drawn into the combustion zone by the buoyancy uplift at distances higher than the zone radius, and entrainment mechanisms commence to take over. If we choose $\frac{r}{\alpha} > D^o > r/4$ (where α is the entrainment factor), the above calculations for flux into and out of the zone as defined will be accurate. In this case, $D^o = r$ has been chosen.

The heat supply responsible for the buoyant uplift is, of course, provided by combustion, and the energy equation gives

$$\frac{Q_c}{W_c} = C_p\, (T - T_a) , \tag{3.16}$$

where T_a is atmospheric temperature. This equation, together with the equation of state

$$\frac{T}{T_a} = \frac{\rho_a}{\rho} , \tag{3.17}$$

and the vertical momentum eq (3.13), enables us to determine the flux and density of the gas leaving the zone.

Thus,

$$W_c (Q_c + W_c T_a C_p)^2 = A^2 g\, \rho_a{}^2 T_a C_p Q_c r , \tag{3.18}$$

and if we write

$$W_c = \left(\frac{Q_c}{T_a C_p}\right) \overline{W}_c , \tag{3.19}$$

then we obtain the following cubic equation for $\overline{W}_c$

$$\overline{W}_c (1 + \overline{W}_c)^2 - A_2 = 0, \tag{3.20}$$

where

$$A_2 = A^2 g \rho_a^2 \left(\frac{T_a C_p}{Q_c} \right)^2 r \ . \tag{3.21}$$

An examination of eq (3.20) and (3.21) shows that the above theory suggests the mass flux drawn in by a heat source varies with its size in the following limiting ways:

$$W_c \propto A^{5/2} \ , \quad \text{for "small" source Areas, A,}$$

and

$$W_c \propto A^{5/6} \ , \quad \text{for "large" source areas,} \tag{3.22}$$

where small means $A_2 << 1$.
The appropriate solution branch of the cubic is the $\overline{W}_c > 0$ branch.

3.2.3 Plume Analysis

We now know the mass flux, W_c, and density of gas leaving the combustion zone, so that we can determine the buoyancy flux and use traditional plume theory to determine the additional mass flux of air entrained before the ceiling gas layer is reached (see Morton, Turner, and Taylor[19,20,21]). If we assume the plume is surrounded by uniform-density atmospheric air (until entering the ceiling layer) and make the simple entrainment assumption (that the inflow velocity is some fraction, α, of the upward velocity), then the following well known relations of simple plume theory result[20]:

1) The proportional rate of change of mass flux, $W_p(z)$, transported by the plume is inversely proportional to the "effective" radius, r', of the plume*, i.e.,

$$\frac{1}{W_p(z)} \frac{dW_p(z)}{dz'} = \frac{2\alpha}{r'} \ , \tag{3.23}$$

where z' is the distance up from the combustion zone (see Figure 3.1); and

*A top hat profile is normally assumed, and r' is the effective width of the profile.

2) The plume is cone shaped (neglecting initial stages of adjustment) with

$$\frac{dr'}{dz'} = 6\alpha/5 \ , \tag{3.24}$$

where α is the entrainment coefficient.
Equation (3.24) can be integrated to give

$$r' = \frac{6\alpha}{5} z' + z'_o \ , \tag{3.25}$$

and, after substituting this expression into eq (3.23), the resulting expression can be integrated to give

$$\frac{W_p(z')}{W_{PO}} = \left(1 + \frac{6\alpha z}{5r_o}\right)^{5/3} \ , \tag{3.26}$$

where W_{PO} and r_o are constants to be adjusted so that mass and buoyancy fluxes of gas leaving the combustion zone match those obtained from the combustion zone analysis. It is sufficiently accurate for our purposes to match mass fluxes at the combustion zone exit (so that $W_{PO} = W_c$ at $r' = r$)* and use the result

$$\frac{W_p(z')}{W_c} = (1 + \frac{z'}{5r})^{5/3} \ . \tag{3.27}$$

The plume enters the ceiling gas layer at a height $z' = L\text{-}b\text{-}D^o\text{-}R\text{-}h_t$ (see Figure 3.1), so that the mass flux of heated gas arriving at the ceiling layer via the plume (denoted by W_o) is given by

$$\frac{\text{Flux arriving at Ceiling}}{\text{Flux leaving the combustion zone}} = \frac{W_o}{W_c}\left(1 + \frac{6\alpha(L\text{-}b\text{-}D^o\text{-}R\text{-}h_t)}{5r}\right)^{5/3} . \tag{3.28}$$

*A slight shift in the cone base will not affect the predicted entrainment mass greatly.

It is interesting to examine this flux ratio as a function of the source radius for fixed plume height (taken here as the distance from the bed top to the door frame top, i.e., $L-b-h_t$ in Figure 3.1) to get a feel for the effect plume entrainment has on the overall flux and temperature development in the room as the fire grows. A plot of eq (3.28) with $\alpha = .116$ is shown in Figure 3.3. Clearly, in the early stages of the fire, there is proportionally a large amount of entrainment (e.g., greater than four times as much air is entrained in the plume as initially leaves the combustion zone for a flame radius $r < 20$cm); however, once the flame radius exceeds a size of the order α times plume height, i.e., about 40 cm here, there is first a rapid reduction in the proportional amount of entrainment, and then a leveling off (see Figure 3.3). This result, in part, explains the slow buildup in ceiling gas - layer temperatures during the early fire stages.

This entrainment result (eq (3.28)) is accurate if the ratio of the plume gas density to that of its environment is close to unity, and an entrainment coefficient $\alpha = .116$ seems to best fit experimental results[21]. If this density ratio is not everywhere small, then the amount of entrainment is dependent on the local density ratio, and $\alpha = .116 \sqrt{R^1(z)}$, (where R^1 is this density ratio) seems to fit the data. The plume shape is no longer conical, and a relatively greater fraction of air is entrained in the cooler higher regions of the plume than in the flame region. For the plume sizes of interest in our calculations (considering the shape of the curve in Figure 3.3), the expression

$$\alpha = .116 \sqrt{R} \quad , \tag{3.29}$$

where $R = \frac{\rho}{\rho_a}$ and ρ is the density of the ceiling gas layer when used in conjunction with eq (3.26), provides an accurate assessment of the amount of plume entrainment.

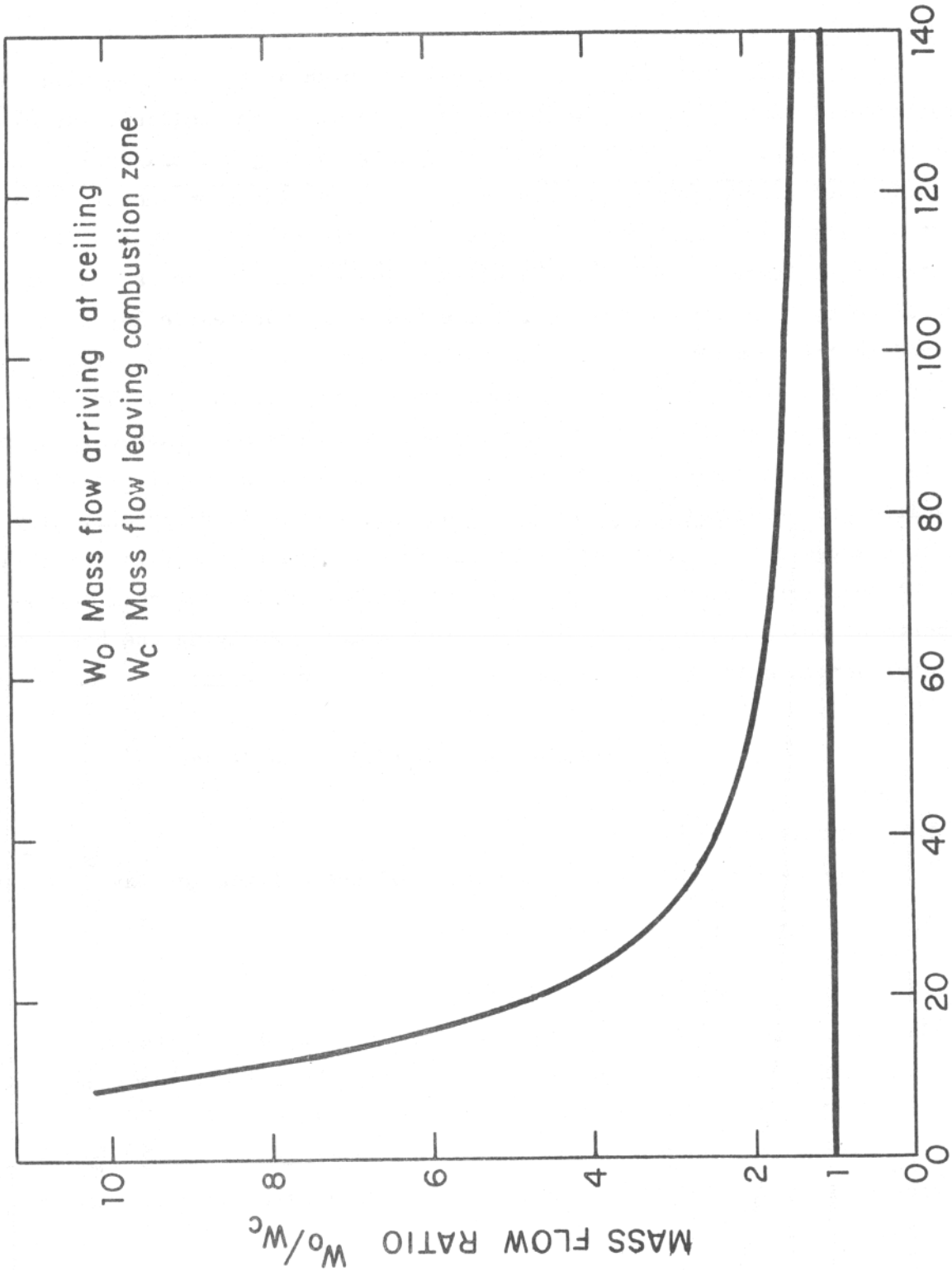

FIGURE 3.3 RATIO OF MASS FLOW ARRIVING AT CEILING TO MASS FLOW LEAVING COMBUSTION ZONE VERSUS RADIUS OF SOURCE FIRE

3.2.4 The Ceiling Gas Layer

It is assumed that the hot plume gas arriving at the ceiling mixes instantaneously and completely with the gas already at the ceiling, and also that the heat loss processes affect the hot ceiling layer gases uniformly. In practice, of course, the gases arriving at the ceiling from the plume(s) and heated walls, etc., arrive with a temperature distribution and tend to layer according to temperature. This layering process is, to a certain extent, nullified by turbulent mixing, but there was still noticeable layering observed in the room fire test. The most worrisome feature of our simple, two-fluid model is that, because the lower cooler gases of the hot-gas ceiling layer fall through the door, whereas the hotter layers are trapped under the ceiling, an estimate of heat flux from the room using the two-fluid model may significantly underestimate the heat flux through the door. Preliminary estimates suggest that the two-fluid model is not significantly in error as far as the room fire tests were concerned, although clearly one could devise an experiment which could defeat the two-fluid model. Applying the heat conservation principle over the time interval t to t+dt, we obtain:

$$H_2(t) - H_1(t) = Q_c(t)dt + R_N(t)dt - LOSS(t)dt. \qquad (3.30)$$

In this expression:

1) H_1 denotes the heat content (in cal.) of the ceiling gas layer at time t, so that

$$H_1 = C_p\,(T(t) - T_a)E(t), \qquad (3.31)$$

where

$$E(t) = h(t)\,A_R\,R(t)\,\rho_a \qquad (3.32)$$

is the mass (gm) of the ceiling gas layer at time t, with A_R being the cross sectional area of the room (in cm^2), h(t) the ceiling layer depth (cm), $R(t) = \rho(t)/\rho_a$, and C_p the specific heat (0.45 cal/gm);

2) H_2 is the heat content evaluated at t + dt of the original mass of gas at time t together with the plume mass flux added over the time interval dt(sec), so that

$$H_2 = C_p\ (T(t+dt) - T_a) \left[E(t) + W_o(t)dt\right] ; \qquad (3.33)$$

3) Q_c dt is the heat transported to the ceiling via the plume as a result of combustion* over the time interval dt;

4) LOSS dt is the heat loss through the ceiling and walls due to conduction; and

5) $R_N$dt is the net radiative heat gain by the ceiling layer over time dt.

In the limit as dt→0 the heat eq (3.30) reduces to

$$\frac{dT}{dt} = \frac{Q_c + R_N - LOSS - C_p(T-T_a)\ W_o}{C_p\ h\ A_R\ R\ \rho_a} \quad . \qquad (3.34)$$

3.2.4.1 Radiation Exchanges To and From the Ceiling Layer - The total amount of heat radiated from the fire is Q_r. This is radiated in all directions and may or may not be absorbed in the ceiling gas layer, depending on how smoky this layer is. Markstein's work[22] shows that a considerable proportion of the heat radiated to this layer is absorbed and emitted from this layer when the layer is smoky (i.e., after about 5 min from ignition). Once the ceiling gas layer reaches a significant temperature, there will be radiative loss to other parts of the room. Putting in approximate view factors and assuming blackbody emission and absorption, the net rate of radiative heat gain is given by

$$R_N = Q_r \left(\frac{A}{A_R}\right) - \sigma \left[(T)^4 - (T_a)^4\right] (A_R - \pi r^2) \quad . \qquad (3.35)$$

Both terms will only become numerically significant (relative to Q_c) near flame-over so there is no harm in including both terms for the early stages of the fire development (even though the gas layer may be completely transparent at this early stage). The above radiation estimates are crude, and,

*We assume here no time delay between the gas leaving the combustion zone and this same gas arriving at the ceiling.

unfortunately, the last term in particular is sensitive to errors in the various factors involved (because of the fourth power of temperature behavior). Because of the sensitivity in the calculation of this last term, it was felt that more serious errors are likely to be made by keeping it in than by leaving it out, so it has been left out of the calculations to date.*

3.2.4.2 Wall Heat Loss - The plume gas penetrates the ceiling gas layer on arrival, both because of inertia and because the plume gas is hotter on the average than the surrounding ceiling gas. Thus, the gas in immediate contact with the ceiling will be continuously replaced by "newer", hotter plume gas, and the resulting heat transfer to the ceiling will be significantly enhanced as a result of this exchange process. The assumption that the ceiling surface is "effectively" always in contact with gas at the mean temperature of the ceiling gas layer seems, therefore, appropriate, and the conduction problem we are faced with (assuming Newtonian cooling from the external surface of the ceiling material of thickness ℓ) is

$$K \frac{\partial^2 \phi(x,t)}{\partial x^2} = \frac{\partial \phi(x,t)}{\partial t} \quad , \tag{3.36}$$

with $\phi(o,t) = T(t)$, (3.37)

and

$$\frac{\partial \phi(\ell,t)}{\partial x} = - C\phi(\ell,t) \quad . \tag{3.38}$$

In the 1973 and 1974 tests, the outside walls were relatively warm at the end of the test, so that the semi-infinite problem with the boundary condition of eq (3.37) seems an appropriate first approximation+. The solution to this

*This term becomes important near and after flame-over. Many factors complicate the radiation balance at this stage. It is conceivable that this term should be zero at this stage because the whole room is filled with hot gas after flame-over.

+We can perturb about this solution to get a more accurate answer.

semi-infinite problem (see Carslaw and Jaeger[23]) is given by:

$$\phi(x,t) = \frac{x}{2\sqrt{\pi K}} \int_0^t T(\tau) \frac{\exp\left[-x^2/4K(t-\tau)\right]}{(t-\tau)^{3/2}} d\tau \ , \tag{3.39}$$

and the amount of heat flux conducted away from the gas is given by*

$$\text{LOSS/area} = \lim_{x \to o} \frac{k}{2\sqrt{\pi K}} \int_0^t T(\tau) \frac{\exp\left[-x^2/4K(t-\tau)\right]}{(t-\tau)^{3/2}} d\tau \ . \tag{3.40}$$

Thus, the total amount of heat per unit time conducted through the ceiling and walls of the room is given approximately by

$$\text{LOSS} = (\text{LOSS/area}) \left[A_R + 2(\ell_1 + \ell_2)(h_t + h)\right] \ , \tag{3.41}$$

where ℓ_1 and ℓ_2 are the room length and width, and $(h_t + h)$ is the thickness of the hot gas ceiling layer. The heat conservation eq (3.34) and the loss eq (3.40) are, of course, coupled via the wall loss term.

3.2.5 Flow Through the Door

Cool air of mass flux W_i, where

$$W_i = W_o - \frac{dm}{dt} \tag{3.42}$$

and $\frac{dm}{dt}$ is the mass added by the fire, is drawn into the fire zone and entrained by the plume, and, thus, removed from the cool air layer in the room. At the same time, hot gas of mass flux W_o either collects under the ceiling or flows out the door. Some, or all, of the cool gas flux removed by the plume plus fire will be replaced by cool air sucked in the door. The amount of cool

*For numerical evaluation, this integral needs to be processed further.

air drawn in the door (and the amount of hot gas going out the door) will depend on the opening size, the hot gas layer depth, and conditions outside the door. Eventually, if steady burning rate conditions are maintained, and the opening is large enough*, steady state conditions will be reached. Under these conditions, all the cool gas removed by the fire and plume is replaced by air coming in the door, and the hot gas flux to the ceiling is balanced by the hot gas flux out the door. This steady state situation is accurately described by the Emmons model[9, 10]. The transient buildup to steady state is described by Fowkes[24]. The response time of the system (i.e., the time taken to reach steady state conditions) is of the order of the time taken for the room to fill to the steady state depth in the absence of an opening[24]. Under the bedroom test fire conditions (with the door open, and with an initial slow burning-rate buildup), the response time scale is sufficiently small compared with the burning-rate time scale that steady state conditions can be assumed to be reached instantaneously+.

The flows into and out of the door (see Emmons[9], two-fluid model) are given by

$$\frac{W_o}{\phi} = C \frac{\sqrt{8}}{3} \left[R(1-R)\right]^{1/2} \left(\frac{h_o}{H}\right)^{3/2}, \tag{3.43}$$

and

$$\frac{W_i}{\phi} = C \left[2(1-R)\right]^{1/2} \left[\frac{2}{3}\left(\frac{\delta}{H}\right)^{3/2} + \left(\frac{\delta}{H}\right)^{1/2} \left(\frac{H-h_o}{H} - \frac{\delta}{H}\right)\right], \tag{3.44}$$

where h_o is the depth of hot gas outflow <u>at the door</u>; where

$$h = \delta + h_o \tag{3.45}$$

*so that choked conditions are not realized.

+Rapid burning-rate changes occur near to flame-over, so that the quasi-static assumption is no longer valid. This just means, however, that our estimate of flame-over time will miss slightly (of the order of 1 sec).

defines δ , h being the ceiling gas layer depth inside the room measured from the top of the door frame (see Figure 3.1); where

$$R = \rho/\rho_a = \frac{T_a}{T} \; ; \tag{3.46}$$

where $\phi = g^{1/2} \rho_a \, A \, H^{1/2}$, with A the door area and H the door height; and C(=.68) is the doorway flow coefficient. (In our case H = 222.2 cms, A = 18,520 cm^2 and g = 980 cm/sec^2 so that ϕ = 10180 gm/sec). The solution procedure is as follows: The mass fluxes W_o and W_i have already been determined from the combustion zone and plume analysis (see eq (3.26) and (3.42)), and the density ratio R has been determined from the ceiling gas layer analysis (see eq (3.34) and (3.40)); the depth of outflow at the door (h_o) follows from eq (3.43). Substituting for h_o in eq (3.44), we obtain a cubic equation in δ, with the smallest positive δ solution being the relevant one. The ceiling gas layer depth, h, then follows from eq (3.45).

3.2.5.1 Maximum Flux (Choked) Conditions - The plume analysis, the combustion-zone analysis, and the outflow/inflow steady-state discussion all assume that the mass flux "called on" by the fire can (and will) be supplied through the door, so that the fire and plume behave as if there were no room surrounding them. Now, there is a maximum possible air flux that can be drawn in the door and hot gas flux that can be expelled through the door. If the fire "calls on" more flux than this, the extra cannot be supplied from outside the room, and the hot gas layer will descend until steady state conditions are again realized*. Maximum flux conditions are realized[9] when h = H, i.e., when the ceiling gas layer essentially "fills" the room.+ Since no more than the maximum flux can

*As choked flow conditions are approached, ceiling layer depths become large, so that there is "effectively" a large range of depth corresponding to the "almost choked" flow situation.

+There is still the region near the door that is not occupied by hot gas, and it is through here that the air enters.

enter through the door, this flux level will finally limit the burning rate in the room.

Setting h = H in eq (3.43) and (3.44) and dividing these two equations, we obtain

$$\frac{W_i}{W_o} = \frac{1}{R^{1/2}}\left(\frac{H-h_o}{h_o}\right)^{3/2}, \tag{3.47}$$

i.e., $$\frac{W_i}{W_i + \frac{dm}{dt}} = \frac{1}{R^{1/2}}\left(\frac{H-h_o}{h_o}\right)^{3/2}. \tag{3.48}$$

since $\frac{dm}{dt} << W_i$ * , we can approximate this expression by

$$1 = \frac{1}{R^{1/2}}\left(\frac{H-h_o}{h_o}\right)^{3/2}. \tag{3.49}$$

Solving for h_o, we obtain the depth of hot gas outflow under choked conditions,

$$\frac{h_o}{H} = \left(\frac{1}{1+R^{1/3}}\right). \tag{3.50}$$

As we might expect under maximum flux conditions, half the door is covered with hot gas if R ≈ 1. If the density ratio is much less than one, considerably more outflow depth is needed for the escaping hot gas, with the result that less fresh air can enter into the room. Using eq (3.50) with eq (3.42) and (3.43), we can determine W_{iMAX}, i.e.,

$$W_{iMAX} = C\phi\frac{\sqrt{8}}{3}(R(1-R))^{1/2}\left(\frac{1}{1+R^{1/3}}\right)^{3/2}. \tag{3.51}$$

*The fuel-air ratio is of the order 1/18.

3.2.5.2 A Note on Solution Procedure - If the flux calculations based on plume and combustion zone theory do not exceed W_{iMAX}, so that

$$W_i < W_{iMAX},$$

then the calculations proceed as indicated above. If the plume and combustion zone analysis leads to the result

$$W_i > W_{iMAX},$$

then, based on the above model (i.e., the idea that only W_{iMAX} can be absorbed by the plume), we set

$$W_i = W_{iMAX}$$

and proceed with the normal ceiling gas layer calculations.

3.3 FLAME-OVER AND FLASHOVER

Flame-over is defined as the phenomenon of the rapid spread of fire over the ceiling (and usually other parts of a fire enclosure). Flame-over conditions may or may not be realized before choked conditions are realized at the door. If choked conditions are realized first, we assume that the burning rate within the room can still continue to increase.* In the discussion to follow, the term "flashover" is used to describe the flames-out-the-door situation.

3.4 SPECIES CONCENTRATIONS IN THE ROOM

Smoke is the major life hazard in the building fire, so an understanding of the processes of smoke production and movement is essential. The smoke-

*It is assumed here that the fire is not significantly "blanketed" by the hot gas layer.

production process is not understood to the extent that we know what tests to perform on building materials. It is well known that both the amount and composition of smoke produced by fire depend strongly on the fire conditions (whether the combustion is smoldering, flaming (rapid or slow), or the conditions are flashover conditions). The tunnel test[25,26] attempts to "simulate" flame spread conditions under basically adequate oxygen-supply conditions without radiant input, while the smoke chamber tests[25,26] attempt to simulate post-flashover conditions. The I.I.T.R.I. full-scale material tests for the Society of the Plastics Industry[27] seem to suggest that the tunnel test works reasonably well for the corridor flame spread conditions, that the smoke chamber results are difficult to assess, and that neither describes the rapid smoke production that occurs under rapid spread conditions. The fire conditions we are considering are not similar to those of the tests. Based on these tests and the work of Gross, et al[28], Nelson[29] has suggested a means of assessing smoke load. Depending on size, smoke particles will tend to diffuse or settle out into the appropriate temperature layer in the room, so that significant stratification can occur.

Smoke particles may be reconsumed by the fire or carried by the gas flow to other parts of the building. None of these processes has been investigated. We have insufficient knowledge about the basic particle properties to attempt a study. Some useful references in this area are[27-36]. We will attempt here to see if there is a significant correlation between the optical density measurements, as recorded in the 1974 fire test, and the following, primitive, production-movement model. If we assume that species-production rate is proportional to burning rate, and that the species mixes uniformly in the hot-gas, ceiling layer, then the species concentration, (SC), in the gas layer will be given by

$$\frac{d(SC)}{dt}\left[A_R \text{ (ceiling layer depth)}\right] = \beta \frac{dm}{dt} - \frac{W_o}{\rho} (SC). \qquad (3.52)$$

On the basis of this model, one would expect the species concentration (and optical density per unit length*) at a particular position in the room to be zero until the hot gas layer descends to the designated position, and thereafter be given by eq (3.52).

3.5 EXPERIMENTAL RESULTS AND THEORY

Three theoretical computations have been made. The "Simple theory" computation is based on the "Simple Model" combustion-zone theory (Section 3.2.2.2). Both of the other two computations are based on the "Buoyancy" combustion-zone theory (Section 3.2.2.3). One of these computations ("The Buildup Theory") ignores "flame-over" processes. This computation not only predicts the onset of "flame-over", but also (because it continues to make non-"flame-over" calculations) gives us a good indication of whether or not flame-over conditions would have been either avoided or postponed significantly if burning conditions were slightly altered. The "Flame-over Theory" attempts to follow the complete fire history. The dashed curves in the figures to follow are measured full-scale test results, while the solid curves are the "Buildup Theory" and "Flame-over Theory" calculations. The dotted results are "Simple Theory" output. Heat losses through the walls have been ignored in the results to be presented. Preliminary calculations suggest that the losses are significant only in the early fire stages and will be included in later more-detailed models.

3.5.1 The 1974 Bedroom Fire

In the figures to follow, the approximate times (based on observations) at which flames appeared under the ceiling (flame-over), flames billowed out the door (flashover), and extinguishment commenced are shown.

*assuming a linear relation between the two (not completely justified)

In Figure 3.2 the following results are plotted:

1) Experimental curves

a. The bed weight-loss rate, based on Pagni's laboratory tests over the first 5 1/2 min and as directly recorded in the room fire over the remaining time, is shown. Note that there is an extremely rapid increase in weight loss rate at 5 1/2 min coinciding with pillow involvement and/or rapid increase in local radiative fire enhancement. After flame-over, the weight loss curve tells us little about the burning rate in the room because other items in the room are pyrolyzing and so contribute to the room burning rate. Thus, the curve should be ignored after the 6 1/2 min mark for our purposes. Note that the vertical scale for this curve is magnified by a factor 10 so that comparisons can be made with the other mass fluxes of interest.

b. The mass flux of hot gas leaving the room, based on velocity and temperature measurements in the doorway[32], is shown. The results are crude (being based on at most three velocity probes), so we cannot really tell if the apparent jumps were really present in the room test. Note that there is a rapid increase in flux coinciding approximately with the rapid, bed weight-loss increase, and also that, after "flame-over", the flux levels off at a maximum value, appears to drop sharply and then return to the maximum value.

2) Theoretical Curves

a. The burning rate input curve is shown. This is simply a least-squares exponential fit to the early (pre-flame-over) weight-loss experimental data. It is this input upon which all theoretical calculations are made.

b. The room burning rate curve is shown. This is a prediction of the burning rate of all fuel in the room. Until "flame-over" the burning rate = bed weight loss rate, so that this curve lies on top of the burning rate input curve. After flame-over, predicted at 6.5 min (cf. 6.6 min experimental), fuel throughout the room is involved, so that the curves separate. There is a rapid increase in burning rate followed by a rapid decrease (arising because the increased burning rate at flame-over results in a rapid

increase in ceiling layer temperature which in turn reduces the flux of air that can enter through the door so that the burning rate decreases again).

The mass flux curves for hot gas leaving the room according to the "Buildup" theory, "Flame-over" theory and "Simple" theory are also plotted in Figure 3.2.

The "Simple" theory results (the dotted curve) are low, as anticipated; more air is drawn into the flames and plume than is required for burning up the fuels at all stages before flame-over.

The "Flame-over" theory predicts a rapid increase in flux at about the 5.5 min mark, when burning rate increased rapidly, and a further instantaneous jump in flux at flame-over, followed by a rapid decrease in flux, (resulting because increases in ceiling temperature cause a decrease in the maximum flux levels through the door). The general character of the solution is right, and the quantitative results are much better than one would expect. The theoretically-predicted flux levels are perhaps low at around the 5-min mark, and the predicted maximum flux level is a little high. The results can be made to fit "on top of" the data if the effective combustion-zone area is taken as being about 1.5 times the flame area at its base. Although this seems a reasonable adjustment to put in, it has no independent experimental justification, so the results have not been recorded on the figure.

The "Buildup" theory indicates that flux levels would have continued to increase had not flame-over occurred.

In Figure 3.4, ceiling temperature levels, as recorded and as predicted by the various theories, are shown. The temperature levels as recorded by channel 91 (a probe located well inside the room at about the level of the top of the door) is shown. This particular probe was selected because something like average ceiling layer temperatures were recorded at this spot. Note that there is very little change in ceiling layer temperature until after 5 min and then there is a rapid increase followed by a leveling off. The flame-over theory result gives a flat temperature profile up till the rapid weight loss change, but the predicted temperature is higher than that

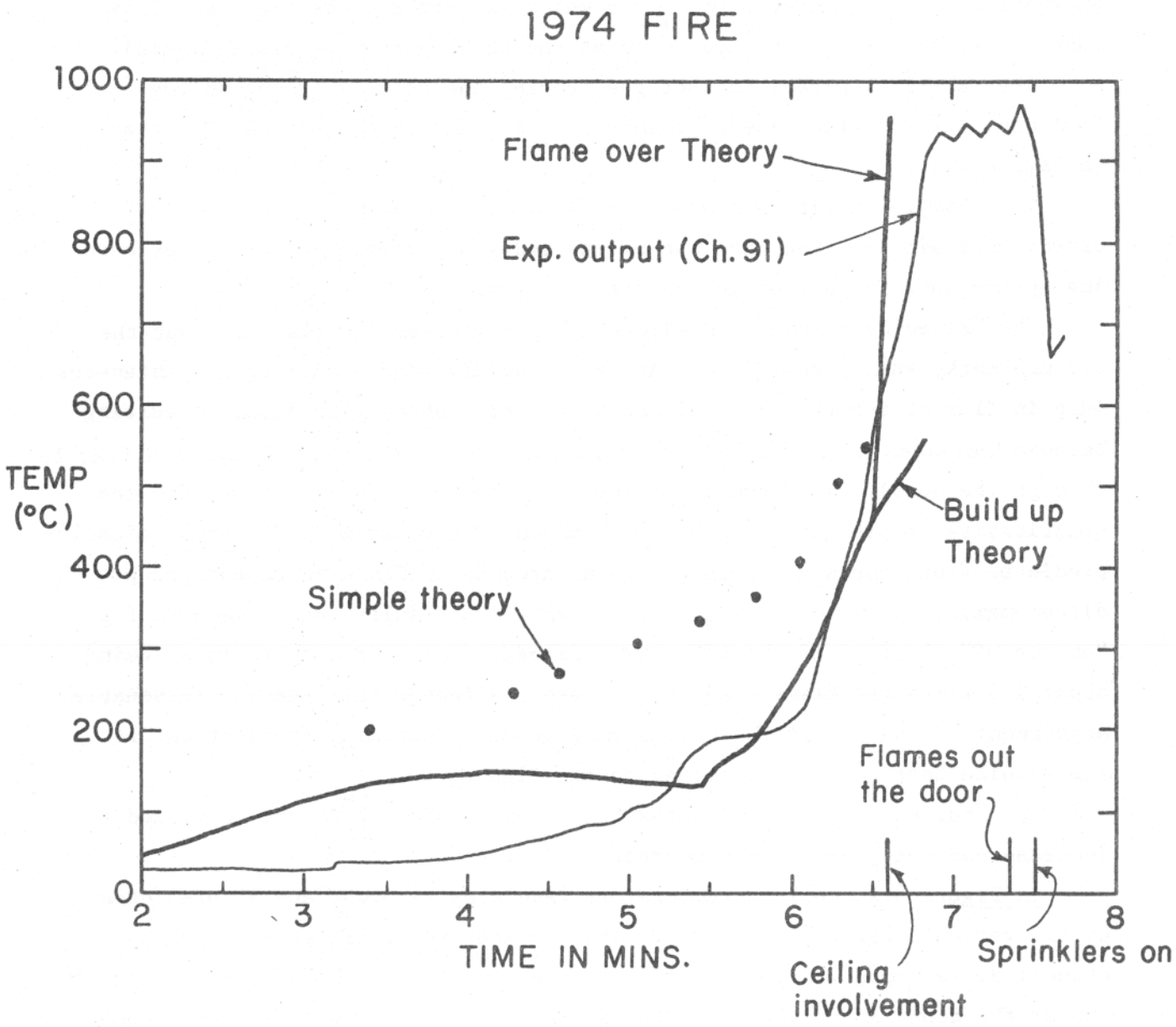

FIGURE 3.4 CEILING LAYER TEMPERATURE VERSUS TIME AFTER IGNITION

actually recorded in the test*. Preliminary calculations suggest that this discrepancy is probably due to conduction losses through the ceiling and walls. The theory predicts a rapid increase in temperature up to flame-over, followed by an extremely rapid increase after flame-over. These results agree well with the test results. Theory does not predict the leveling off of temperature seen in the test just before and after flashover. Clearly, we have underestimated the heat losses from the room (radiation through the door etc.) and/or the amount of heat generated in the room itself during this stage. The "Buildup" theory result is very interesting. It suggests that, since ceiling temperature levels were rapidly increasing at the time of flame-over and would have continued to increase, the event of flame-over at/or near the 6.5-min mark was never in doubt.

Figure 3.5 shows the theoretical result for the ceiling layer depth (measured down from the door frame top) scaled relative to the size of the door. The ceiling layer descends extremely rapidly at around the 6-min mark. Even if flame-over had not occurred, this would have happened. If flame-over does occur, the process is accelerated. The reader will note that it takes only about 30 sec for the layer to descend from head height to the floor.

Figure 3.6 gives the theoretical prediction for the fractional radiative enhancement of the fire (see eq (3.7)) that can be attributed to the ceiling gas layer. Note the rapidly increasing role played by the ceiling layer as flame-over is approached. Everything happens so rapidly near flame-over that it is hard to see which mechanisms dominate; however, this figure suggests that ceiling gas radiation does significantly influence the onset of flame-over. Further numerical experiments should enable us to decide this issue.

Figure 3.7 displays optical density measurements made in the room at points 18" (channel 149) and 30" (channel 151) from the ceiling. Note that there is significant stratification. The theoretical species concentration

*Since there is little heat in this layer (of depth $\approx h_t$ in Figures 3.1 and 3.5), this error in the early calculations will only weakly affect the calculations for later times.

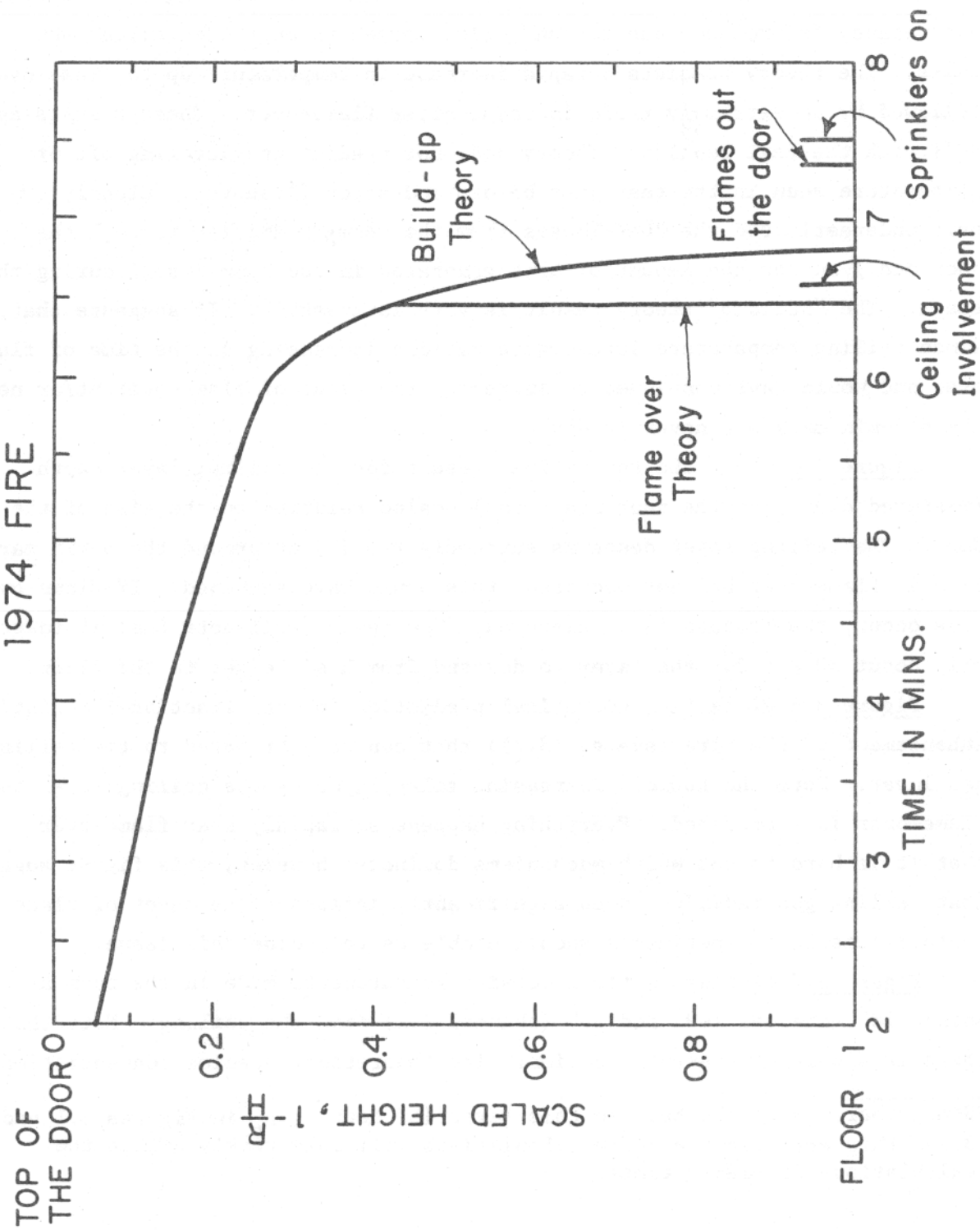

FIGURE 3.5 SCALED GAS LAYER HEIGHT VERSUS TIME AFTER IGNITION

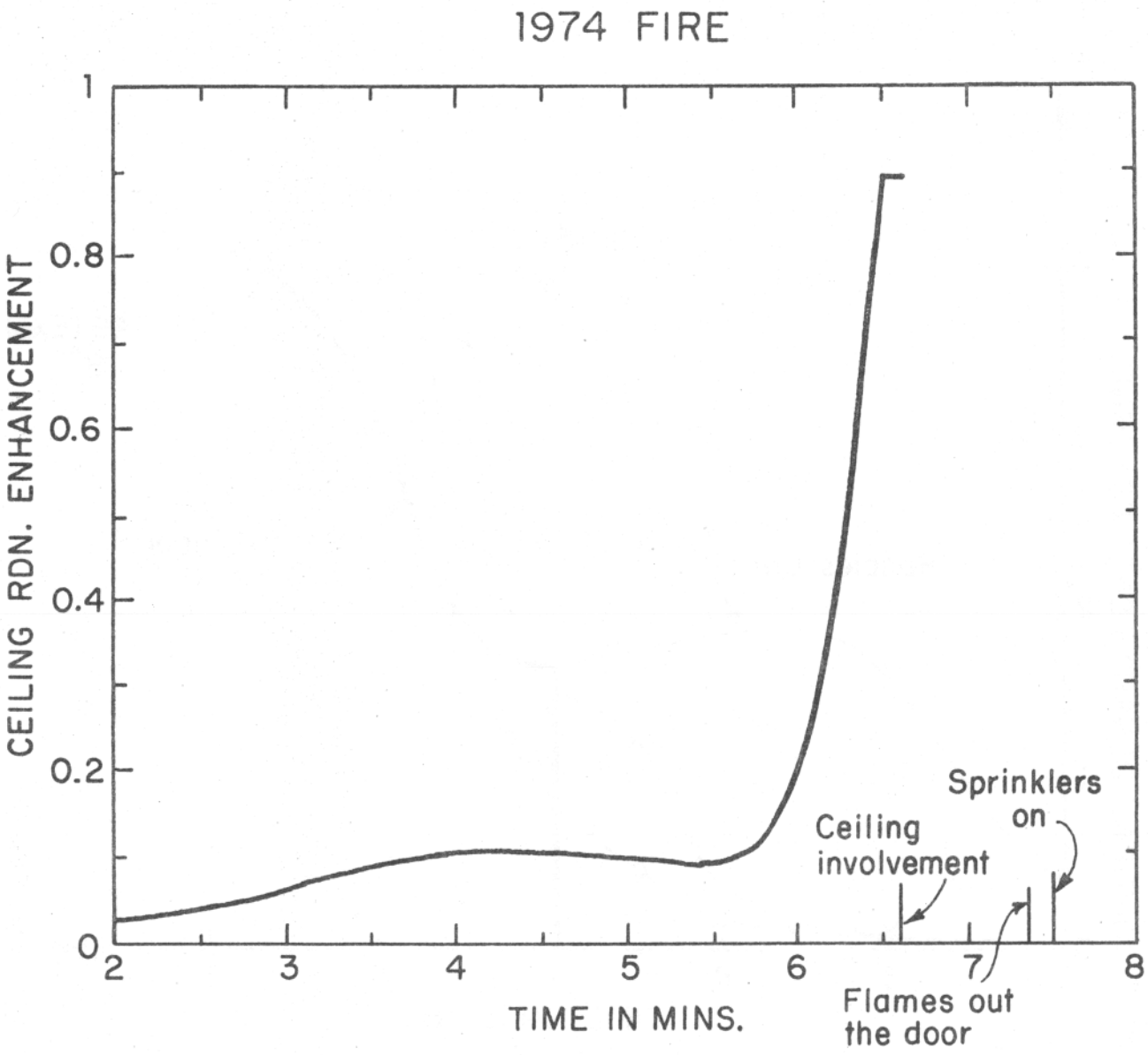

FIGURE 3.6 CEILING RADIATION ENHANCEMENT VERSUS TIME AFTER IGNITION

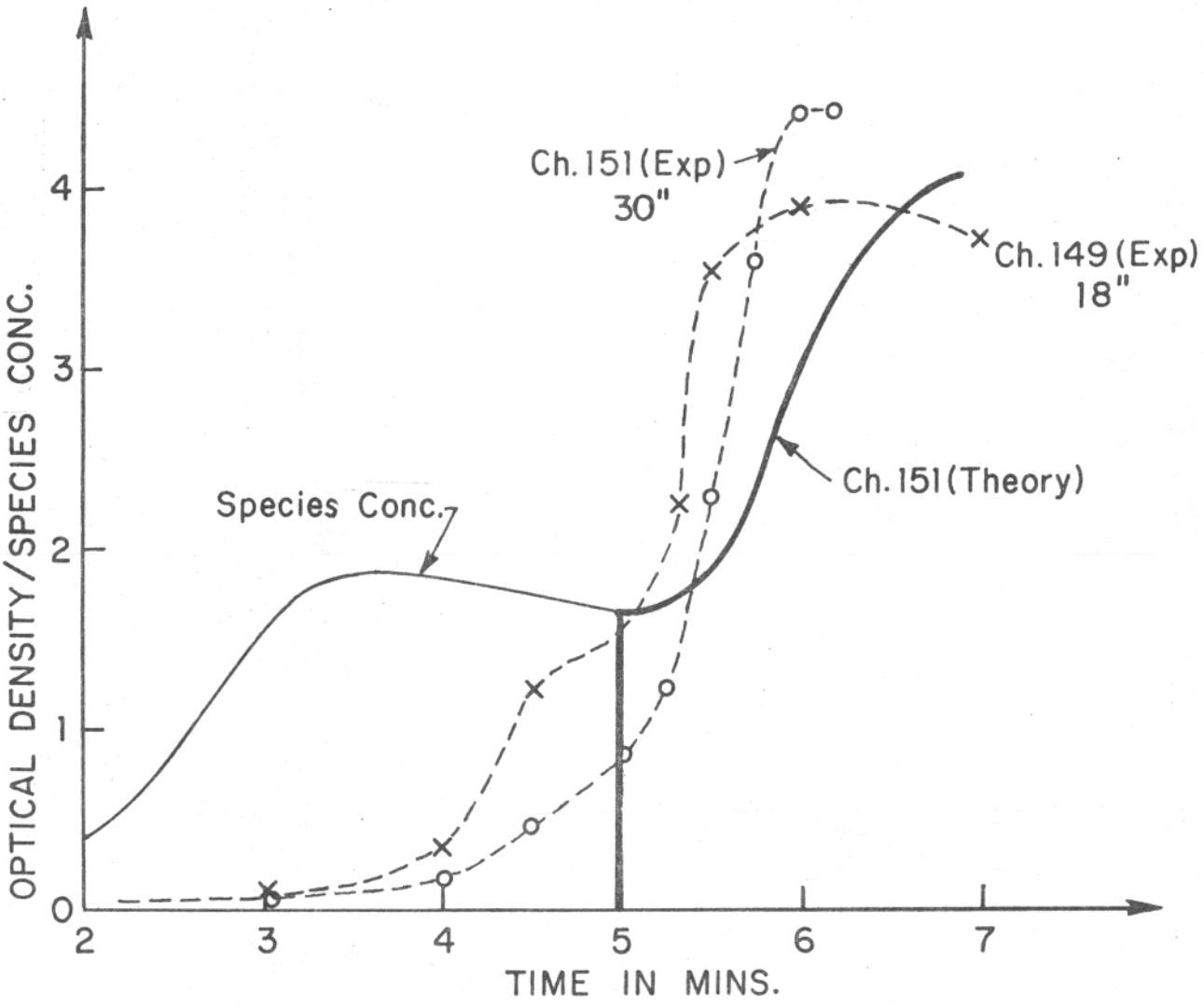

FIGURE 3.7 SPECIES CONCENTRATION AND OPTICAL DENSITY VERSUS TIME AFTER IGNITION

curve is drawn (scaled in the manner shown), and also the theoretical prediction for optical density measurements at the channel 151 probe is shown.* Our theoretical model predicts no obscuration until the hot gas layer descends to the probe, and then there is an instantaneous jump, as shown, followed by a leveling off and further rapid increase at the 5.5-min (rapid burning rate increase) mark. Qualitatively the behavior is right, but quantitatively we seem to have underestimated the rapid production rate increase at the 5.5-min mark. Also, smoke is clearly much more uniformly spread throughout the room in the early fire stages than anticipated.

Figure 3.8 shows the theoretical and observational estimates of flame height. Clearly the theory is not good enough.

3.5.3 Comparison Between the 1974 and 1973 Tests

Unfortunately, there were no direct, bed weight-loss measurements made during the 1973 test, so the type of comparisons we would like to make cannot be made. Indirect estimates of the burning rate were made by several different methods[10] and these results will be used as basic input to our model. Since different estimates gave significantly different results, it is appropriate to think of work to follow as being a numerical experiment related to the 1973 fire, rather than as being an actual numerical simulation. The major computational results for both tests are shown in Figure 3.9.

The burning rate curves (based on experimental data) used as computational

*The optical-density versus mass-concentration relation, $M = 50D$ (where M is the mass concentration in milligrams/ft^3 and D is the optical density/ft), that is sometimes used to relate these two quantities[28] did not work here, so I have just scaled the species concentration curve (as shown) so that comparisons can be readily made with the experimental optical density curves.

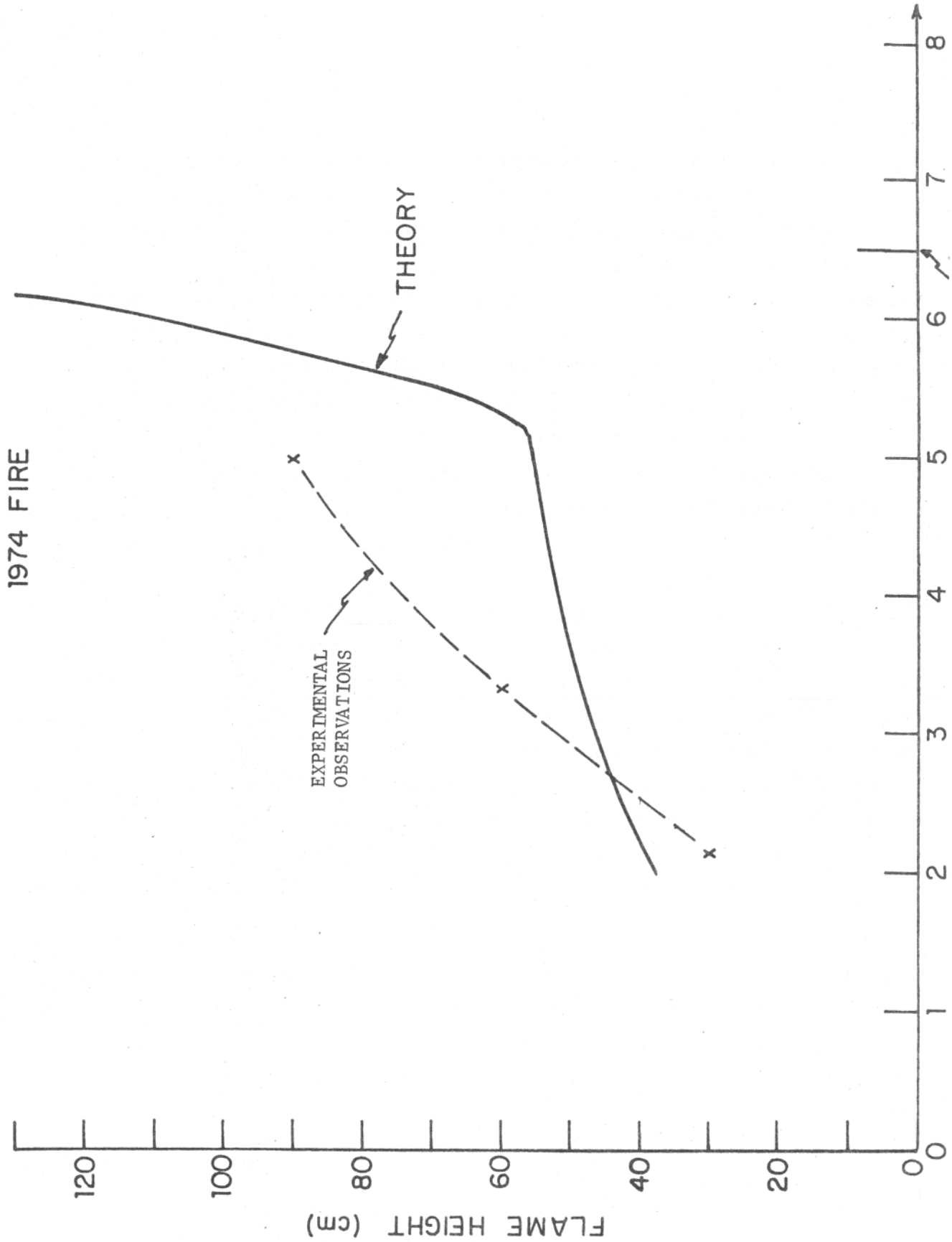

FIGURE 3.8 FLAME HEIGHT VERSUS TIME AFTER IGNITION

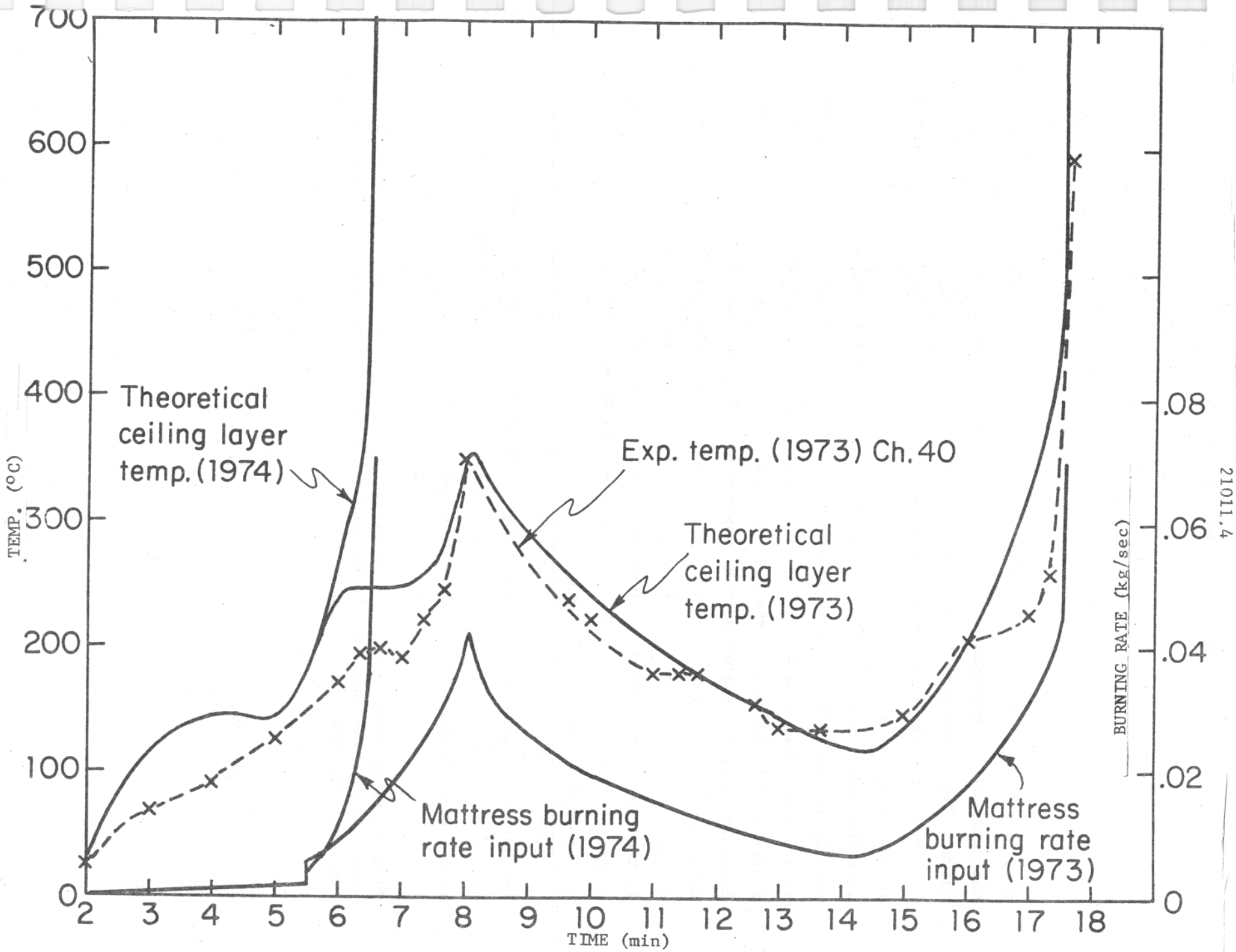

FIGURE 3.9 COMPARISON OF 1973 AND 1974 BEDROOM TESTS SHOWING BURNING RATES AND CEILING LAYER TEMPERATURES

input are shown.* Note the scale on the right hand side of the figure. The theoretically-determined, ceiling gas layer temperatures for the tests are shown. The temperature history as recorded in the 1973 test is also shown.

Note that there was a much more rapid increase in burning rate "recorded" in the 1974 test than in the 1973 test after 5.5 min, (i.e., during Stage 2) with the result that the ceiling gas-layer temperature increased much more rapidly in the 1974 test with flame-over conditions (T = 450°C) being reached by 6.6 min. The closest the 1973 fire approached to flame-over in the early stages of the test was at the 8.11-min mark. At that stage, the ceiling gas-layer temperature reached a local maximum of 350°C, so that flame-over conditions were not nearly reached. After the 8.11-min mark, the burning rate dropped off considerably so there was no chance of flame-over until the further rapid increase in burning rate later on in the test. The theoretically-predicted flame-over time for this test was 17.56 min, very close to the observed flame-over time (17.58 min).

The obvious question that arises out of the above is: what caused the bed burning rate to increase much more rapidly in the 1974 test than in the 1973 test? Possibly, the most likely guess is that local radiative enhancement from the headboard provided much more assistance to the 1974 fire at the

---

*Least-square exponential fits to experimental data were used for the 1973 case, with three such fits being required to cover the various burning rate stages. The best-fit curves were:

$$\frac{dm}{dt} = 2\,\pi r d \rho_m \frac{dr}{dt} \qquad \text{for } 0 < t < 330 \text{ sec}$$

$$\frac{dm}{dt} = .00011228 \exp (.0122378\ t) \qquad \text{for } 330 < t < 487 \text{ sec}$$

$$\frac{dm}{dt} = .27372 \exp (-.0043043\ t) \qquad \text{for } 487 < t < 855 \text{ sec}$$

$$\frac{dm}{dt} = .15335\ 10^{-5} \exp (.00973255\ t) \qquad \text{for } t > 855 \text{ sec}$$

critical (5.5 min) stage. (The fire appeared to move toward the headboard in the 1974 fire and away from it in the 1973 fire). A careful examination of the video tapes,together with local radiation estimates based on these tapes, could perhaps settle this question.

3.6 CONCLUSIONS

The model works extremely well, predicting the onset of flame-over for both tests (given the burning rate input) to within 6 sec. Further tests of the model are necessary before we can conclude that we "understand" the nonlocal aspects of the room fire, and that we "know" the flame-over mechanism, but the results so far are very encouraging.

It may seem extremely surprising (given the crudeness of the component models) that we can predict so accurately the flame-over event. This is something of an illusion, for the following reason: although one second is a short time for us, for the fire it is an extremely long time near flame-over. Events happen extremely rapidly as flame-over is approached, so that even if we "miss" flame-over badly in "fire time" terms, we will not be far out in human terms.

REFERENCES

1. Croce, P.A. and Emmons, H.W., "The Large-Scale Bedroom Fire Test, July 11, 1973," FMRC Technical Report RC74-T-31, Serial No. 21011.4, July 1974; and Volume I, this report.
2. Labes, W.G., "The Ellis Parking and Gary Dwelling Burns," Fire Technology 2 (4), August 1966.
3. Christian, W.J. and Waterman, T.E., "Characteristics of Full-Scale Fires in Various Occupancies," Fire Technology, 17, August 1971.
4. Harmathy, T., "A New Look at Compartment Fires," Part II, Fire Technology, 8, 1972.
5. Kawagoe, K. & Sekine, T., "Estimation of Fire Temp. Time Curves in Booms," BRI Occasional Report No. 11, Building Research Institute, Ministry of Construction, Tokyo, 1967.
6. Block, J.A., "A Theoretical and Experimental Study of Nonpropagating Free-Burning Fires," 13th Symposium on Combustion, p. 971, The Combustion Institute, 1971.
7. Heskestad, G., "Modeling of Enclosure Fires," 14th Symposium on Combustion, The Combustion Institute, 1973.
8. Croce, P.A., "Modeling of Vented Enclosure Fires," paper presented at the Fall Technical Meeting of the Eastern Section of the Combustion Institute, November 1974.
9. Emmons, H.W., "Natural Convective Flow Through an Opening," Home Fire Project Report, No. 1, November 1974.
10. Emmons, H.W., "Flow Through the Doorway," Appendix F in "The Large-Scale Bedroom Fire Test, July 11, 1973," FMRC Technical Report RC74-T-31, Serial No. 21011.4, July 1974.
11. Prahl, J. and Emmons, H.W., "Fire Induced Flow Through an Opening," Combustion & Flame, 1975 (in press).
12. Pagni, P.J., "Preliminary Summary of Some Mattress Burning Experiments," Appendix to this Section.

13. Thomas, P.H., "The Size of Flames from Natural Fires," Proceedings, 9th Symposium on Combustion, p. 844-859, 1953.
14. Kosdon, F.J., Williams, F.A. and Buman, C., "Combustion of Vertical Cellulosic Cylinders in Air," Proceedings, 12th Symposium on Combustion, p. 253-264, 1969.
15. Emmons, H.W., "A Study of Flame Heights," Appendix I in "The Large-Scale Bedroom Fire Test, July 11, 1973," FMRC Technical Report RC74-T-31, Serial No. 21011.4, July 1974.
16. Alpert, R.L., "The Role of Ceiling Thermal Radiation in Flashover Mechanism," Appendix E in "The Large-Scale Bedroom Fire Test, July 11, 1973," FMRC Technical Report RC74-T-31, Serial No. 21011.4, July 1974.
17. Knight, C., Technical Report - Home Fire Project (to be published).
18. Smith, R.K., Leslie, L.M. and Morton, B.R., "The Role of Dynamic Pressure on Generating Fire Wind," Geophysical Fluid Dynamics Laboratory, Report No. 54, Monash University.
19. Morton, B.R., "On Modeling Plume Fires," Proceedings, 10th Symposium on Combustion, p. 973-983, August 1964.
20. Morton, B.R., Taylor, G.J. and Turner, J.S., Proc. Roy. Soc. (London), A234, 1956.
21. Turner, J.A., Annual Rev. of Fluid Mechanics, Vol. 1, 1969.
22. Markstein, G., "Full-Scale Test Data Obtained with the Scanning Radiometer," Section VIII in this Volume.
23. Carslaw, H.S. and Jaeger, J.C., Conduction of Heat in Solids, Clarendon Press, p. 247, 1947.
24. Fowkes, N.D., "Natural Convective Flow Caused by a Fire," Technical Report for Home Fire Project, 1974.
25. Standard Methods of Fire Tests of Building Construction and Materials, NFPA No. 251, ASTM Eng. 1958.
26. Standard Method of Test for Surface Burning Characteristics of Building Materials, ASTM, Annual Book of ASTM Standards, Par. 14, 1968.

These experiments were performed on the weight-loss apparatus described by Tamanini.[4] The mass burning rate, some of the temperature field in and above the urethane, the flame spread rate and the flame geometry were measured as functions of time. Two types of covered urethane samples were burned: one with the original cover and a cotton-polyester blend sheet,[1] the other similarly covered but with a 10-cm diameter hole in the coverings around the ignition point. The latter configuration was designed to simulate both full-scale bedroom tests.[1,5]

The flame spread results for this hole-in-the-cover sample showed three distinct regimes: 1) in the first 40 sec, the flame went through an initial transient and then spread rapidly over the surface until it reached the edge of the 10-cm hole; 2) in the next 80 sec, the flame propagated with a downward velocity on the order of 0.1 cm/sec, with little radial movement until it reached the thin aluminum pan beneath the urethane; and 3) in the remaining minutes of the test the flame moved radially (horizontally) and uniformly through the mattress at a slowly increasing rate, of the order 0.1 cm/sec. During the last time period, the burnt region had a cylindrical geometry with its interior uniformly filled with a turbulent luminous flame. A regular fluctuation was observed in the flame attached to the coverings at the upper periphery of the cylinder.

The sample with an uncut cover and sheet was ignited in a similar fashion. It eventually reached a state of slowly increasing radial (horizontal) spread with a flame and burnt-region geometry identical to that described above in the third time period. However, the time to develop this quasi-steady cylindrical geometry was increased by approximately 4 min as the covering fabric burned, charred, and tore.

IV

FLOW THROUGH THE DOORWAY

D. Kligler and H.W. Emmons
Harvard University

The rate of burning in an enclosure can be approximated from the temperature distribution of the gases flowing through the opening - in our case - the doorway. Buoyancy-driven flow is calculated from a hydraulic point of view[1], using a measured flow coefficient to correct for the effect of the vena contracta, friction, and other approximations. The fuel-air ratio, calculated from doorway temperature and the properties of the fuel, is then used to find the rate of burning as a function of air flow.

It should be noted that the temperatures used in calculations are, in general, higher than the actual gas temperatures, due to the effects of radiation. Figure 4.1 shows the difference between the temperatures of unaspirated and aspirated thermocouples, placed in pairs throughout the room. Large differences between the corrected (aspirated) and uncorrected temperatures occur only late in the burn, when temperatures are high; and thus, the error of even 100°C causes only small errors in the calculations of flow and burning rate.

Figure 4.2 shows the model and defines the notation[2]. The fire gas density ρ appears in the formulae in the ratio to the density of the incoming air, ρ_a, $r = \frac{\rho}{\rho_a} = \frac{T_a}{T}$. Plots of doorway temperature (cf. Figure 4.3) suggest two approximations:

1) a linear temperature gradient $r = \frac{1}{1 + \alpha\zeta}$, $\zeta = \frac{y}{H}$ and

2) a two-fluid model, with temperature, and thus r, assumed constant throughout the buoyant layer. To use this two-fluid model, we select a temperature

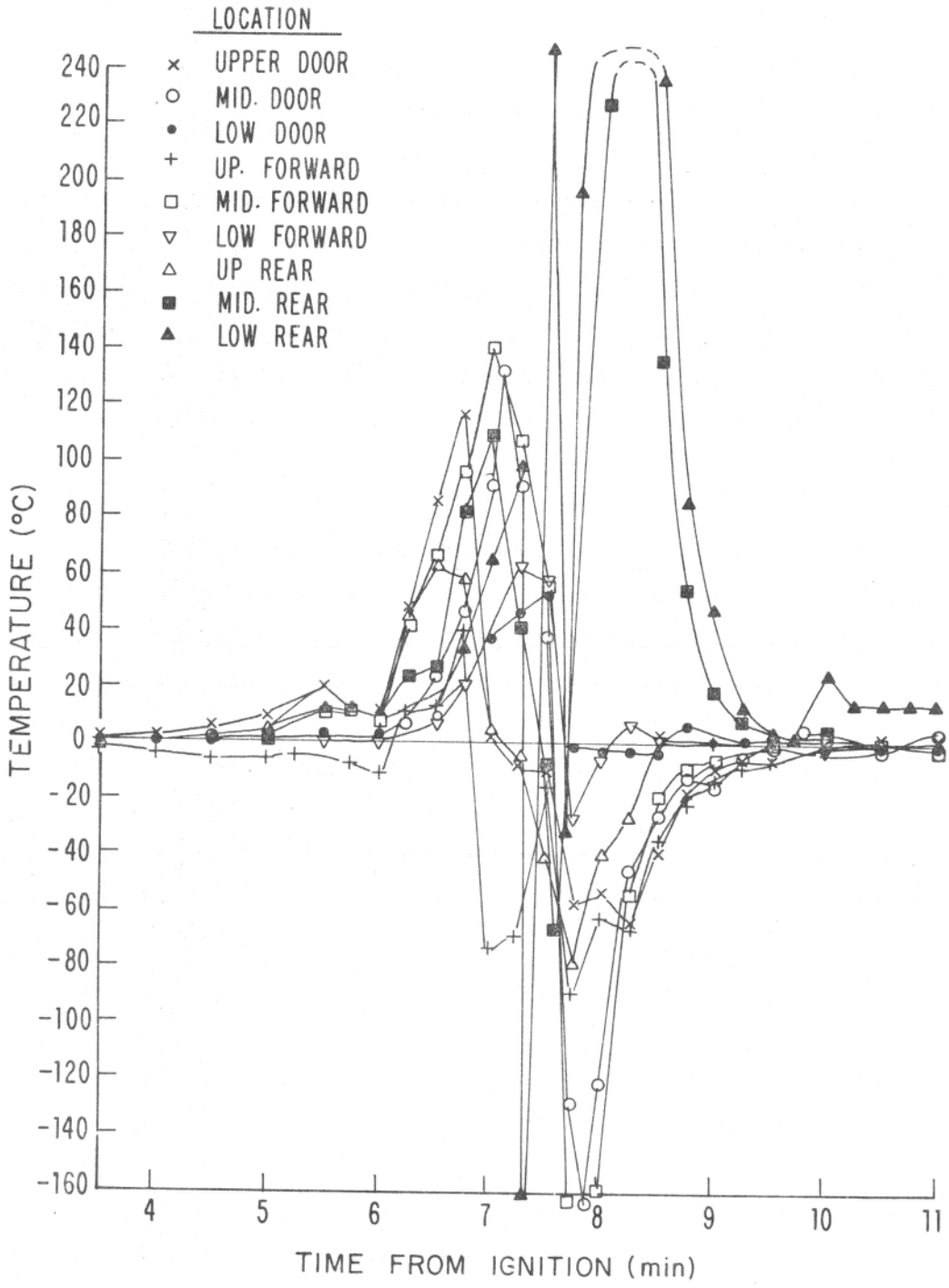

FIGURE 4.1 TEMPERATURE DIFFERENCE (T bead - T asp) VERSUS TIME FROM IGNITION FOR NINE PAIRS OF ASPIRATED AND BARE BEAD THERMOCOUPLES IN BEDROOM TEST

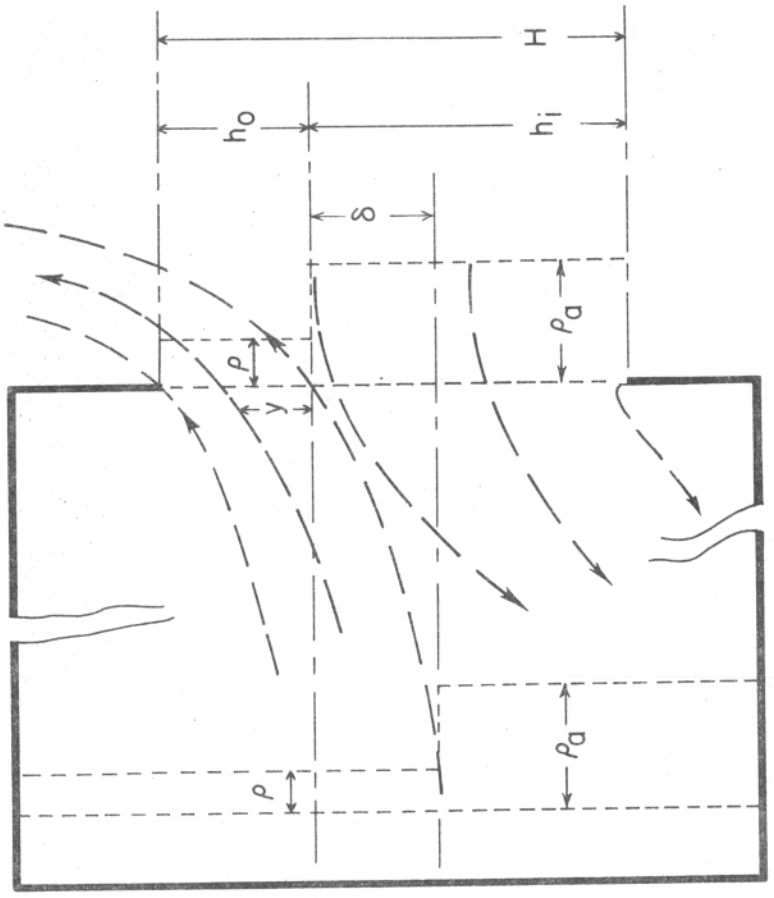

FIGURE 4.2 THE BUOYANT FLOW OF GASES THROUGH THE DOORWAY

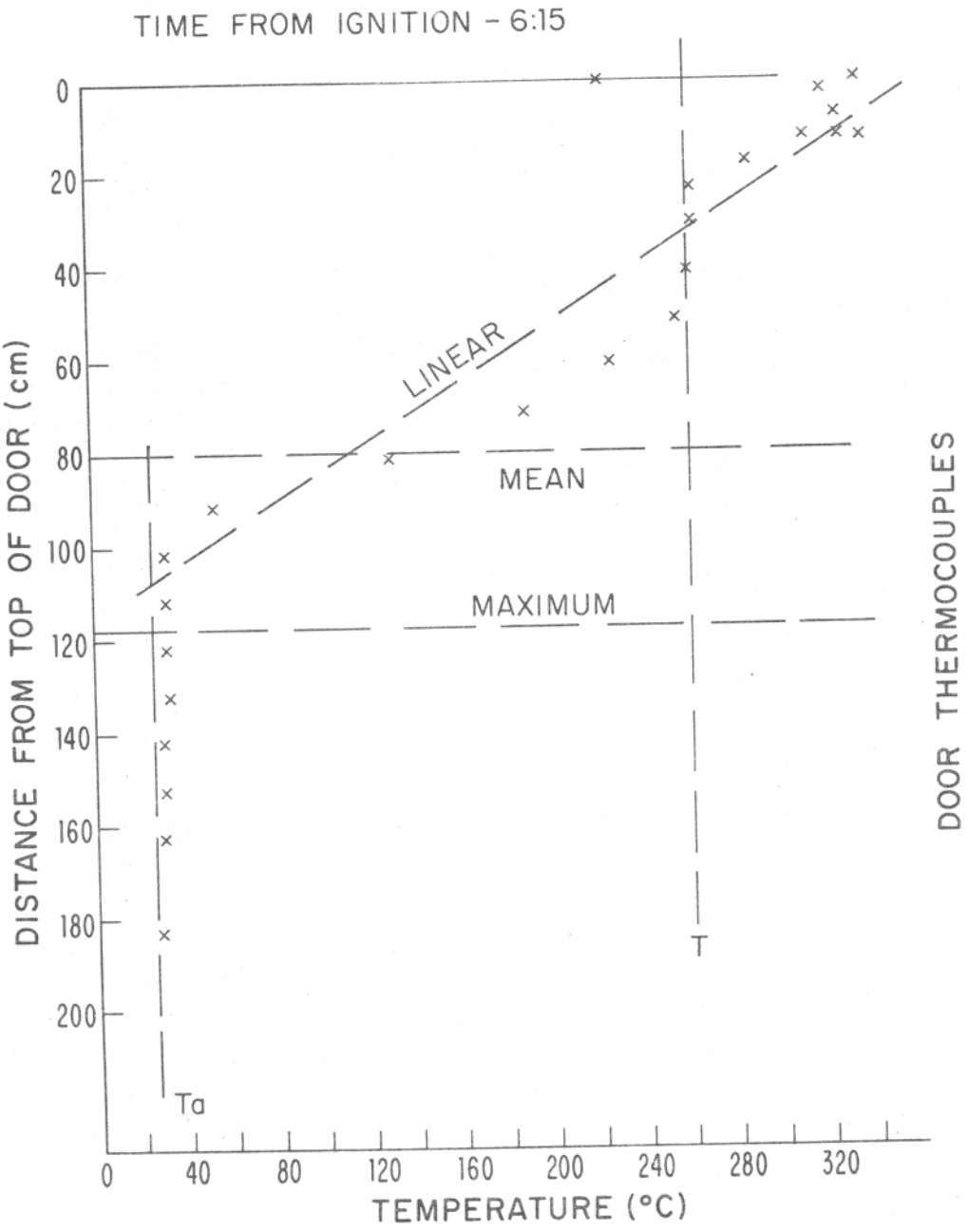

FIGURE 4.3 TEMPERATURE DISTRIBUTION IN DOORWAY AT 6:15 AFTER IGNITION

near the maximum and a buoyant layer depth either a) at a mean position or b) at the lower position which defines the maximum flow for the given r. The formulae for doorway velocity are:[1]

1) linear temperature gradient

$$\frac{v_o}{\sqrt{2gH}} = \left(\frac{1 + \alpha\zeta}{\alpha} \left(\alpha\zeta - \ln \left(1 + \frac{\alpha\zeta}{1 + \alpha \frac{\delta}{H}} \right) \right) \right)^{1/2} \tag{4.1}$$

$$\frac{v_i}{\sqrt{2gH}} = \frac{1}{\alpha^{1/2}} \begin{cases} \left(\alpha\zeta + \ln \left(1 - \dfrac{\alpha\zeta}{1 + \alpha \frac{\delta}{H}} \right) \right)^{1/2} & \zeta \leq \dfrac{\delta}{H} \\ \left(\dfrac{\alpha\zeta}{H} - \ln \left(1 + \alpha \dfrac{\delta}{H} \right) \right)^{1/2} & \zeta \geq \dfrac{\delta}{H} \end{cases} \tag{4.2}$$

2) two-fluid model

$$\frac{v_o}{\sqrt{2gH}} = \left(\left(\frac{1}{r} - 1 \right) \zeta \right)^{1/2} \tag{4.3}$$

$$\frac{v_i}{\sqrt{2gH}} = \begin{cases} \left((1 - r)\, \zeta \right)^{1/2} & 0 \leq \zeta \leq \dfrac{\delta}{H} \\ \left((1 - r) \dfrac{\delta}{H} \right)^{1/2} & \dfrac{\delta}{H} \leq \zeta \leq \dfrac{h_i}{H} \end{cases} \tag{4.4}$$

While agreement of calculated and experimental results for doorway velocity was not usually as good as that shown in Figure 4.4, in general the two-fluid model with mean flow depth gave the best results. For this reason, and because it is much simpler to calculate than the linear model, this method of approximation was chosen for use in all later calculations.

Next, the flow through the doorway throughout the test was calculated for this model using the following formula obtained by integrating eq 4.3:

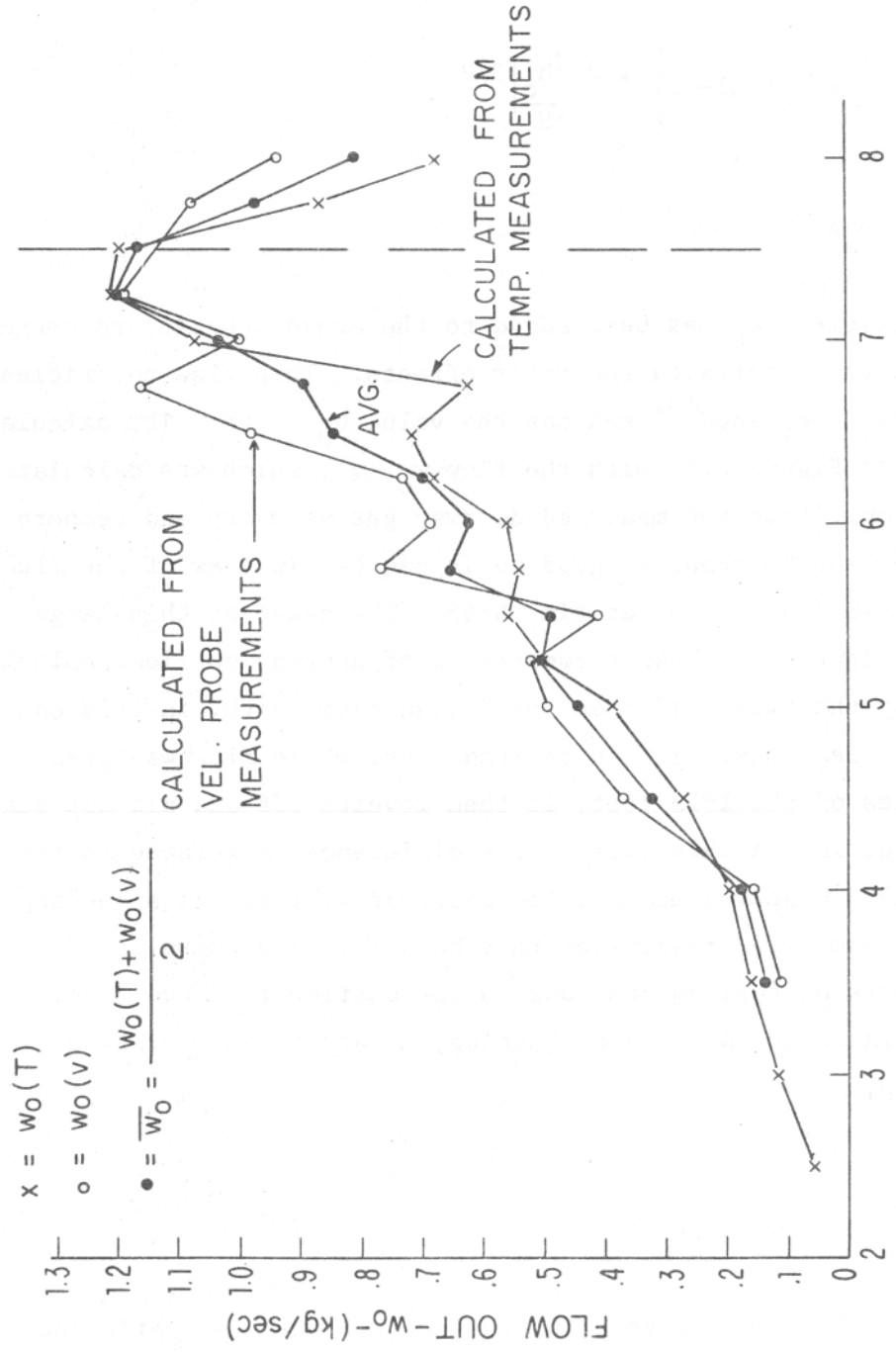

FIGURE 4.5 MASS FLOW OUT THE DOORWAY VERSUS TIME FROM IGNITION

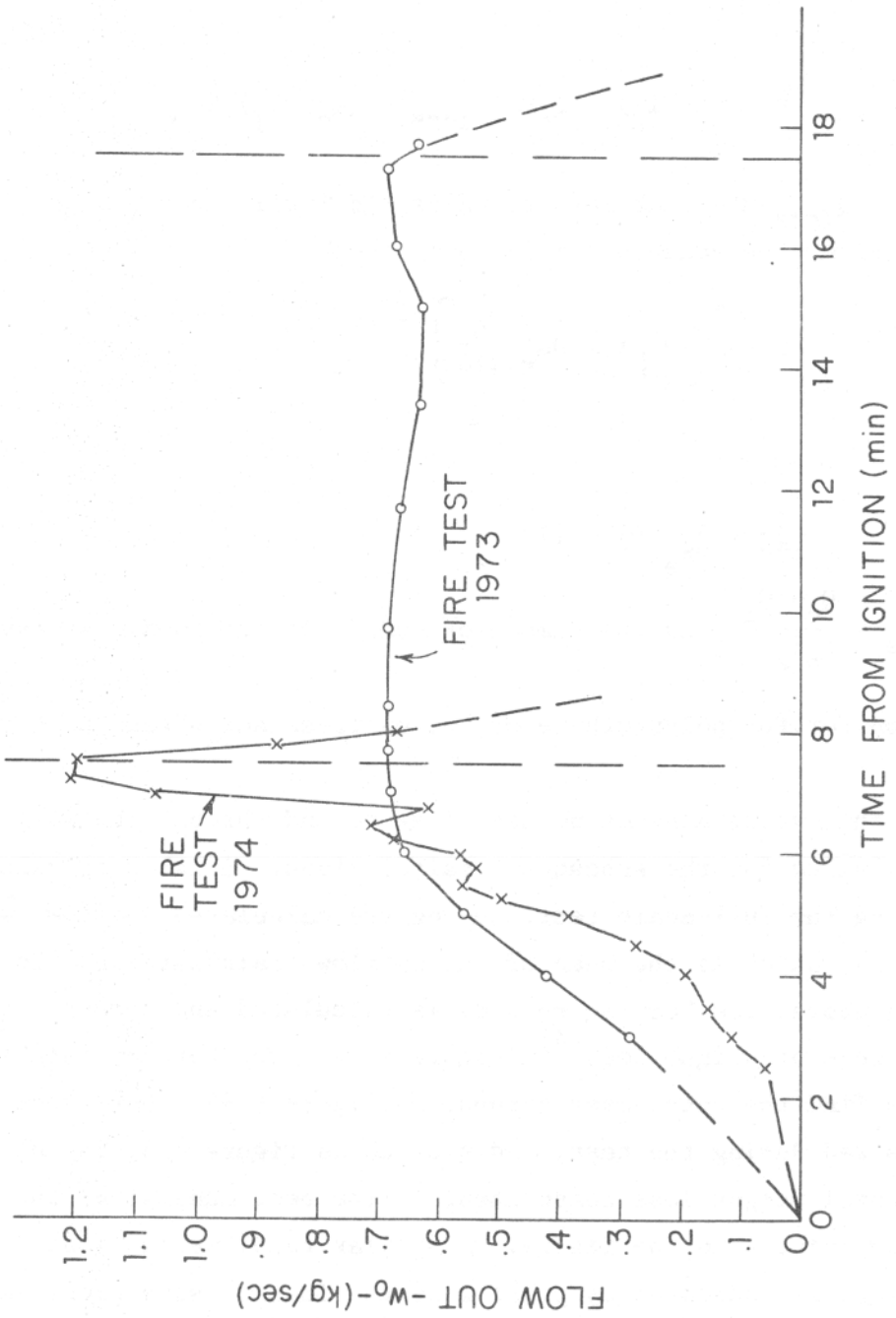

FIGURE 4.6 MASS FLOW OUT THE DOORWAY VERSUS TIME FROM IGNITION: COMPARISON OF 1973 AND 1974 TESTS

$$w_o c_p (T - T_a) = Q_c \dot{M} - Q_{loss} = (Q_c - Q_l) \dot{M} \quad , \tag{4.8}$$

where $Q_l = Q_{loss}/\dot{M}$ = heat loss to walls and furnishings per unit mass of fuel burned. From this equation, r is found to be:

$$r = \frac{T_a}{T} = \left(1 + Da_e \frac{\Delta}{1+\Delta}\right)^{-1} \tag{4.9}$$

Thus,

$$\frac{\Delta}{1+\Delta} = \frac{1}{Da_e} \left(\frac{1}{r} - 1\right) \tag{4.10}$$

where $Da_e = \dfrac{Q_c - Q_l}{c_p T_a}$, is the Damköhler number of the room. We assume complete combustion for the polyurethane of the mattress and obtain $Da = \dfrac{Q_c}{c_p T_a} = 49.$ (4.11)

Although this value assumes no heat loss to and through the walls, we nonetheless used this value for the subsequent calculations. Δ takes on values up to about 0.07 during the full-scale test. Using the calculated outflow, $\overline{w_o}$ (shown in Figure 4.5), which is the mean of the outflows calculated by the two methods described above, the burning rate $\dot{M}$, is calculated and compared to the bed's measured rate of weight loss[4] (Figure 4.7). The burning rate is then integrated to find the total mass burned, M (Figure 4.8). Note that the weight loss measured during the test, and plotted in Figure 4.8, is only that of the bed. A total weight loss measurement of the bed, made after the test, is indicated by point A in the figure. A similar total weight loss measurement of <u>all</u> contents is indicated by point B in the insert (same plot, expanded ordinate) to Figure 4.8. The dashed line to point A represents the estimated weight of the bed after the sprinkler was activated (t=40 sec), while the dashed line to point B shows the hypothetical weight loss of <u>all</u> room contents.

These calculations show good agreement with experimental results. The fact that the calculated burning rate is about 75 percent of that measured,

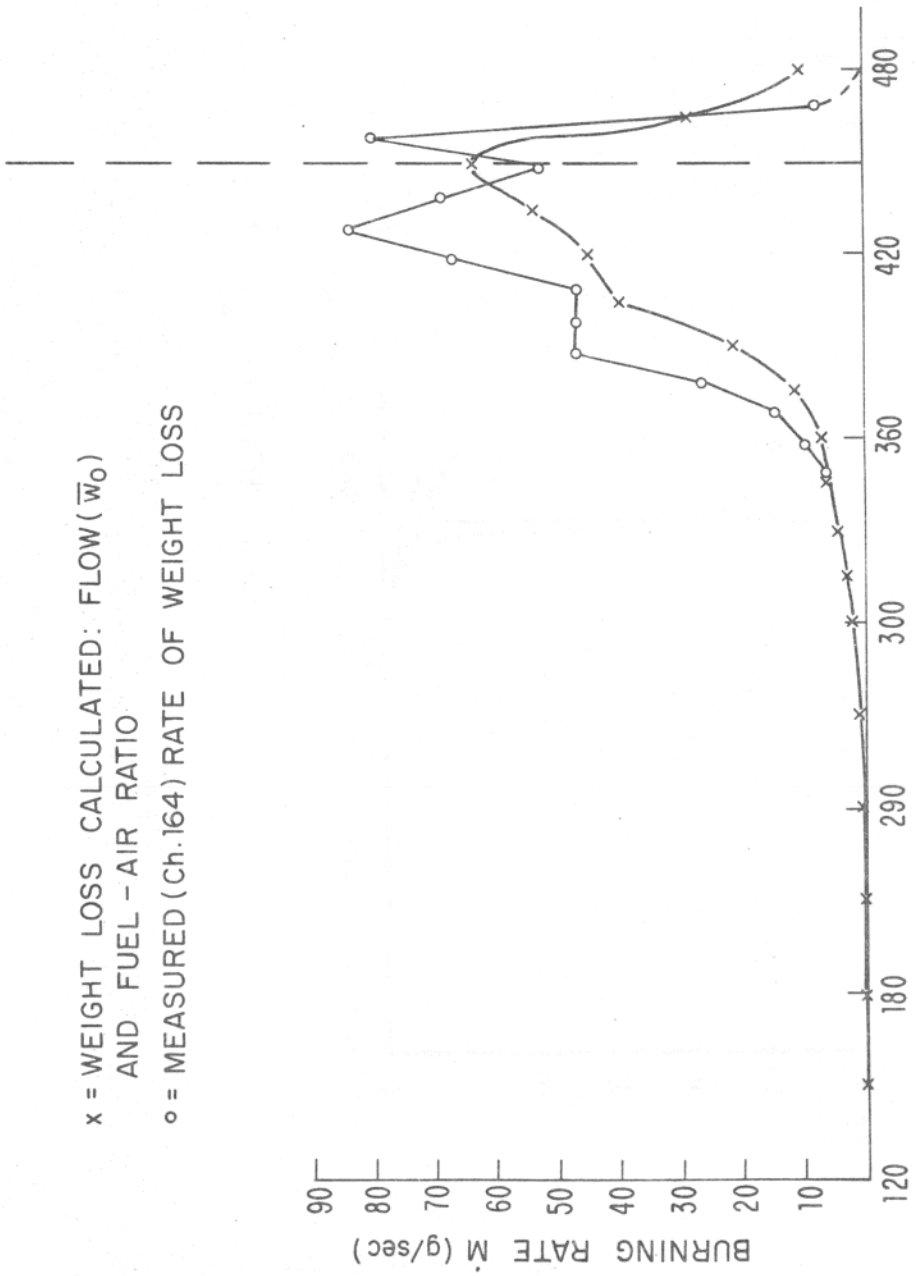

FIGURE 4.7 BURNING RATE VERSUS TIME FROM IGNITION

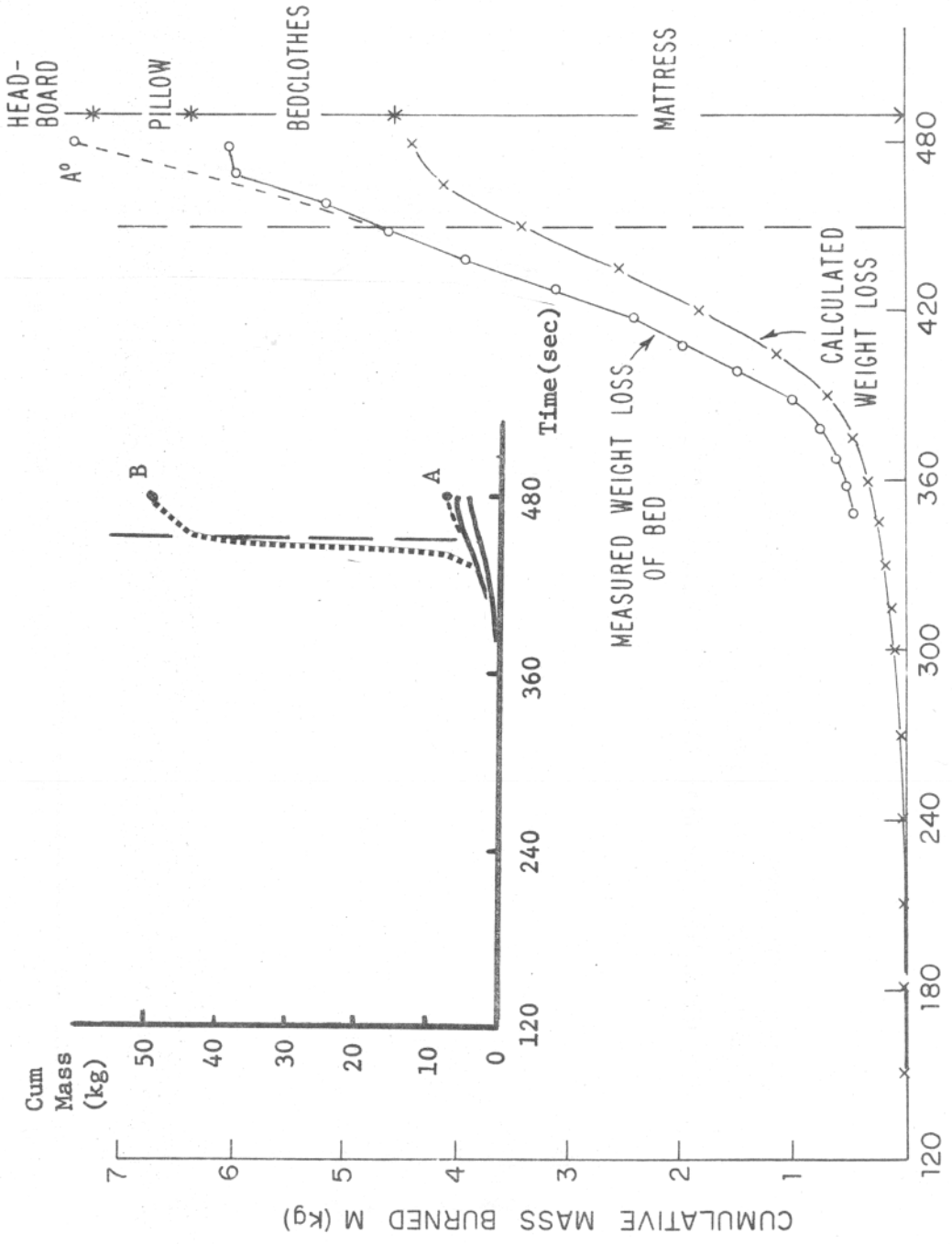

FIGURE 4.8 CUMULATIVE MASS BURNED VERSUS TIME FROM IGNITION

indicates that the fuel-air ratio used was too low. This is confirmed by a comparison of the value calculated by eq (4.10) with one calculated from experimental burning rate and outflow (calculated from eq (4.7), shown in Figure 4.9). The primary reason for this inaccuracy is our choice of a constant Da = 49 without regard to wall and other heat losses. In actuality, the Damköhler number used to determine Δ must take into account the properties of the enclosure, as well as the fuel, and the fraction of the fuel actually burned (rather than pyrolyzed and lost as smoke). Thus $Da_e < 49$, and Δ will take on larger values. In addition, late in the burn, other items in the room are involved, besides the mattress, and the fuel qualities of these items must be taken into account as well. A plot of Da_e (Figure 4.10), as calculated from eq (4.7) and (4.10), using experimental data, shows that its actual value is between about 25 and 30.

LIST OF SYMBOLS

A	Area of doorway
C_D	Flow coefficient
Da	Damköhler number for fuel
Da_e	Damköhler number of enclosure
H	Height of door
M	Mass loss
Q_c	Heat of combustion per unit mass of fuel burned
Q_l	Heat loss per unit mass of fuel burned
Q_{loss}	Heat loss to enclosure
T	Temperature
T_a	Ambient temperature
c_p	Heat capacity of air
g	Gravitational acceleration
h_i	Height of inflow layer
h_o	Height of outflow layer
r	Hot-to-cold air density ratio

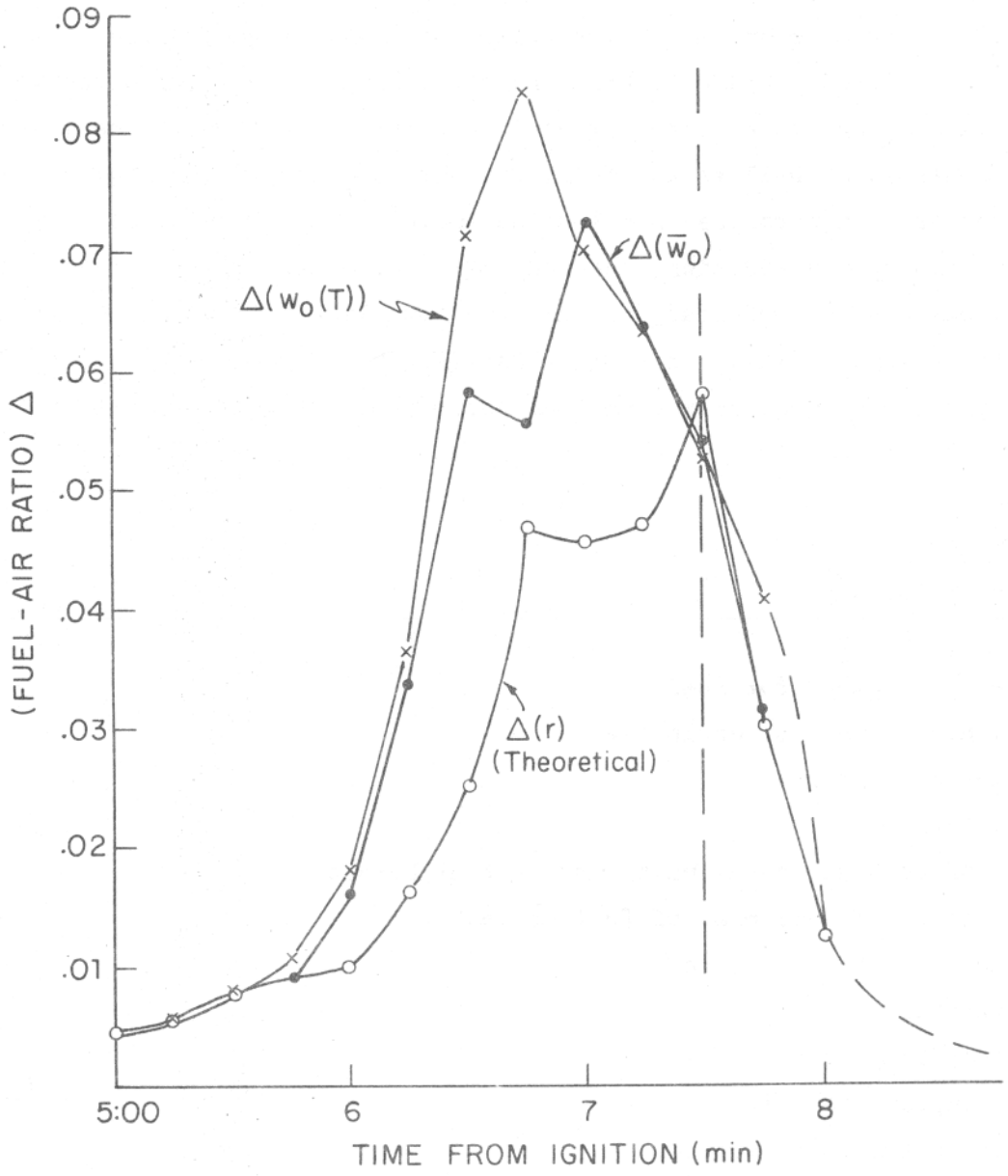

FIGURE 4.9 FUEL-AIR RATIO VERSUS TIME FROM IGNITION

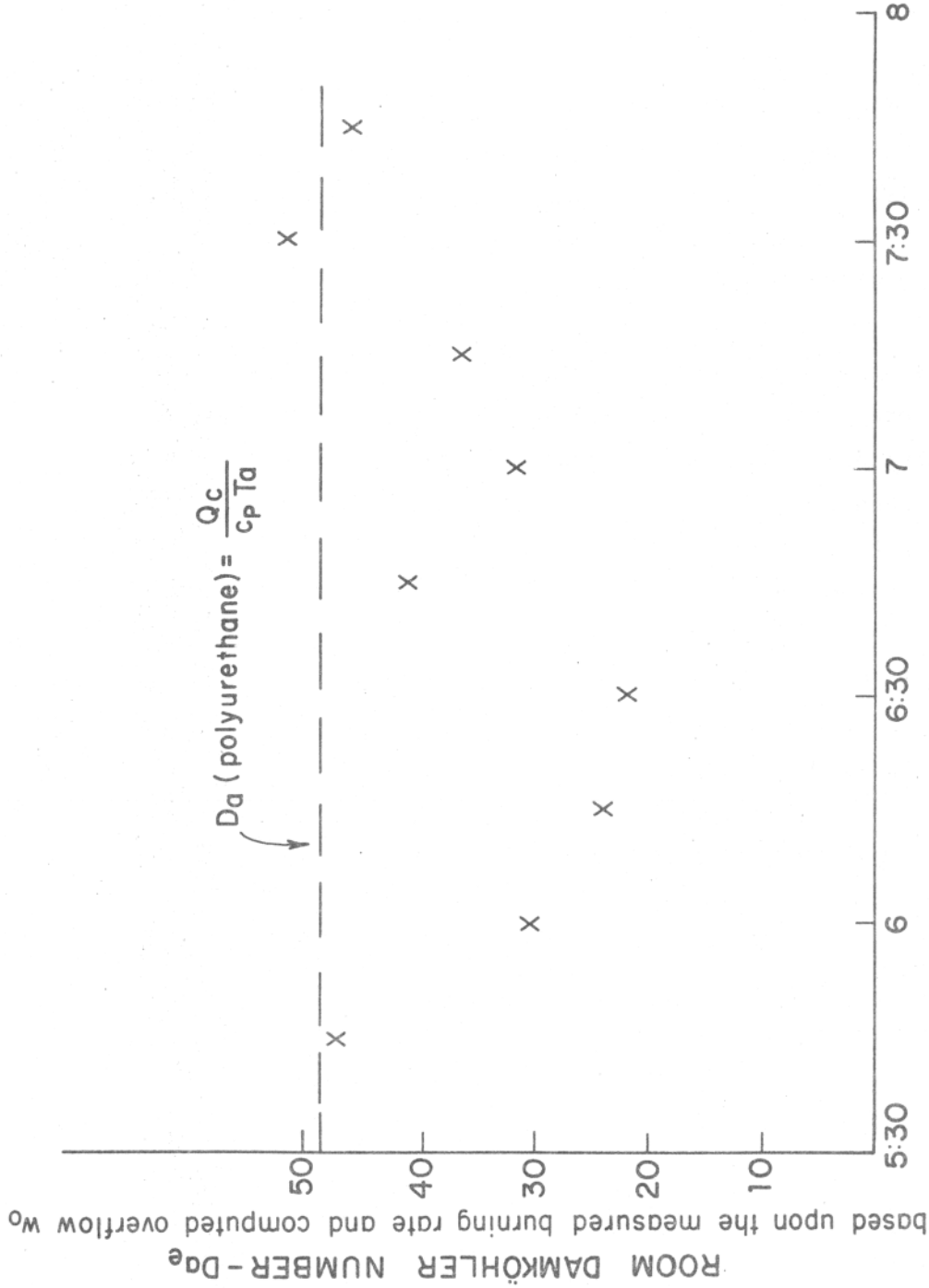

FIGURE 4.10 ROOM DAMKÖHLER NUMBER VERSUS TIME FROM IGNITION

LIST OF SYMBOLS (Cont'd)

v_i Gas velocity - in

v_o Gas velocity - out

w_i Gas flow - in

w_o Gas flow - out

y Distance from neutral axis

Δ Fuel-air ratio

α Constant temperature gradient

δ Difference of hot gas level in opening and in enclosure

ζ Fractional distance from neutral axis

ρ Gas density

ρ_a Ambient gas density

ϕ Flow parameter

REFERENCES

1. Emmons, H.W., "Natural Convective Flow Through An Opening," Home Fire Project Technical Report No. 1, 1973

2. Emmons, H.W., "Flow Through The Doorway," in "The Large-Scale Bedroom Fire Test, July 11, 1973," FMRC Technical Report No. RC74-T-31, Serial No. 21011.4, July 1974.

3. Prahl, J. and Emmons, H.W., "Fire Induced Flow Through An Opening," paper in preparation

4. Volume I, this Report

V

THE EXISTENCE OF A NEUTRAL PLANE: EXPERIMENTAL CHECK OF HYDRAULIC FLOW MODEL

J. Prahl and D. Kligler
Harvard University

The hydraulic model used to approximate flow through the doorway in fire tests (see Section IV) requires that pressure inside the room at the level of the zero-velocity point in the doorway be equal to that of the surrounding atmosphere at the same height.(1) This assmmption was tested by calculations from delicate pressure measurements taken during the July 1974 full scale bedroom fire test.(2)

Inside-outside differential pressure, $\Delta p = p_a - p_{in}$, was measured at floor level at the center-rear of the room (channel 166). The pressure above this level is then given by

$$\frac{dp}{dz} = -\rho g = -g\rho_a \left(\frac{p}{p_a}\right)\left(\frac{T_a}{T}\right) ,$$

$$p(z) = p_o \exp\left(-\frac{g\rho_a T_a}{p_a}\int_0^z \frac{dz'}{T(z')}\right). \qquad (5.1)$$

Temperature in the rear of the room was measured by thermocouples No 87-100, so that the integral of eq (5.1) becomes a sum:

$$\int_0^z \frac{dz'}{T(z')} \cong \sum_{n=1}^{z} \frac{(z_n - z_{n-1})}{(T_n + T_{n-1})/2} \quad . \qquad (5.2)$$

In this formula, the temperature between vertical positions z_{n-1} and z_n is assumed to be the mean of the temperatures measured at the two levels. Finally,

since

$$p_{a>>} \frac{g\rho_a T_a H}{T} \quad ,$$

a first-order Taylor expansion of eq (5.1) is a good approximation:

$$p\ (z) \cong p_o \left(1 - \frac{gp_a T_a}{p_a} \sum_{n=1}^{z} \frac{2\left(z_n - z_{n-1}\right)}{T_n + T_{n-1}}\right) \quad . \tag{5.3}$$

Using this result, pressures inside and outside the room were calculated as functions of height at various times throughout the test. Figure 5.1 shows the typical result at 7:15 min after ignition: as expected, near the floor pressure is greater outside than inside, drawing cool air into the room; at higher levels, pressure is greater inside, forcing hot air and fire gases out. Note that h_i marks the zero-velocity level in the doorway, while $(h_i - \delta)$ marks the boundary between hot and cool gas layers inside the room.

Figure 5.2 shows h_i, $h_i - \delta$, and the level at which pressures are equal, inside and outside of the room. Throughout the test, the level where $p_{in} = p_{out}$, while usually within 15-20 percent of h_i, still is almost always below this theoretically predicted position. As the height of the zero-velocity level in the doorway is not measured exactly during the test, the h_i shown in the figure may be incorrectly determined. (h_i is found on the basis of doorway temperature data in Section IV). In addition, the differential pressure measurements used in calculations are between .002 and .02 mm Hg, so that their accuracy may be a problem. On the other hand, as the two-fluid hydraulic model is not a fully accurate approximation to the flow of fire gases, some modification of the theory may be needed to correct for the discrepancy noted here in the level of h_i. The accuracy required by fire calculation does not warrant any additional effort until other parts of the problem can be predicted with the same (low) accuracy which is not possible at present.

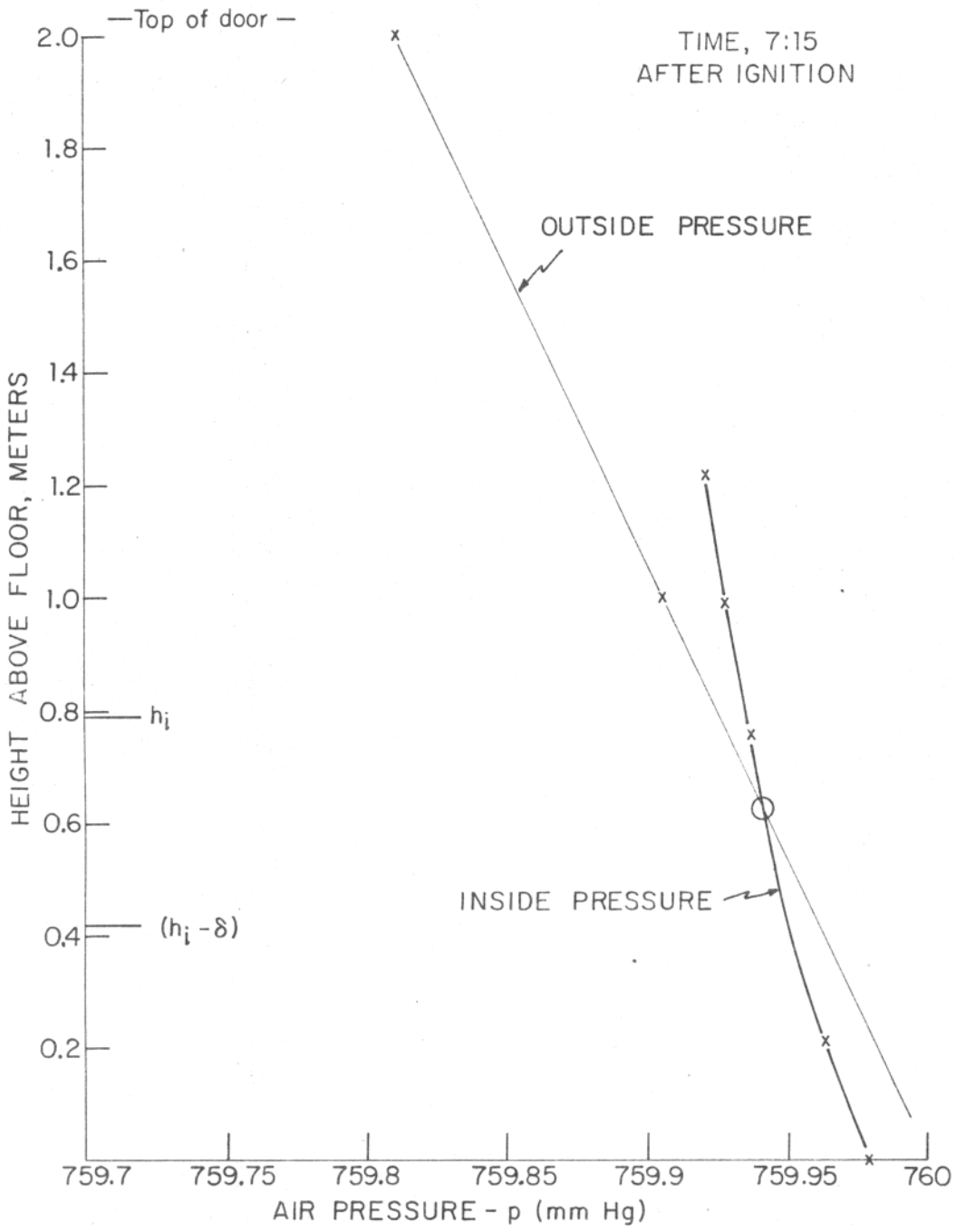

FIGURE 5.1 INSIDE AND OUTSIDE PRESSURES VERSUS HEIGHT AT 7:15 AFTER IGNITION

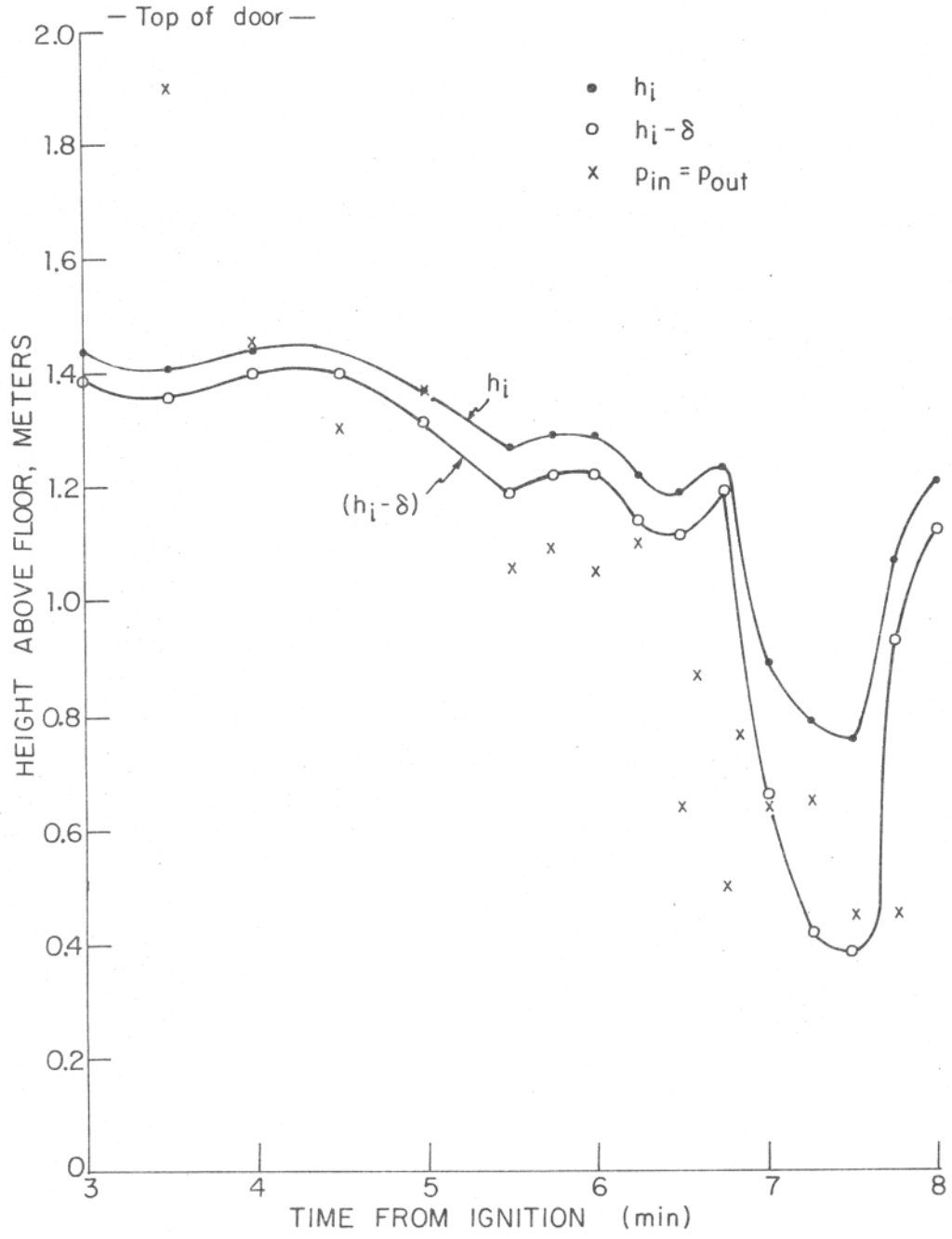

FIGURE 5.2 DOORWAY INFLOW LAYER DEPTH, COOL GAS LAYER DEPTH IN ROOM AND EQUAL PRESSURE LEVEL VERSUS TIME AFTER IGNITION

LIST OF SYMBOLS

g	Gravitational acceleration
H	Height of doorway
h_i	Height of doorway inflow layer
p	Pressure
p_a	Ambient atmospheric pressure, 760 mm Hg
p_o	Pressure at floor level (= p_a, outside the room)
p_{in}	pressure inside room
p_{out}	pressure outside room
T	Temperature
T_a	Ambient temperature
z	Vertical coordinate measured up from floor
ρ	Density of air
ρ_a	Ambient air density
δ	Hot layer depth in room below level in doorway

REFERENCES

1. Emmons, H.W., "Natural Convective Flow Through An Opening," Home Fire Project Technical Report No. 1, 1973.
2. Volume I, this report.

VI

ENERGY BALANCE FOR THE BEDROOM ENCLOSURE

P. A. Croce
Factory Mutual Research Corporation

An energy balance for the bedroom fire enclosure was performed in order to ascertain the energy losses during the fire as well as to estimate the burning rate history. Consider the control volume shown in Figure 6-1. The boundary B corresponds to any solid-gas interface inside the bedroom with the gas being inside the control volume and the solid surface outside; the opening in the boundary, D, corresponds to the bedroom doorway that was left open during the test. The quantities depicted in Figure 6-1 are the following: $\dot{m}_i\ h_i$ - the product of inward mass flow and enthalpy (relative to ambient); $\dot{m}_e\ h_e$ - the product of outward mass flow and enthalpy (relative to ambient); $\dot{Q}_{Dr}$ - the net radiative energy exchange rate through the doorway; $\dot{Q}_W$ - the net energy exchange rate to the walls, ceiling and floor; $\dot{Q}_C$ - the net energy exchange rate to the contents (bed, bureau, desk, etc); mu - the product of mass and specific internal energy of the gases in the control volume; and E.R.R. - the energy release rate of the fire. Heat transfer into the control volume is positive. An energy balance thus yields

$$\dot{m}_i\ h_i + \text{E.R.R.} - \dot{Q}_C - \dot{Q}_W - \dot{Q}_{Dr} - \dot{m}_e\ h_e = \frac{d}{dt}\,(\text{mu}). \qquad (6\text{-}1)$$

Solving for E.R.R., we have

$$\text{E.R.R.} = \dot{Q}_{Dc} + \dot{Q}_{Dr} + \dot{Q}_W + \dot{Q}_c + \frac{d}{dt}\,(\text{mu}), \qquad (6\text{-}2)$$

where $\dot{Q}_{Dc}$ is the net convective energy exchange rate through the doorway given by

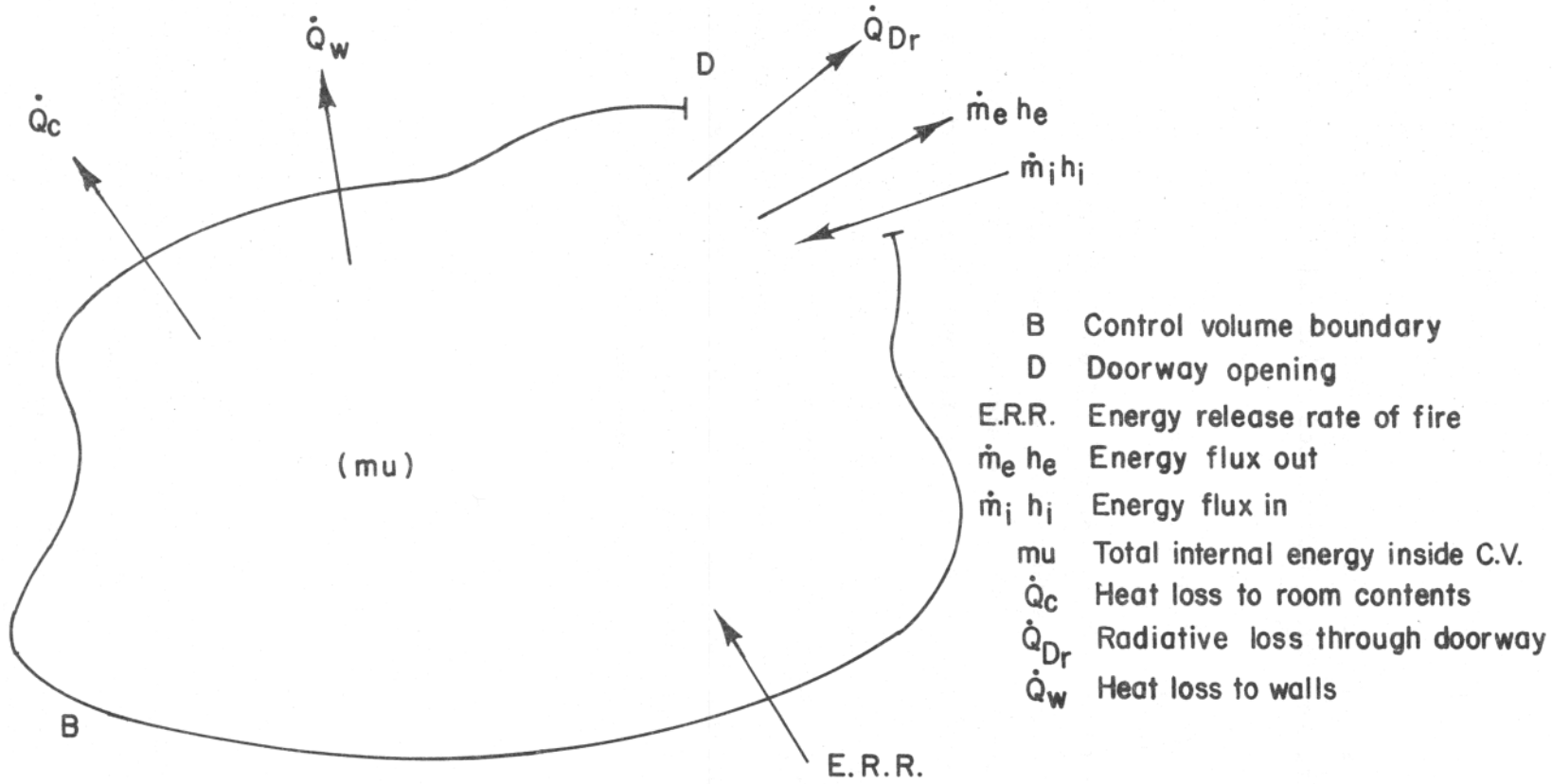

FIGURE 6.1 CONTROL VOLUME FOR BEDROOM ENERGY BALANCE

$$\dot{Q}_{Dc} = \dot{m}_e h_e - \dot{m}_i h_i. \tag{6-3}$$

The quantity d(mu)/dt is typically small (less than 5 percent of the total heat release rate during the first bedroom test) and will be neglected*; thus,

$$E.R.R. = \dot{Q}_{Dc} + \dot{Q}_{Dr} + \dot{Q}_W + \dot{Q}_C. \tag{6-4}$$

Equation (6-4) was applied at 30 sec intervals from ignition to 5:30 after ignition, and at 10 sec intervals thereafter up to 7:30, the time the sprinkler was activated. Each term on the right hand side of eq (6-4) was evaluated separately at each time interval. These calculations were performed as follows:

The net convective energy exchange rate through the doorway, $\dot{Q}_{Dc}$, was calculated by dividing the doorway opening into full width areas corresponding to the six bidirectional probes. The individual heights of these sections, top to bottom, were 30.5 cm, 35.6 cm, 35.6 cm, 35.6 cm, 35.6 cm and 30.5 cm. In each section, the velocity and temperature were assumed constant over the sectional area+. Perfect gas behavior was also assumed. Accordingly, for each area, A_j,

$$\dot{m}_j = \rho_j A_j U_j, \tag{6-5}$$

and

$$\dot{Q}_{Dcj} = \dot{m}_j c_p (T_j - T_a), \tag{6-6}$$

$$= \frac{P A_j U_j c_p}{R T_j} (T_j - T_a), \tag{6-7}$$

where ρ is the gas density, U is the measured velocity, T is temperature, P is the pressure in the doorway (assumed atmospheric) and c_p is the constant

*On the assumptions of perfect gas behavior, constant specific heat, constant pressure and uniform temperature, this quantity is identically zero.

+Since the data from one probe (channel 157) was lost during the test, the velocity at this station was assumed to be the average of two adjacent velocity values.

pressure specific heat. The subscript, a, refers to ambient conditions. The net transfer was then obtained by

$$\dot{Q}_{Dc} = \sum_j \dot{Q}_{Dcj}. \tag{6-8}$$

To evaluate the net radiative exchange rate through the doorway, $\dot{Q}_{Dr}$, the signal measured by the radiometer outside the bedroom (channel 163) was assumed to be the response to radiation from a black Lambertian surface in the plane of the doorway. Thus,

$$\dot{Q}_{Dr} = e_b A_{door} = \frac{A_{rad}}{F_{dr}} \dot{E}_r,$$

$$= \pi L^2 \dot{E}_r, \tag{6-9}$$

where e_b is the black body emissive power, A_{door} is the area of the doorway, A_{rad} is the sensing area of the radiometer, F_{dr} is the view factor for radiative transfer from the doorway to the radiometer, L is the distance from the door to the radiometer, and $\dot{E}_r$ is the measured irradiance.

The heat exchange rate with the walls, ceiling and floor was obtained from the one-dimensional heat transfer equation

$$\frac{\partial T}{\partial t} = \alpha \frac{\partial^2 T}{\partial x^2} \tag{6-10}$$

in which t is time, α is the wall thermal diffusivity and x is the perpendicular distance measured from the inner surface. The exposed wall, ceiling and floor surfaces were divided into areas corresponding to thermocouple pairs monitoring inner and outer surface temperature. For each section, eq (6-10) was solved numerically with the measured, time-dependent surface temperatures as boundary conditions and a linear temperature distribution through the wall as initial condition*. Equation (6-10) is not a complete

*A few wall thermocouples registered slightly non-ambient temperatures prior to ignition due to nearby instrumentation; the resulting effect on the energy balance was small, as indicated in Table 6.1 at t=0:30.

representation of the physical situation, since effects of the release and transpiration of the water of hydration in gypsum are not included. It was felt, however, that the use of an adjusted value of α, one which yielded heat transfer rates at the outer surface consistent with those obtained from free-convection empirical relationships, was satisfactory for these calculations.*

With the solution to eq (6-10) for each wall or ceiling** section (of area A_i), heat losses were obtained by calculating the conduction heat transfer rate at the inner surface, i.e.,

$$\dot{q}_i = - k A_i \left(\frac{\partial T}{\partial x} \Big|_{x=0} \right)_i , \qquad (6\text{-}11)$$

and summing over all sections, i.e.,

$$\dot{Q}_W = \sum_i \dot{q}_i . \qquad (6\text{-}12)$$

The rate of energy storage in the contents, $\dot{Q}_{cs}$, was determined by assuming the energy input per unit area of each piece of furniture, etc., was the same as that to the adjacent wall area. Accordingly, for each item m, the heat flux $\dot{q}''_m$ was determined for the appropriate wall area+ of that item, i.e.,

$$\dot{q}''_m = - k \left(\frac{\partial T}{\partial x} \Big|_{x=0} \right)_m , \qquad (6\text{-}13)$$

and applied to the exposed surface areas, a_m, of the item. The total heat loss to the contents was then given by

$$\dot{Q}_{cs} = \sum_m \dot{q}''_m \, a_m . \qquad (6\text{-}14)$$

*These thermal property values were: $k = .036 \frac{kw}{m°C}$, $\alpha = .0044$ cm^2/sec compared with reported values of virgin gypsum of $k = .024$ kw/m°C and $\alpha = .0027$ cm^2/sec[1].

**Heat losses to and through the floor were small, and therefore, not included.

+The "appropriate" wall area was chosen by considering elevation, proximity and orientation of each major surface of each item. The uncertainty introduced by this approach is not so severe to the overall balance since these quantities are typically small (see Table 6.1).

Values of energy release rate, E.R.R., were then computed using eq (6-4). Table 6.1 lists all of the terms of eq (6-4), the mass inflow and outflow, and values of equivalent burning rate, R, calculated by assuming 100-percent combustion efficiency of the polyurethane mattress, i.e.,

$$R = \frac{E.R.R.}{\Delta H_c} \quad , \tag{6-15}$$

where ΔH_c = 29,500 kJ/kg[2]. The fact that mass inflow and outflow differ by significantly more than the burning rate is not surprising. The probes used to measure these flows are not very sensitive to direction; a correction for actual flow direction could reduce the outflow by ~25 percent. In addition, the amount of "excess" outflow can be accounted for by two-thirds of the available water in the gypsum wallboard.

The results in Table 6-1 are accurate, at best, to $\pm$ 20 percent. Principal sources of error in the energy balance occur in the doorway convective term, where two-dimensional flow is assumed, and in the heat loss to the walls, where, perhaps, an over-simplified approach is used. The assumption of 100-percent combustion efficiency also introduces additional error into the values for burning rate.

Some recent work[3] on fire-induced flows through enclosure openings indicates a flow coefficient, C_f*, for the bedroom doorway geometry of C_f= 0.68 for both inflow and outflow. If this is applied to the convective energy term of eq (6-4), the energy balance yields values of E.R.R. that are lower by ~15 percent than those given in Table 6-1. Figure 6-2 shows the calculated burning rate history (with C_f= 1.0 and C_f= .68) compared with the burning rate determined from the measured weight loss of the bed.

The uncertainty in the heat loss to the walls, which, as seen in Table 6-1, constitutes approximately half the total heat loss, can be reduced by improving the measurement of heat flux to the walls. In the present test, prototype calorimeters were employed at several locations and more

---

*defined as the ratio $C_f = \frac{\text{actual mass flow rate}}{\text{2-dimensional mass flow rate}}$.

TABLE 6-1

ENERGY BALANCE FOR THE BEDROOM ENCLOSURE

Time After Ignition (min:sec)	Mass Flow In, $\dot{m}_i$ (kg/sec)	Mass Flow Out, $\dot{m}_o$ (kg/sec)	Conv. Flux Thru Door, $\dot{Q}_{Dc}$ (kw)	Rad. Flux Thru Door, $\dot{Q}_{Dr}$ (kw)	Heat Loss To Wall, $\dot{Q}_W$ (kw)	Heat Loss To Contents $\dot{Q}_c$ (kw)	Energy Rel. Rate, E.R.R. (kw)	Burning Rate, R (kg/sec)
0:30	0.05	0.03	0.03	0.0	-0.55	0.02	-0.50	-.00002
1:00	0.09	0.06	0.07	0.0	0.01	0.07	0.15	.000005
1:30	0.14	0.09	0.20	0.0	0.78	0.11	1.09	.00004
2:00	0.19	0.13	0.33	0.0	0.45	0.10	0.88	.00003
2:30	0.22	0.16	0.67	0.0	0.96	0.14	1.8	.0006
3:00	0.27	0.19	1.3	0.0	2.0	0.17	3.5	.00012
3:30	0.31	0.23	2.9	0.0	4.3	0.52	7.7	.00026
4:00	0.36	0.30	6.2	0.0	8.2	1.3	15.7	.00053
4:30	0.43	0.52	18.7	0.0	20.6	2.9	42.2	.0014
5:00	0.49	0.75	42.8	0.0	34.4	5.1	82.4	.0028
5:30	0.65	0.56	88.3	0.0	77.7	10.2	176.3	.0060
5:40	0.58	0.86	102.7	0.0	73.8	10.2	186.7	.0063
5:50	0.57	0.83	100.8	0.0	71.2	9.4	183.9	.0062
6:00	0.45	0.93	125.3	0.0	82.4	10.9	218.7	.0074
6:10	0.53	1.15	211.5	0.0	175.8	21.1	408.4	.014
6:20	0.69	0.95	289.8	4.3	310.3	39.9	644.2	.022
6:30	0.62	1.33	399.3	12.2	482.3	59.2	953.0	.032
6:40	0.59	1.46	597.5	26.5	587.5	84.0	1295.5	.044
6:50	0.57	1.64	968.5	60.2	1032.6	157.6	2218.9	.075
7:00	0.93	1.35	999.9	71.3	929.5	184.6	2185.2	.074
7:10	0.73	1.50	1059.1	89.2	877.1	171.5	2196.9	.074
7:20	0.71	1.73	1267.7	126.0	892.4	185.5	2471.6	.084
7:30	0.92	1.52	1126.2	124.2	853.7	238.7	2342.7	.079

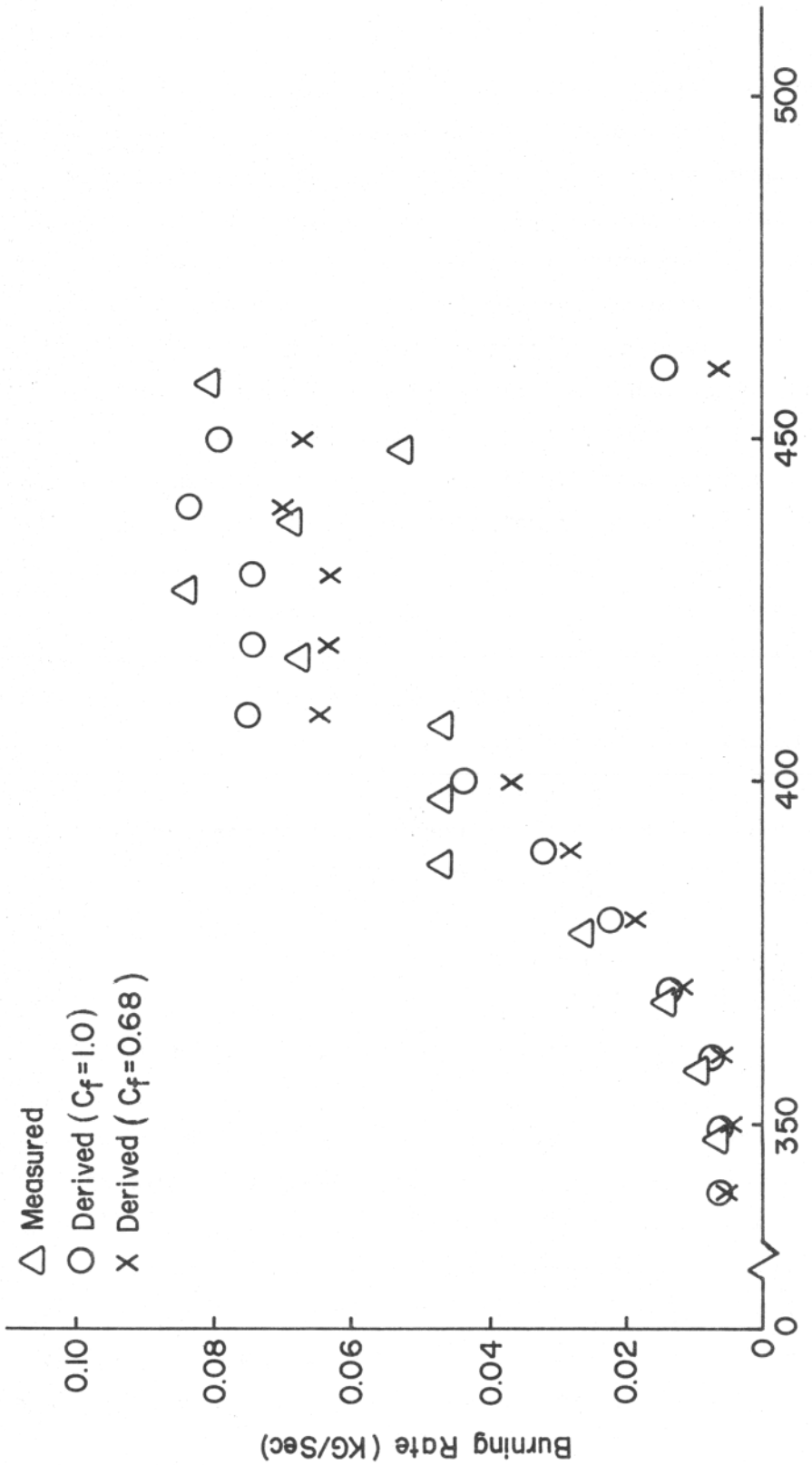

FIGURE 6.2 BURNING RATE VERSUS TIME AFTER IGNITION

expensive (and reliable) heat flux gauges used in a few locations. The calorimeters, it appears, lack the accuracy desired, and the heat flux gauges are too expensive for full-scale energy balance applications. Use of the simple heat transfer equation is subject to error with materials such as gypsum. A simple, inexpensive, and reliable method is needed.

To examine the assumption of 100-percent combustion efficiency, it may be possible, by means of a chemical species balance, to obtain some information on the true combustion efficiency as a function of time. Accurate gas species concentration histories, which have been adjusted for delays and distortions due to tubing lengths, filters, condensers, pumps, analyzers, etc., are required. Except for simple shifts for time delay, the data of the current test have not been so corrected. It will, however, be possible to make full corrections[4] to similar data from our next test.

Consider gas concentration measurements from the present test averaged over the time interval 7:00-7:30, when effects of signal distortion were not so significant. The average concentrations (volume percents) were: 2.87 percent O_2, 14.55 percent CO_2, 2.01 percent CO, and 1.63 percent THC for the central sampling port. If we assume polyurethane, $C_{6.3}H_{7.1}NO_{2.1}$[5], to be the burning fuel, a species balance yields

$$C_{6.3}H_{7.1}NO_{2.1} + 4.16\ O_2 + 15.64\ N_2 \rightarrow$$

$$2.97\ CO_2 + 2.89\ H_2O + 0.41\ CO + 2.59\ C(s) + 0.33\ CH_4 + 0.59\ O_2 + 16.14\ N_2.$$

From these results, using the heats of formation of the various compounds involved, an effective heat of combustion can be determined. This value can then be compared with the stoichiometric heat of combustion to estimate combustion efficiency. For example, in the above case, the effective heat of combustion was 2790 cal/g, the stoichiometric heat of combustion was 5640 cal/g, giving a combustion efficiency of .49, or 49 percent. If we consider that, during the 7:00 to 7:30 interval, the fire had involved most of the room, and the

sampling port was immersed in flames (i.e., the combustion zone), the value of 49 percent may not be unreasonable.*+ Information can also be obtained on the fuel-air ratio as a function of time, e.g., fuel/air = 0.23 (mass) for the above case, a not unreasonable value considering the location of the sampling port and the extent of the fire development during the time interval examined. If the sampling port were positioned to sense only products of combustion and remain out of the combustion zone, improved accuracy in these quantities would result.

*Involvement of fuels other than polyurethane during the burning interval considered is also a factor.

+This technique has already been applied successfully in a study of similar full-scale situations[6].

REFERENCES

1. Castle, G.K., Alexander, J.G., Tempesta, F.L. and Belason, E.B., "Analytical Prediction of the Thermal Response of Decomposing Materials in Fire Environments," J. Testing and Evaluation, Vol. 1, No. 5, September 1973.
2. Volume I, this report.
3. Prahl, J. and Emmons, H.W., "Fire Induced Flow Through an Opening," Submitted for Publication, May 1975.
4. Croce, P.A., "A Method for Improved Measurement of Gas Concentration Histories in Rapidly Developing Fires," Submitted for Publication, June 1975.
5. Throne, J.L. and Griskey, R.G., "Heating Values and Thermochemical Properties of Plastics," Modern Plastics, November 1972.
6. Kung, H.C., Residential Sprinkler-Protection Study, FMRC Technical Report, Serial No. 22442, July 1975.

VII

THE RESPONSE OF A FUEL ELEMENT TO A FIRE ENVIRONMENT

F. Tamanini

Factory Mutual Research Corporation

7.1 INTRODUCTION

The rate of growth of a fire in an enclosure is one of the critical aspects of the fire problem because of its bearing on the amount of property loss and on the margin of safety for the occupants. If the conditions are appropriate, the growth of a developing fire can take the connotations that are usually associated with a runaway process. When this happens, the rate of increase of temperatures, heat fluxes and burning rates in the enclosure increases dramatically over the values at previous times. Usually, this corresponds to a qualitative change in the appearance of the fire, which spreads rapidly from the fuel element initially involved to other major fuel elements and, eventually, to the whole enclosure. The occurrence of the process of rapid spread is commonly described (by people in the scientific community if not by firemen) by saying that the fire has reached the stage of flashover. What this means in more rigorous quantitative terms has yet to be established, and the problem remains open to contributions.

If one accepts the concept that this critical condition is accompanied, if not characterized, by the "jump" of the fire from the item initially ignited to at least another major fuel element in the enclosure, it becomes important to study the response of such an element to the fire environment. For this reason, this section reports the results of an analysis concerning data obtained during the realistic full-scale bedroom fire of 1974. Attention will concentrate on a selected item (the bureau in the rear right corner of the room) located near the fuel element first to be involved in the fire (the bed). Reference 1 contains the detailed description of the layout of the room and the list of the measuring devices used for the experiment.

7.2 EXPERIMENT

The experiment reported here consisted of two parts:

1) The weights of the front panels of the nine drawers in the bureau were measured before and after the fire;

2) The temperature histories at two different depths in the middle of the top center drawer (No. 1) were recorded (channel 102-103).

7.2.1 Weight Measurements

Table 7.1 shows the results of the weight measurements. The values reported for the weights after the fire are those measured after the bureau had been left to dry from the water absorbed during the extinguishment phase and the wood allowed to reach equilibrium with room conditions. Later, the panels were oven dried and weighed again. The moisture content referred to the dry weight turned out to be:

$$MC = 7.50 \pm .25\%$$

It was possible to make an estimate of the dry weight of each panel before the fire by looking at the values of MC after the fire and relative humidity of the air (RH) before and after the fire. In particular, it was assumed that MC had varied proportionally to RH. The estimated fraction of the initial dry weight lost during the fire did not differ appreciably from the one evaluated including the moisture as presented in Table 7.1.

The different panels were labeled as indicated in Figure 7.1. A quick look at the numbers in the fourth column of Table 7.1 shows that the upper part of the bureau suffered more extensive damage than the lower. This result could be expected considering that the lower sections had greater convective cooling and that the energy received by radiation was lower because of the reduction in viewing angle.

The data show another consistent pattern in the distribution of heat fluxes, which cannot be justified by a simple argument. The right part of the bureau appears to have lost more mass and, hence, to have been subjected to larger heat fluxes.

TABLE 7.1

WEIGHT CHANGES FOR FRONT PANELS OF BUREAU DRAWERS*

Panel No.	Original+ Weight (g)	Weight§ After Fire (g)	Fraction Lost During Fire (%)
1	295.7	244.7	17.2
2	290.0	250.4	13.7
3	242.5	194.7	19.7
4	421.3	363.2	13.8
5	444.1	376.3	15.3
6	475.5	420.7	8.0
7	540.1	481.0	10.9
8	461.4	418.1	9.4
9	488.0	441.5	9.5
Overall	3658.6	3190.6	12.8

* All panels weighed with knob and holding screw left in place (knob + holding screw = ~ 9 g)

+ Weight measured when room relative humidity was RH=63%

§ Weight measured after wood was exposed for about ten days to room condition. At the time of the weighing RH was 49%.

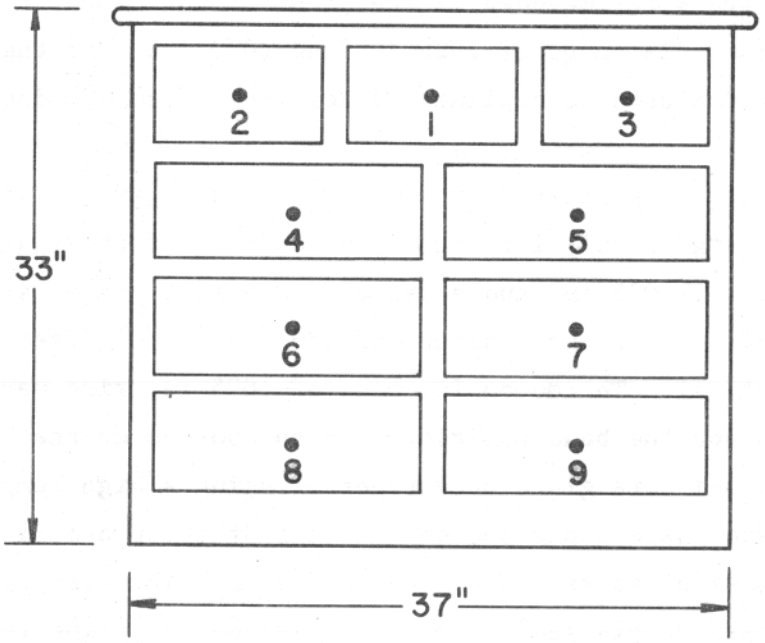

FIGURE 7.1 FRONT OF BUREAU SHOWING PANEL LABELING

This pattern is consistent with the observation that the ignition of the magazines on the top of the bureau occurred right above drawer No. 3 and that the panel of the same drawer was the first surface to ignite on the front of the bureau.

Even though this observed asymmetry is not explained here, it is unlikely that it is practically very relevant, considering the relatively low values of the differences involved.

7.2.2 Temperature Measurements

Two thermocouples were imbedded in the panel of the center top drawer (No. 1) at the nominal distances of .020 in. and .070 in. from the outside surface. The technique used is outlined in Reference 2 and is described here only briefly.

The panel was cut as indicated by section A-A in Figure 7.2 and two holes were drilled in the edge parallel to the front surface of the panel. The holes had a diameter of .025 in. and a depth of .75 in.: their axes were at .020 in. and .070 in. from the surface of the panel and offset by .050 in. in the vertical. Thermocouples made of .005-in. wire were inserted in the holes and the bead positioned at the bottom of the holes. The two halves of the panel were glued back together using a high temperature epoxy. The thermocouple leads were connected on the back of the panel (inside the drawer) to the extension cables. The mounting scheme minimizes conduction errors since the thermocouple leads lie in the isothermal plane for 3/4 in. before they encounter temperature gradients. Additional sources of error might have affected the measurement. For example, the difference between the thermal properties of the wood and those of the thermocouple materials, a bead size comparable to the distance over which large temperature differences exist, and so on. The results of the measurements, shown in Figure 7.3, indicate a maximum temperature difference between the readings of the two thermocouples as being of the order at 200°C. Assuming that the diameter of the thermocouple bead was .010 in., the maximum temperature difference that could be expected across the bead was of the order of 40°C.

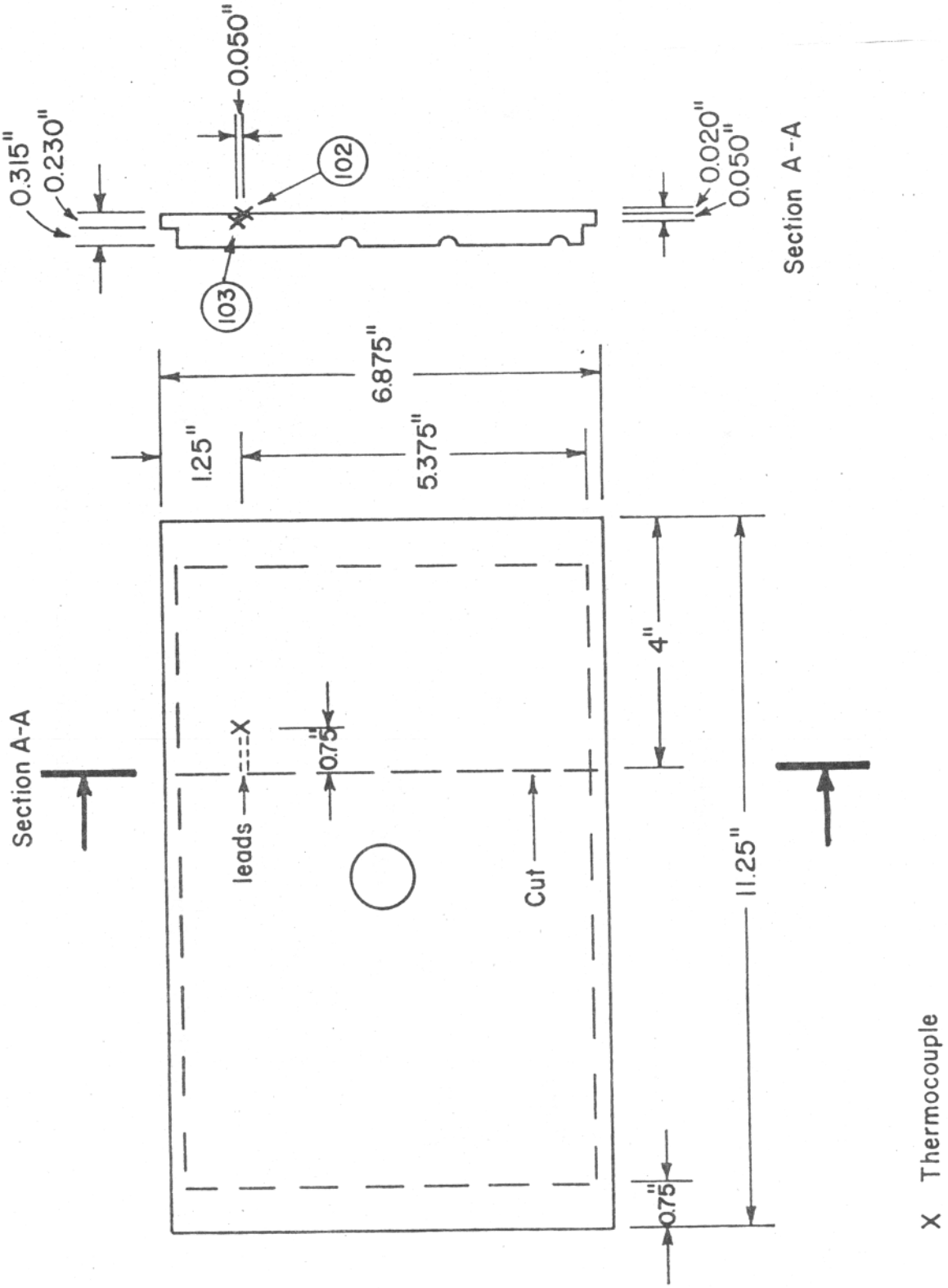

FIGURE 7.2 INSTRUMENTATION LAYOUT: THERMOCOUPLES IN CENTER TOP BUREAU DRAWER

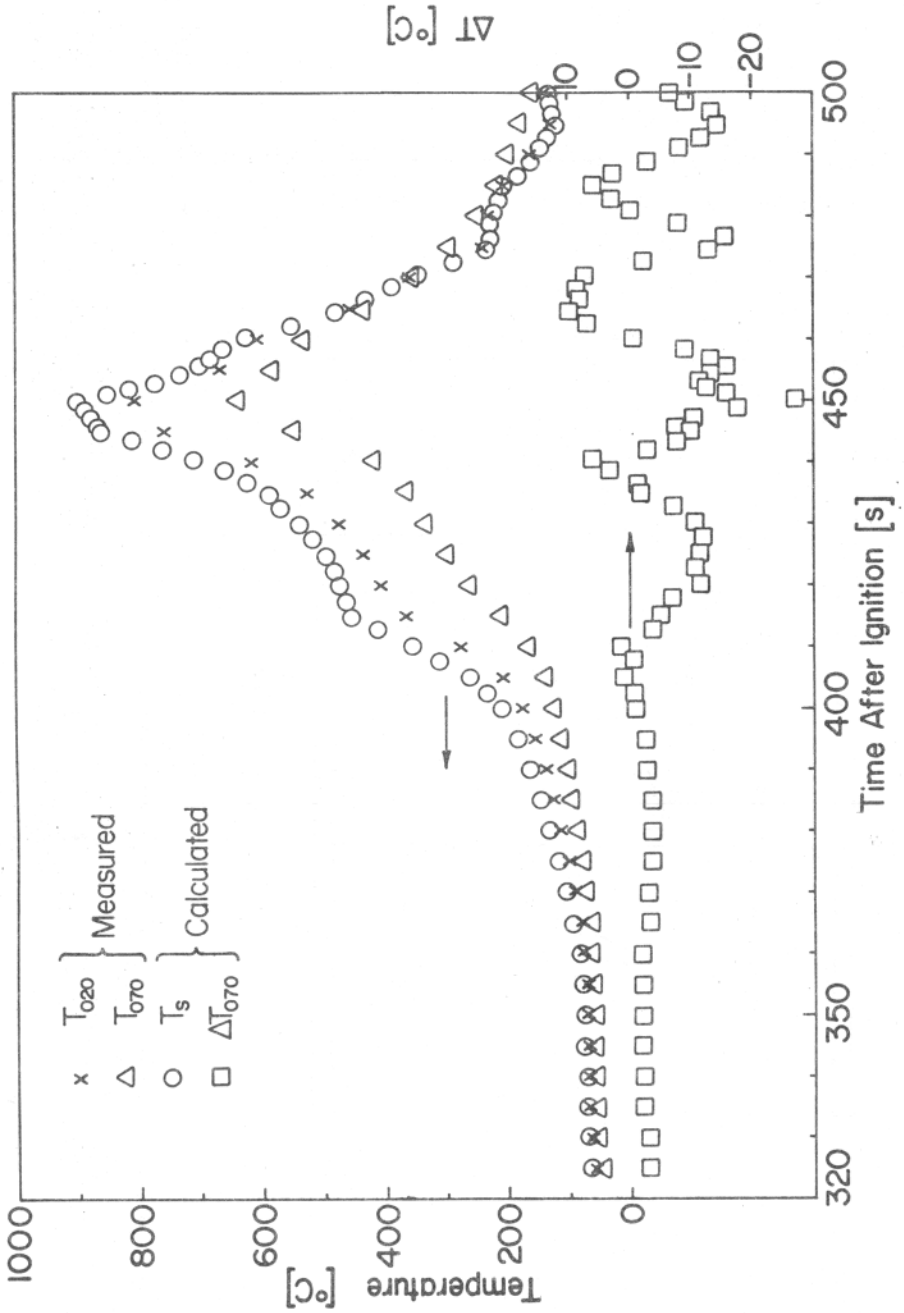

FIGURE 7.3 MEASURED AND CALCULATED TEMPERATURES IN THE PANEL

The most likely source of error was probably due to the actual position of the thermocouple bead with respect to the surface. Even though great care was taken in trying to drill the holes straight, there was no way of actually checking the exact position of the bottom of the holes. Greater confidence could be put on the accuracy of the positioning of the outer thermocouple (.020 in. from the surface) because the small thickness (nominally .0075 in.) of the wall of the hole facing the front surface actually allowed the view of the drill in transparency. Despite all the reasons for uncertainty, no correction of the temperature readings was attempted.

7.3 THEORETICAL MODEL

The temperature measurements were used as inputs to a calculation for the determination of the heat flux received by the front surface of the bureau and its rate of pyrolysis. The calculation was based on a pyrolysis model proposed by Kung[3] and adopted in Reference 2. In the model, the temperature distribution in the slab of wood is obtained by solving the heat equation in one dimension with a source term for the heat generated by the pyrolysis reaction and a convective term for the heat transfer between the gases of pyrolysis and the char. The pyrolysis reaction is assumed to be one step and the rate of pyrolysis to be described by an Arrhenius expression. The heat of pyrolysis is defined at a reference temperature, taken as room temperature for convenience. The model allows for different thermal properties for the wood and the char and uses a linear interpolation based on the local density to calculate the thermal properties of partially pyrolyzed wood. Table 7.2 shows the values used in the calculation for the different quantities. As a general rule, the values used for the calculations of wood burning presented in Reference 2 were maintained. The density of the char was estimated to be 20 percent of the initial density of the wood and the thermal conductivity of the wood adjusted to follow the known dependence on the density.

TABLE 7.2

VALUES USED FOR THE PROPERTIES

Pre-exponential factor	$a_p = 1500\ s^{-1}$
Activation energy	$E = 15000$ cal/g-mole
Gas constant	$R = 1.987$ cal/g-mole °C
Ambient temperature	$T_0 = 297$°K
Thermal conductivity (wood)	$k_w = .00031$ cal/cm s°C
Thermal conductivity (char)	$k_c = .00045$ cal/cm s°C
Specific heat (wood)	$c_{pw} = .33$ cal/g°C
Specific heat (char)	$c_{pc} = .16$ cal/g°C
Specific heat (volatiles)	$c_{pg} = .30$ cal/g°C
Density (wood)	$\rho_w = .48\ g/cm^3$
Density (char)	$\rho_f = .096\ g/cm^3$
Heat of pyrolysis at ambient temperature	$Q_{po} = 40$ cal/g

The calculation was carried out using the temperature history at a depth of .020 in. from the surface (T_{020}) as a boundary condition, with the back surface of the panel assumed to be adiabatic. The later assumption turned out to be fair, as the temperature of the back surface reached 35.2°C at 450 sec and went up to a maximum of 68.1°C at 500 sec. The temperature history calculated at a depth of .070 in. was compared to the measured one (T_{070}). The magnitude of the difference between the calculated and the measured temperatures at that depth (ΔT_{070}) was used in order to optimize the values at the char thermal conductivity (k_c) and the heat of pyrolysis (Q_{po}). The value used for k_c (see Table 7.2) agrees with the one suggested in some recent work by Havens et al[4] and the value of Q_{po} is very close to the result obtained by Roberts[5] from his experiment. Note that a positive value of Q_{po} implies exothermic pyrolysis.

Typically the slab was divided into 27 slices, and the integration of the equations was carried out using a variable time step as required by considerations of accuracy and stability of the calculation. Figure 3 shows the calculated surface temperature (T_s) and the temperature difference ΔT_{070} between the calculated and the measured temperatures at the .070 in. depth. The small values of ΔT_{070} indicate that the model is a realistic one and that confidence can be placed on its predictions. The oscillations in the profile are due to the fact that only values 5 sec apart were known for the temperature T_{020}, and that intermediate temperatures were obtained by linear interpolation. In addition, the program needed the surface temperature (T_s) as a boundary condition, while T_{020} was the temperature known from the experiment. This difficulty was resolved by choosing at each step the value for T_s in such a way that the temperature calculated at the .020 in. depth was equal to the measured one. The algorithm used to obtain that result is responsible for part of the oscillations in the ΔT_{070} profile.

7.4 HEAT FLUXES, RATE OF PYROLYSIS AND IGNITION

One of the results of the calculation was the estimate of the net energy flux ($\dot{q}''_{net}$) required at the surface in order to get the measured temperature histories in the solid.

The magnitude of the total heat flux directed toward the surface by its surroundings is obtained by adding to $\dot{q}''_{net}$ (net flux going into the solid) the radiative and convective cooling ($\dot{q}''_{s,rad}$ and $\dot{q}''_{s,conv}$) of the surface, so that:

$$\dot{q}''_{tot} = \dot{q}''_{net} + \dot{q}''_{s,rad} + \dot{q}''_{s,conv} \tag{7.1}$$

The radiative cooling can be calculated as:

$$\dot{q}''_{s,rad} = \varepsilon_s \sigma T_s^4 \tag{7.2}$$

where, ε_s is the emissivity of the surface and σ is the Stefan-Boltzmann constant.

The convective cooling, which will be present when the surface is at higher temperature than the gas in front of it, can also be estimated using an expression of the type:

$$\dot{q}''_{s,conv} = h\ (T_s - T_\infty) \tag{7.3}$$

where, h is an appropriate heat transfer coefficient and T_∞ is the temperature of what the surface considers as "infinity".

Since T_s is available, the assumption of a value for ε_s allows one to calculate $\dot{q}''_{s,rad}$, from eq (7.2). The result for ε_s=1 is shown in Figure 7.4, where the magnitude of $\dot{q}''_{s,rad}$ can be compared to that of $\dot{q}''_{net}$. The accurate evaluation of $\dot{q}''_{s,conv}$ is more difficult because of uncertainties associated with the determination of the values of T_∞ and h.

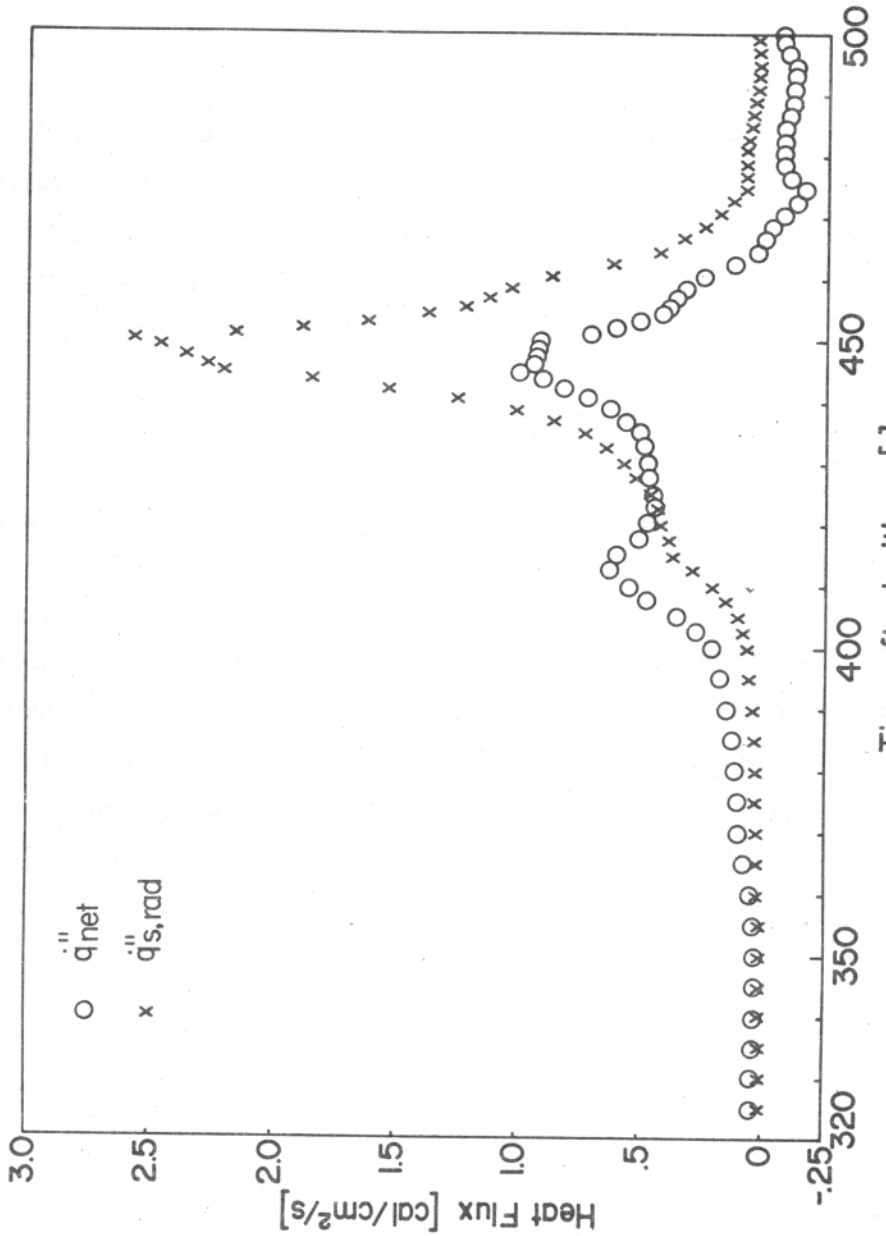

FIGURE 7.4 NET HEAT FLUX TO THE PANEL AND RADIATIVE COOLING

No measurements of the temperature of the gases in front of the panel under scrutiny were available. An indication of the order of magnitude of the difference $(T_s - T_\infty)$ can be obtained by assuming that the right values of T_∞ are those measured by the thermocouple on the rear rack mounted at 30 in. from the floor (channel 99, see report on bedroom fire[1] for instrumentation layout). The location at which the temperature T_∞ was measured was 1 in. higher, 15 in. closer to the door and 25 in. closer to the longitudinal axis of the room than the location of the thermocouples in the drawer panel. The difference $(T_s - T_\infty)$ so estimated varied from 20°C at 325 sec in the fire, to 54°C at 375 sec, 80°C at 400 sec, 155°C at 415 sec, with a maximum of 165°C at 430 sec.

The choice of a reasonable number to be used for h is even more difficult, because of the fact that the natural convection flow established in front of the panel was probably influenced by the general circulation in the room induced by the fire.

On the basis of a simple calculation which assumed natural convective heat transfer and a value for h, taken from a standard heat transfer text[6], $\dot{q}''_{s,conv}$ was estimated to be less than 10 percent of $\dot{q}''_{net}$ at 400 sec after ignition. Even though such an estimate probably represents a lower limit to $\dot{q}''_{s,conv}$, the actual value should not differ by more than a factor of 2.

Because of its small value, $\dot{q}''_{s,conv}$ has been neglected and the total heat flux calculated as:

$$\dot{q}''_{tot} \cong \dot{q}''_{net} + \dot{q}''_{s,rad} \qquad (7.4)$$

This quantity is plotted in Figure 7.5. As can be seen, the total heat flux reached a first maximum of 1 cal/cm^2/sec (4.2 watts/cm^2) at 413 sec, which roughly corresponded to the time of ignition of the panel (as will be discussed later) and then increased further up to about 3.5 cal/cm^2/sec (14.7 watts/cm^2) at 450 sec, at which time the sprinkler was turned on.

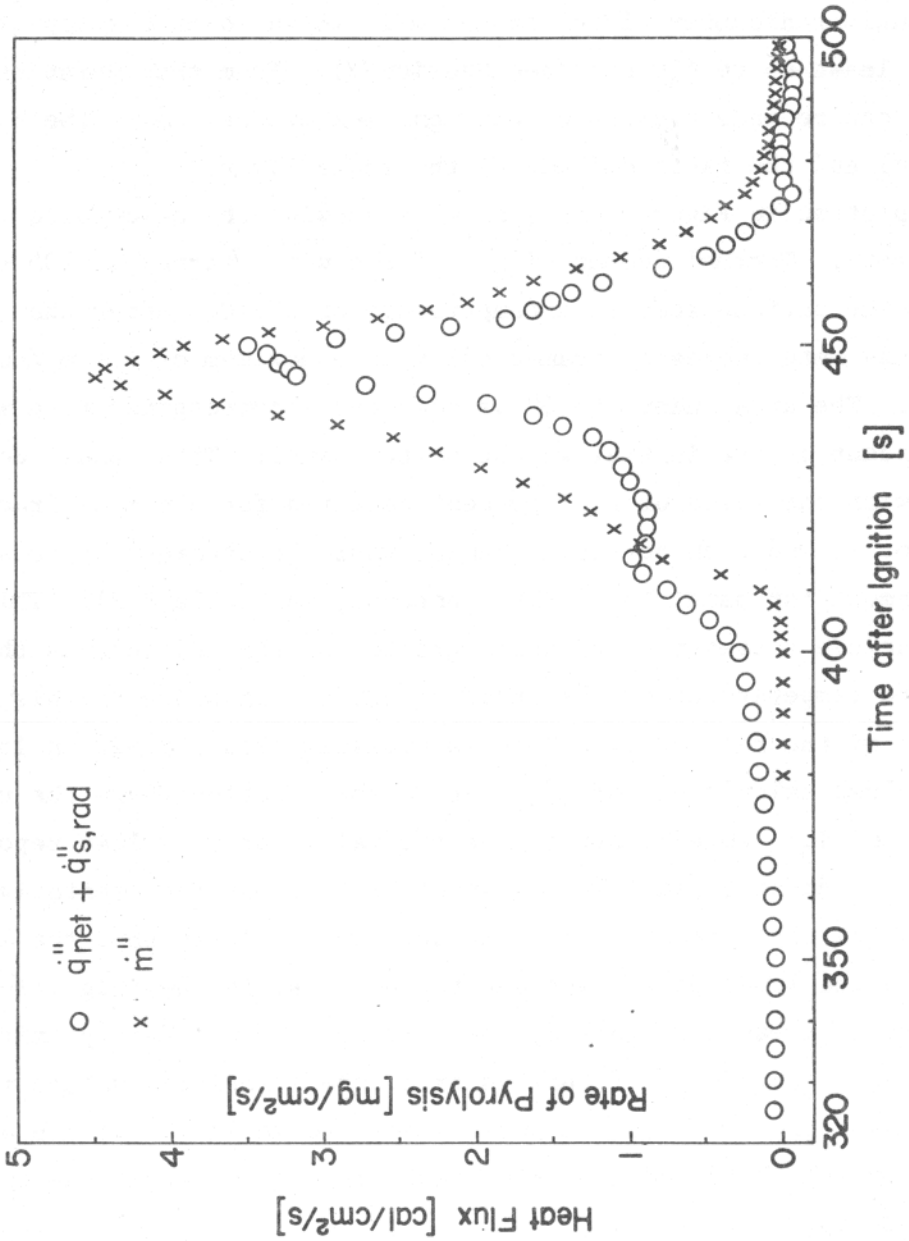

FIGURE 7.5 TOTAL HEAT FLUX AND RATE OF PYROLYSIS OF THE PANEL

The prediction of $\dot{q}''_{tot}$ is consistent with the measurement obtained with the wide angle radiometer placed on the wall 16 in. over the top of the bureau, at least up to 410 sec (see Section IX). From that point on no comparison can be made because of the ignition of the top of the bureau (at 407 sec) and the rapid descent of the smoke layer.

Also plotted in Figure 7.5 is a curve showing the calculated rate of pyrolysis ($\dot{m}''$). Thermal decomposition of the wood started at 405 sec in the fire, when the surface reached a temperature of 255°C. After that time, the pyrolysis rate increased dramatically to a maximum of 4.5 $mg/cm^2/sec$ at 445 sec. The area under the $\dot{m}''$ vs time curve corresponds to a mass loss of 19.7 percent of the initial weight of the panel. This result compares favorably with the value of 17.2 percent measured for the mass fraction lost by panel No. 1, and even better agreement would be obtained by considering the measurement for panel No. 2 (19.7 percent, see Table 7.2). This model does not include a treatment of the migration of the moisture as the wood is heated to temperatures of the order of 100°C. In spite of this, the calculation of the rate of pyrolysis is probably accurate within 15-20 percent.

The values calculated for $\dot{m}''$ refer to the location where the temperatures T_{020} and T_{070} were measured. As the values of mass lost reported in Table 7.1 indicate, panel No. 1 cannot be taken as representative of the behavior of the whole front of the bureau. It is likely that the lower mass lost by the lower panels was due to the delay in their ignition and that once the whole bureau was ignited, the burning rate was fairly uniform over its entire front surface. If this is true, the calculated values for the burning rate of the front of the bureau reported in Table 7.3 are approximations by excess of the real burning rate, in particular in the early stages of burning.

The rate of weight loss for the bed[1] is also reported for comparison. Note that the measurements of char thickness showed that most of the damage was concentrated to the front and the top of the bureau. Even if the contribution due to the burning of the top of the bureau (13.5 in. x 37 in.) had been included, the burning rate calculated for the bureau would not have

TABLE 7.3

RATE OF WEIGHT LOSS FOR THE BED AND THE FRONT OF THE BUREAU

Time (s)	Bed Burning Rate (kg/s)	Bureau Burning Rate* (kg/s)
348	.0063	0
358	.0094	"
368	.0142	"
378	.0263	"
388	.0468	"
398	.0468	"
408	.0468	.0005
418	.0672	.0074
428	.0840	.0137
438	.0687	.0251
448	.0528	.0327
458	.0804	.0149
468	.0078	.0052
478	-	.0012

* The values are calculated assuming that the entire front surface of the bureau (33 in. x 37 in.) was burning at the rate calculated for panel No. 1

quite reached that of the bed. For a detailed study of the flashover phenomenon, the total burning rates estimated this way are not sufficiently accurate and there is a need for more data.

The analysis was also used to give an indication of the time at which the front of the bureau ignited. A theoretical value for the temperature of a diffusion flame fed by the pyrolysis of the bureau was calculated assuming that convection was the only mode of heat transfer and that the environment "seen" by the surface was formed by unvitiated air at room temperature.[2] Piloted ignition is assumed to have occurred when the calculated flame temperature reached a critical value (chosen at 1300°C). The adoption of this ignition criterion would indicate that the panel ignited at 412.5 sec, when the surface temperature was T_s = 410°C and the rate of pyrolysis $\dot{m}''$ = .4 mg/cm^2/sec. This result is in agreement with the time of ignition (413.5 sec) of panel No. 3 as measured from the movie. The agreement is not surprising. In fact, even though the ignition criterion does not account for the effects of oxygen depletion and increased temperature in the room, any reasonably expectable error on, say, the prediction of the minimum rate of pyrolysis required for ignition would reflect itself in a small error on the prediction of the time of ignition. The reason for this lies in the fact that $\dot{m}''$ at the time of ignition was increasing very rapidly.

Accepting the figure of .4 mg/cm^2/sec as the minimum pyrolysis rate required for burning, one can observe that the burning of the panel was brought back to that value in about 22 sec after the sprinkler was turned on (at 450 sec). This indicates an extinguishment time of the order of 20 sec for the bureau; the result can help in the assessment of the effectiveness of the sprinkler head used in the test.

7.5 CONCLUSIONS

The following practical conclusions may be made as a result of the present study:

1) The ignition of the panel was predicted as occurring when the surface temperature had reached 410°C and the rate of pyrolysis, .4 $mg/cm^2/sec$.
2) The in-depth temperature history was successfully calculated.
3) The measured total weight loss agreed well with that predicted by the analysis.

From a more general viewpoint, the analysis has shown that a fair amount of information can be extracted from a very simple temperature measurement. Sufficient data are available in the literature to support the contention that calculations of wood pyrolysis can be done with a high degree of confidence. The process of parameter optimization has emphasized the sensitivity of the prediction on the thermal properties of the char. Even though agreement with the experiment was obtained using the value of char thermal conductivity suggested by a recent study (k_c = .00045 $cal/cm^2/sec$), additional data on the thermal properties of pyrolyzing wood would be welcomed.

Only information on the temperature in the solid at (or near) the surface is required as an input to the analysis; the knowledge of the temperatures at one or more different depths is not indispensable even though it can be used, as it was in this case, to tune the parameters needed in the analysis and increase its accuracy. This technique seems to suggest an easy way to measure heat fluxes to, and rates of pyrolysis from, cellulosic fuel elements.

A better way of estimating convective heat transfer could be devised: a possible scheme would involve placing an aspirated thermocouple at a short distance in front of the surface where the temperature measurement in the solid is being made. Furthermore, some thought might be given to the checking of a better way to embed the thermocouples in the solid, in order to reduce the setup time and/or increase the accuracy in the positioning of the beads.

REFERENCES

1. Croce, P.A., Volume I, this report.
2. Tamanini, F., "A Study of the Extinguishment of Wood Fires," Ph.D. Thesis, Harvard University, May 1974.
3. Kung, H.C., "A Mathematical Model of Wood Pyrolysis," Combustion and Flame, 18, 185-195, 1972.
4. Havens, J.A., Hashemi, H.T., Brown, L.E. and Welker, J.R., "A Mathematical Model of the Thermal Decomposition of Wood," Combustion Science and Technology, 5, 91-98, 1972.
5. Roberts, A.F., "The Heat of Reaction During the Pyrolysis of Wood," Combustion and Flame, 17, 79-86, 1971.
6. McAdams, W.H., Heat Transmission, McGraw-Hill Co., p 172, 1954.

VIII

FULL-SCALE TEST DATA OBTAINED WITH THE SCANNING RADIOMETER

G.H. Markstein

Factory Mutual Research Corporation

The scanning radiometer employed in the full-scale test viewed the ceiling through a 2-in. dia opening in the floor located on the center line 4.5 ft from the front wall. A schematic of the arrangement is shown in Figure 8.1. An 8 1/2-in. x 10-in. water-cooled plate was imbedded in the ceiling above the radiometer, extending 10 in. from the centerline to the left as seen from the room entrance. A scanning mirror deflected the collimated radiometer beam laterally so that it viewed alternately the center of the cold target and a point located symmetrically with respect to the centerline, at a scanning frequency of 33Hz. The mirror deflection as a function of time, as determined by viewing a synchronized oscilloscope trace through the mirror, was trapezoidal, with the times spent at the constant extreme deflections each occupying about 1/3 of the period. The pneumatically operated shutter was located below the floor opening. A sheet metal enclosure was placed around the radiometer assembly below the floor to reduce updrafts through the floor opening as much as possible.

After amplification by a 10^3-gain, chopper-stabilized operational amplifier, the output of the radiometer's thermopile sensor provided two signals. An average signal proportional to the mean radiation was obtained by smoothing the output with an active filter of 1 sec time constant, while a signal proportional to the difference between the cold target and ceiling radiation was obtained from a lock-in amplifier. Calibrations for both the dc and lock-in response of the radiometer were obtained with a blackbody source. Re-calibration of the radiometer after the tests showed no significant change of response (within 3.5 percent of the initial mean value of dc responsivity, and 4.2 percent of the mean lock-in responsivity) even though the fixed plane mirror had been cleaned twice after exposures to soot and water.

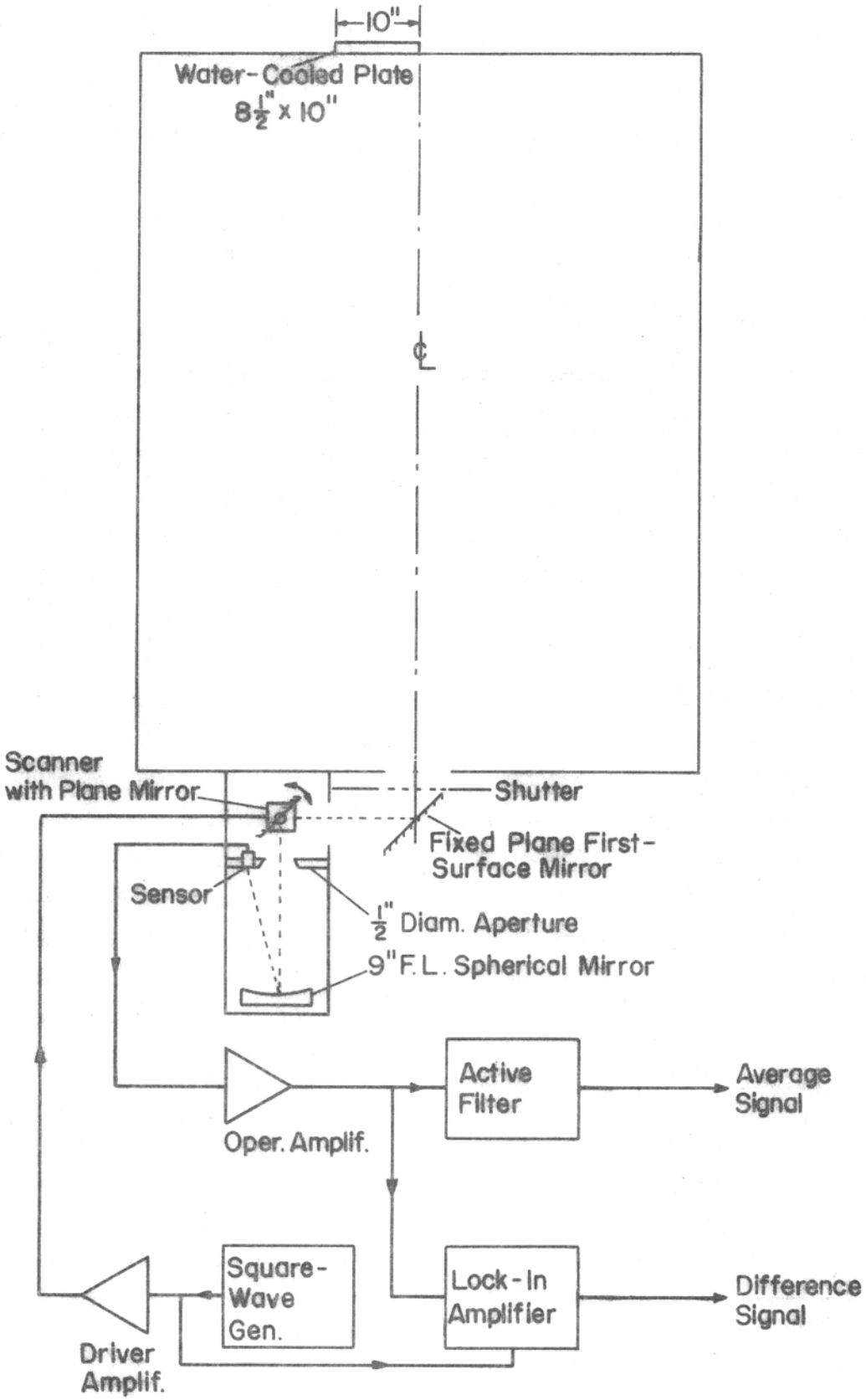

FIGURE 8.1 SCHEMATIC DIAGRAM OF SCANNING RADIOMETER

Results for the full-scale test are shown in Figures 8.2-8.6. The time origin is at ignition. The radiometer shutter was closed at 295 sec and opened at 305 sec, closed again at 348 sec and opened at 365 sec, for the purpose of establishing and resetting baselines. No baseline corrections have been applied to the present data, since the corrections are too small to cause any significant change in the results. The shutter was finally closed at about 470 sec.

Figure 8.2 shows radiance values N_{av} computed from the average dc signal of the radiometer (augmented by the room temperature radiance $\sigma T_o^4/\pi$, $T_o=300°K$). (The signal rise after 535 sec, with the shutter closed, is presumably due to rise of shutter temperature after shutoff of the sprinklers.) Figure 8.3 shows the radiance difference ΔN obtained from the lock-in signal. It should be noted that the data beyond 410 sec are meaningless, since temporary overload of the amplifier occurred. The input sensitivity setting was reduced at this time, but because of the long time-constant setting (30 sec), the instrument did not record a meaningful signal. Up to this time, the difference reading was of the order of 2 percent of the average reading. It is therefore concluded that at least until shortly before flashover, the cold target and therefore also the ceiling was almost completely obscured by the smoke layer.

Figure 8.4 shows the "ceiling" radiance $N_c=N_{av}+.5\Delta N$ and Figure 8.5 the "cold-plate" radiance $N_p=N_{av}-.5\Delta N$. Because of the small values of ΔN these results do not differ significantly from N_{av} shown in Figure 8.2 However, because of the uncertainty of ΔN after 410 sec the actual values of N_c may have been somewhat larger, and of N_p somewhat smaller beyond this instant.

Finally, the "ceiling" radiance has been converted into radiation temperature $T_r=(\pi N_c/\sigma)^{1/4}$ ($\sigma=5.670\times10^{-12}$ W/cm^{2}K^4, Stefan-Boltzmann constant) assuming an emissivity of unity. These temperature values are shown in Figure 8.6 and are further discussed by Modak in Section X.

Data for the paraffin oil fire test are shown in Figures 8.7-8.12. In this run, the shutter was closed at 990 sec, opened at 1020 sec, closed at

1075 sec and opened at 1135 sec. Figure 8.8 shows that in this test the difference readings were about 10 percent of the average readings shown in Figure 8.7. Thus, somewhat less obscuration of the ceiling by the smoke layer seems to have occurred here than in the full-scale bedroom test. No overload of the lock-in amplifier took place and the readings are reliable throughout the plotted time interval. "Ceiling" and "cold-plate" radiances computed in the manner discussed earlier are shown in Figures 8.9 and 8.10. Ceiling values are also shown on an expanded scale in Figure 8.11, and temperatures derived from the ceiling radiances are shown in Figure 8.12. The peak values reached in this test are appreciably lower than those of the bedroom fire test.

Conclusion:

The results demonstrate that the radiative flux received by the floor from above comes almost entirely from the hot smoke layer. The ceiling is obscured by the smoke layer and contributes only a small fraction of the radiative flux. This conclusion is in agreement with results obtained at the National Bureau of Standards.[1]

REFERENCE

1. Quintiere, J., "Some Observations on Building Corridor Fires," Fifteenth Symposium (International) on Combustion (in press).

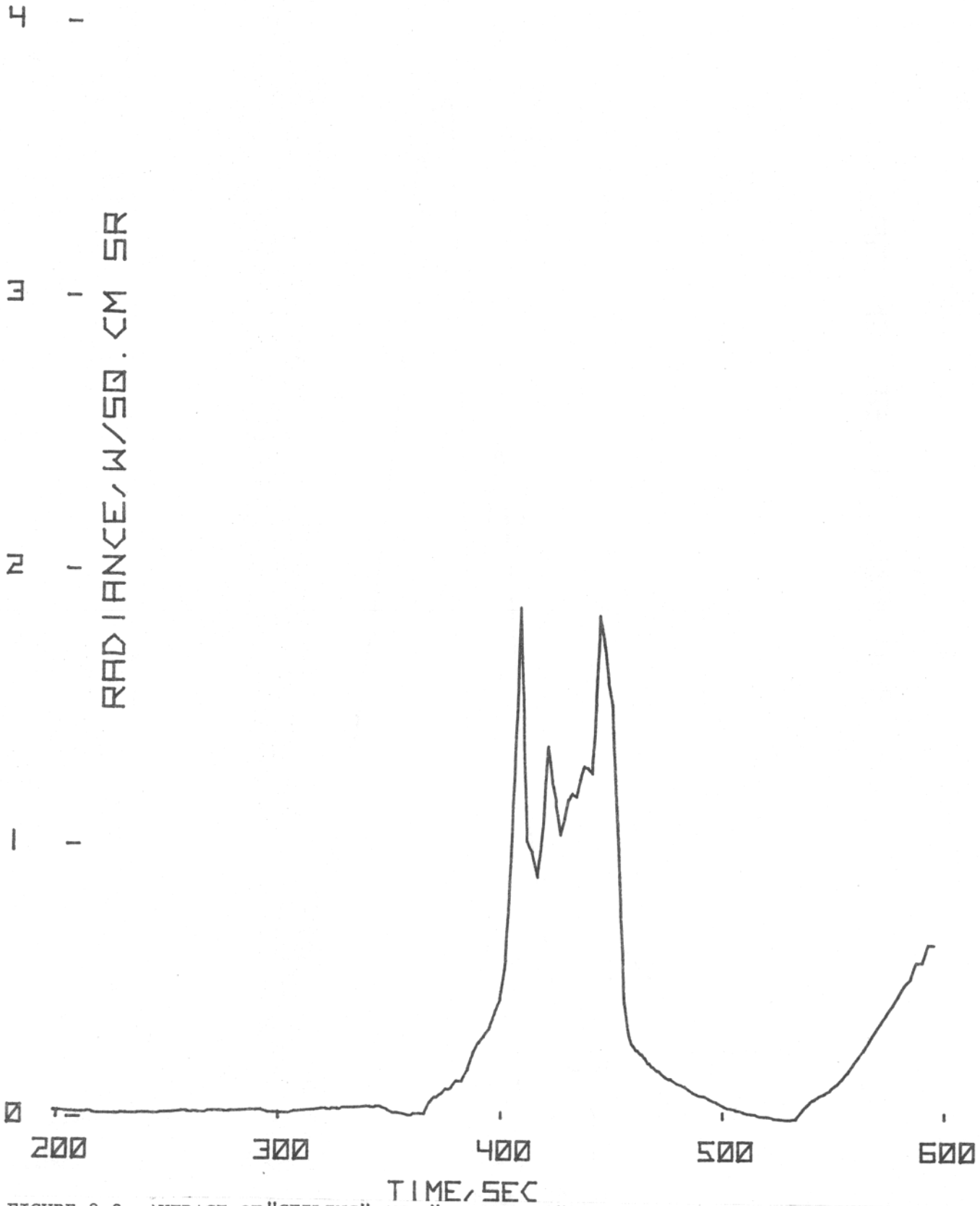

FIGURE 8.2 AVERAGE OF "CEILING" AND "COLD-PLATE" RADIANCE VERSUS TIME AFTER IGNITION FOR THE BEDROOM FIRE

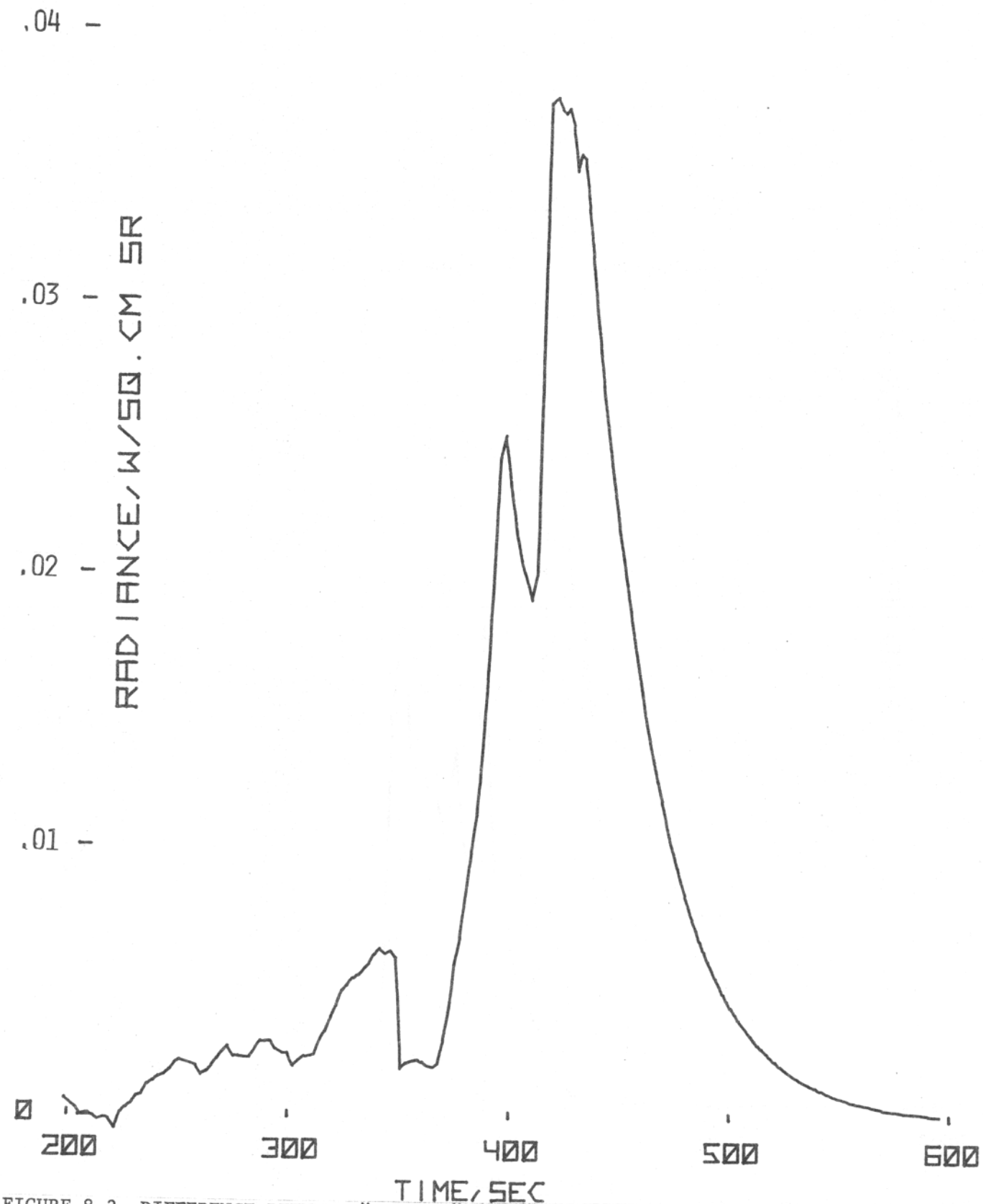

FIGURE 8.3 DIFFERENCE BETWEEN "CEILING" AND "COLD-PLATE" RADIANCE VERSUS TIME AFTER IGNITION FOR THE BEDROOM FIRE

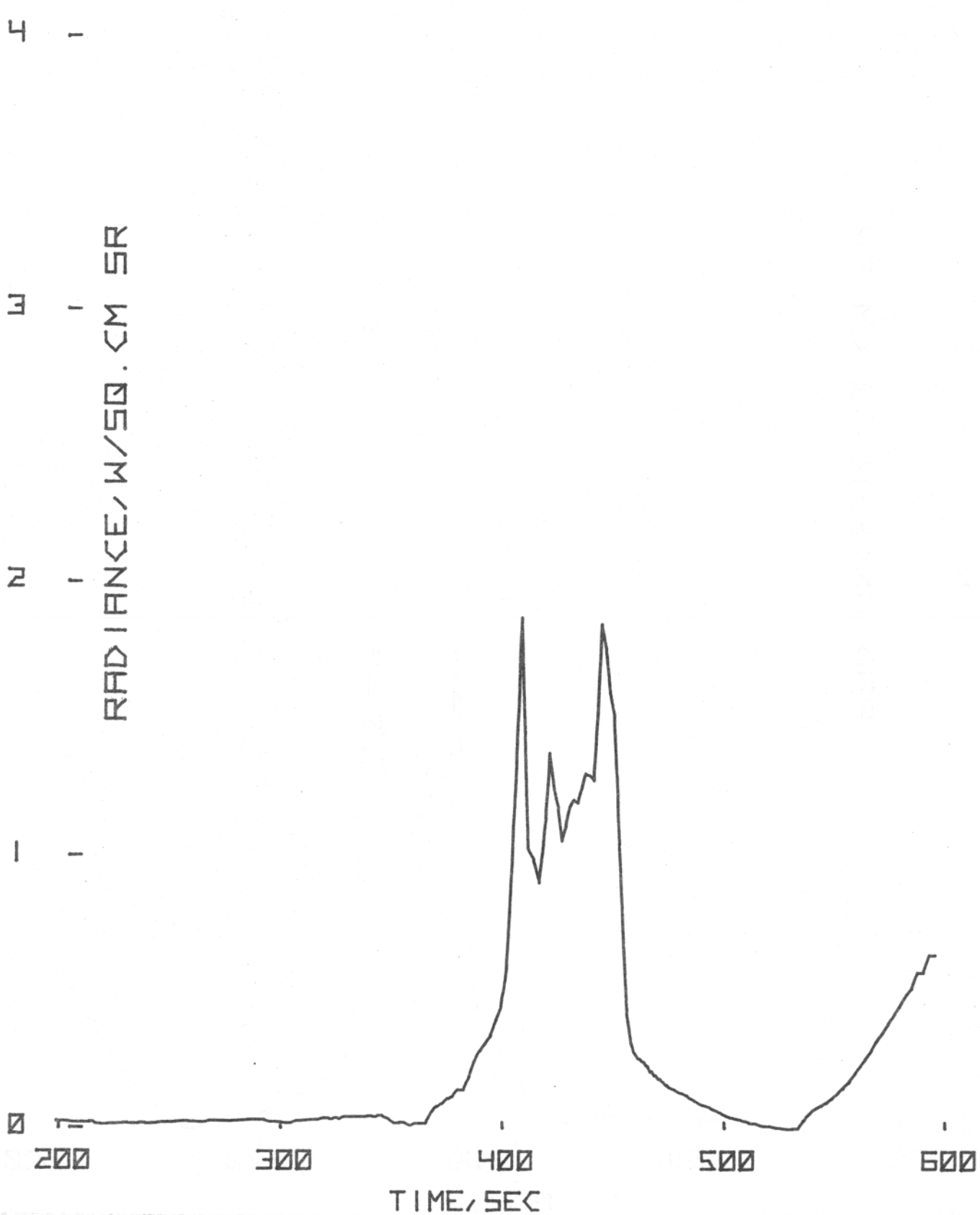

FIGURE 8.4 "CEILING" RADIANCE VERSUS TIME AFTER IGNITION FOR THE BEDROOM FIRE

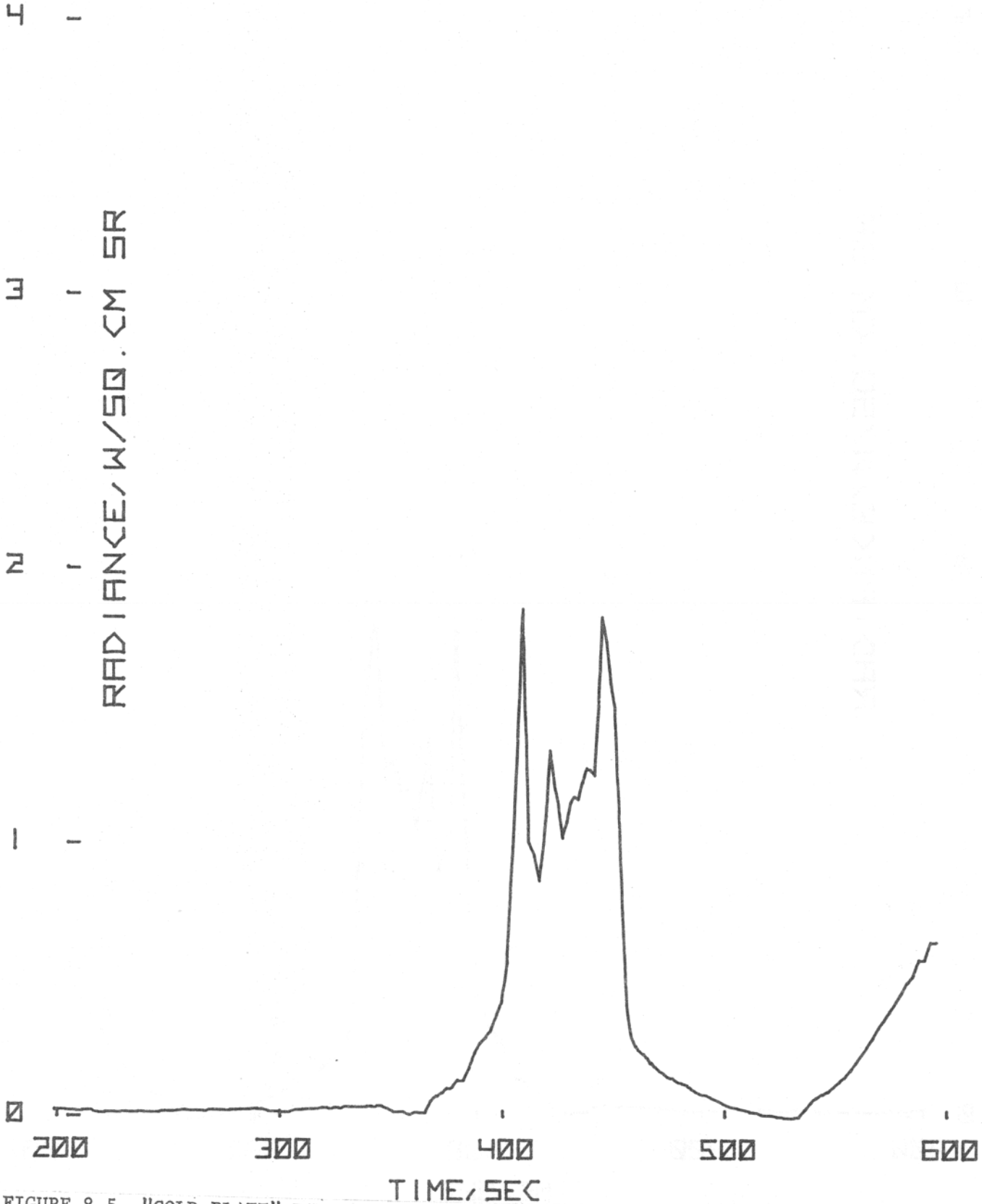

FIGURE 8.5 "COLD-PLATE" RADIANCE VERSUS TIME AFTER IGNITION FOR THE BEDROOM FIRE

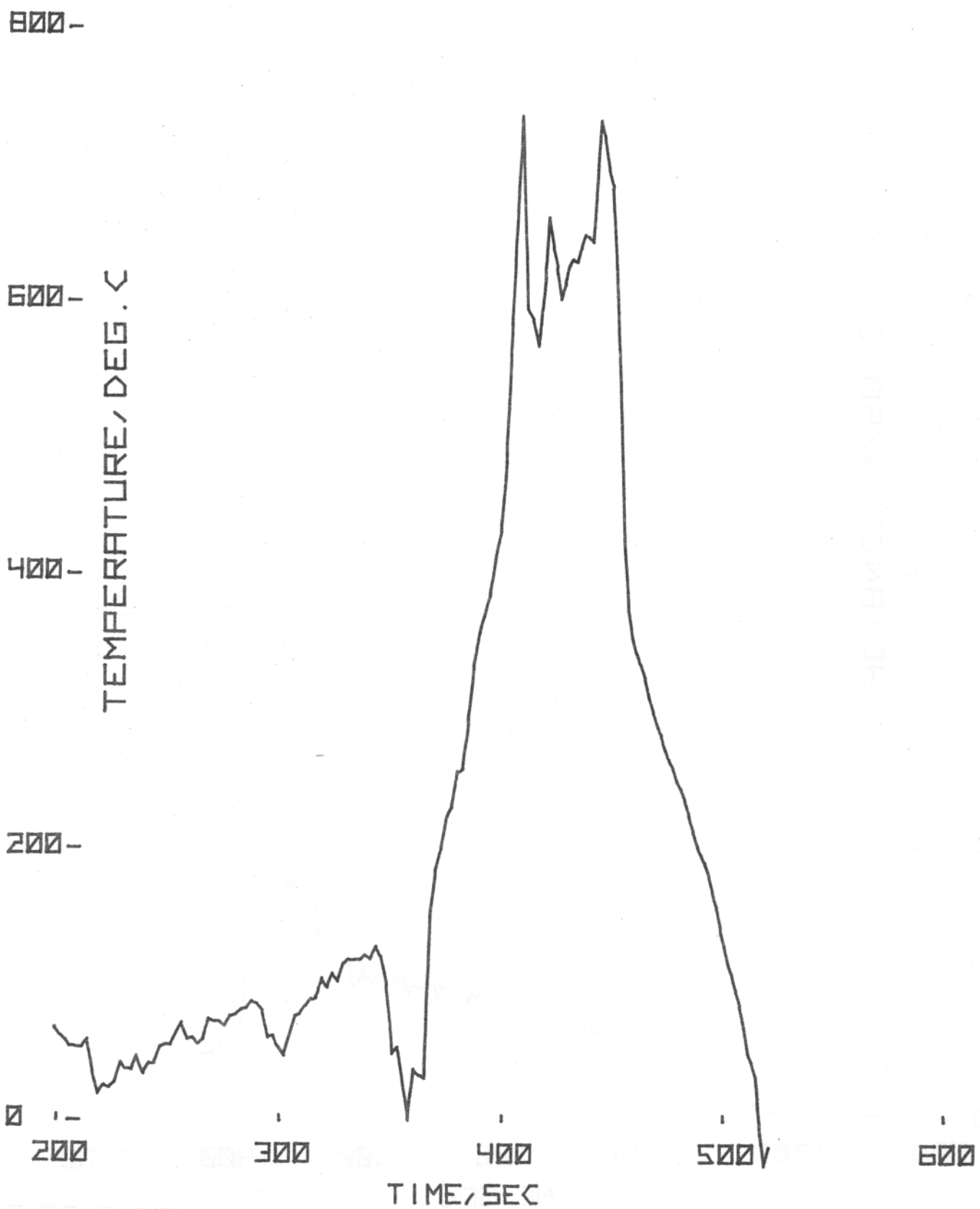

FIGURE 8.6 TEMPERATURE BASED UPON "CEILING" RADIANCE VERSUS TIME AFTER IGNITION FOR THE BEDROOM FIRE

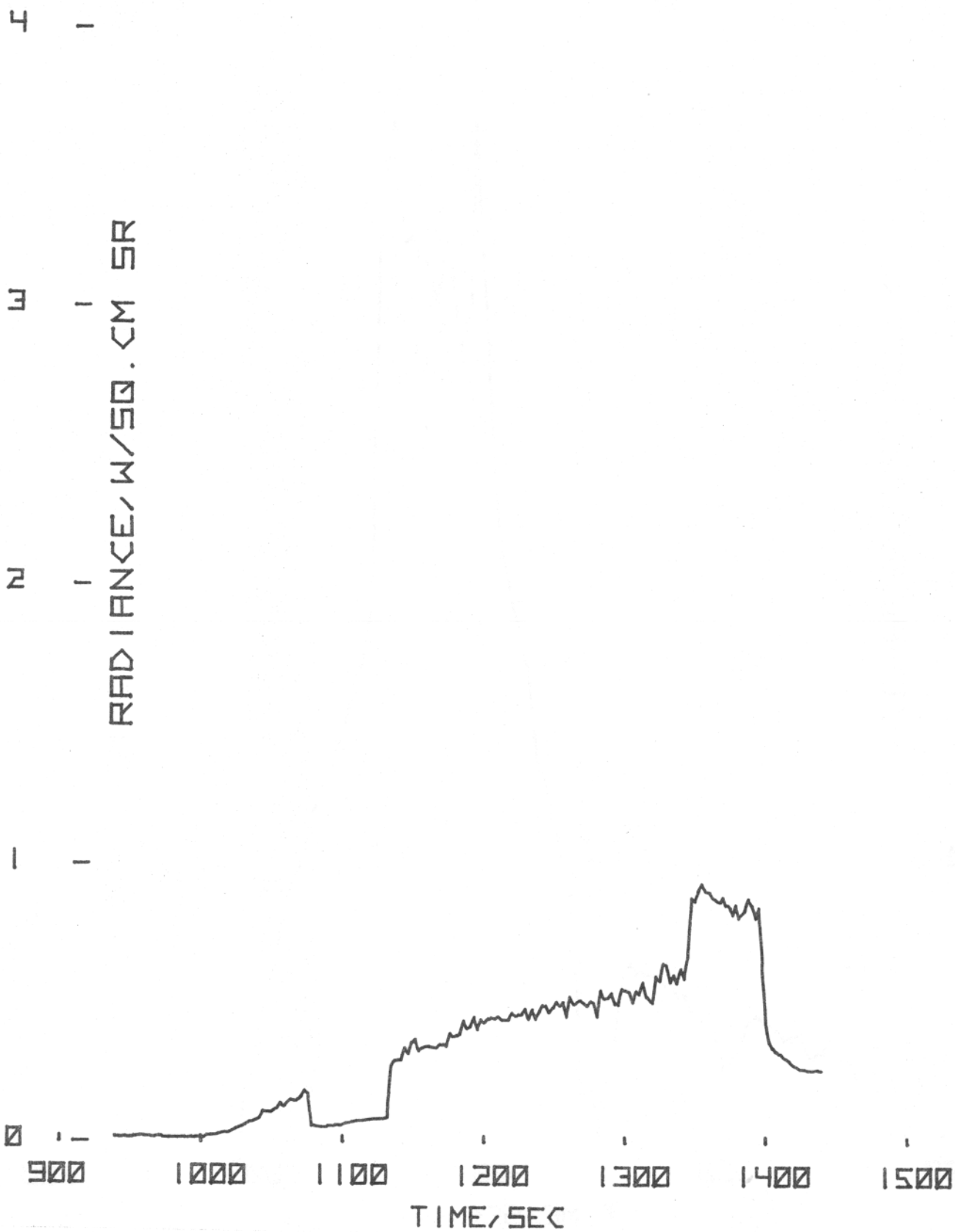

FIGURE 8.7 AVERAGE OF "CEILING" AND "COLD-PLATE" RADIANCE VERSUS TIME AFTER IGNITION FOR THE PAN FIRE

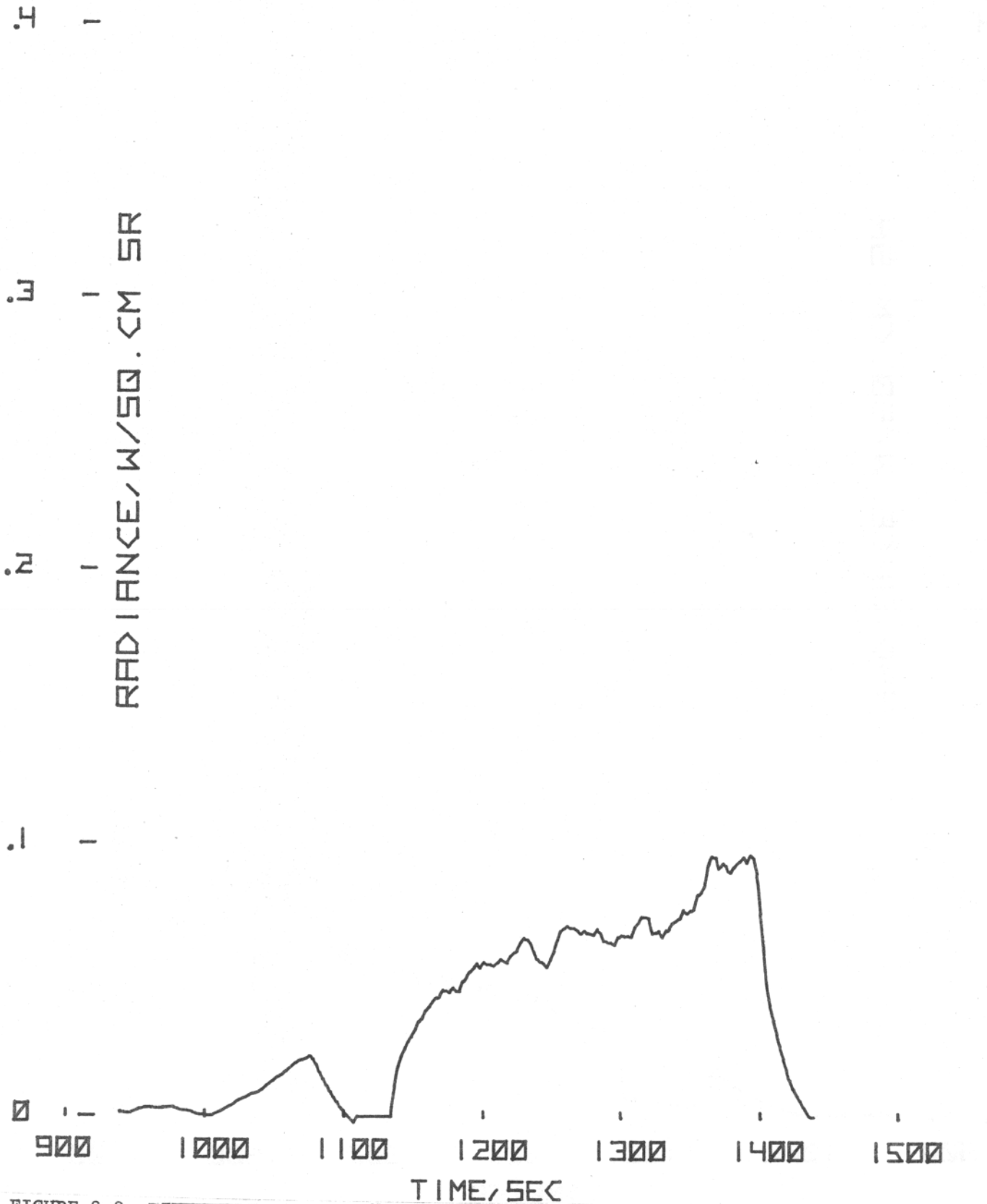

FIGURE 8.8 DIFFERENCE BETWEEN "CEILING" AND "COLD-PLATE" RADIANCE VERSUS TIME AFTER IGNITION FOR THE PAN FIRE

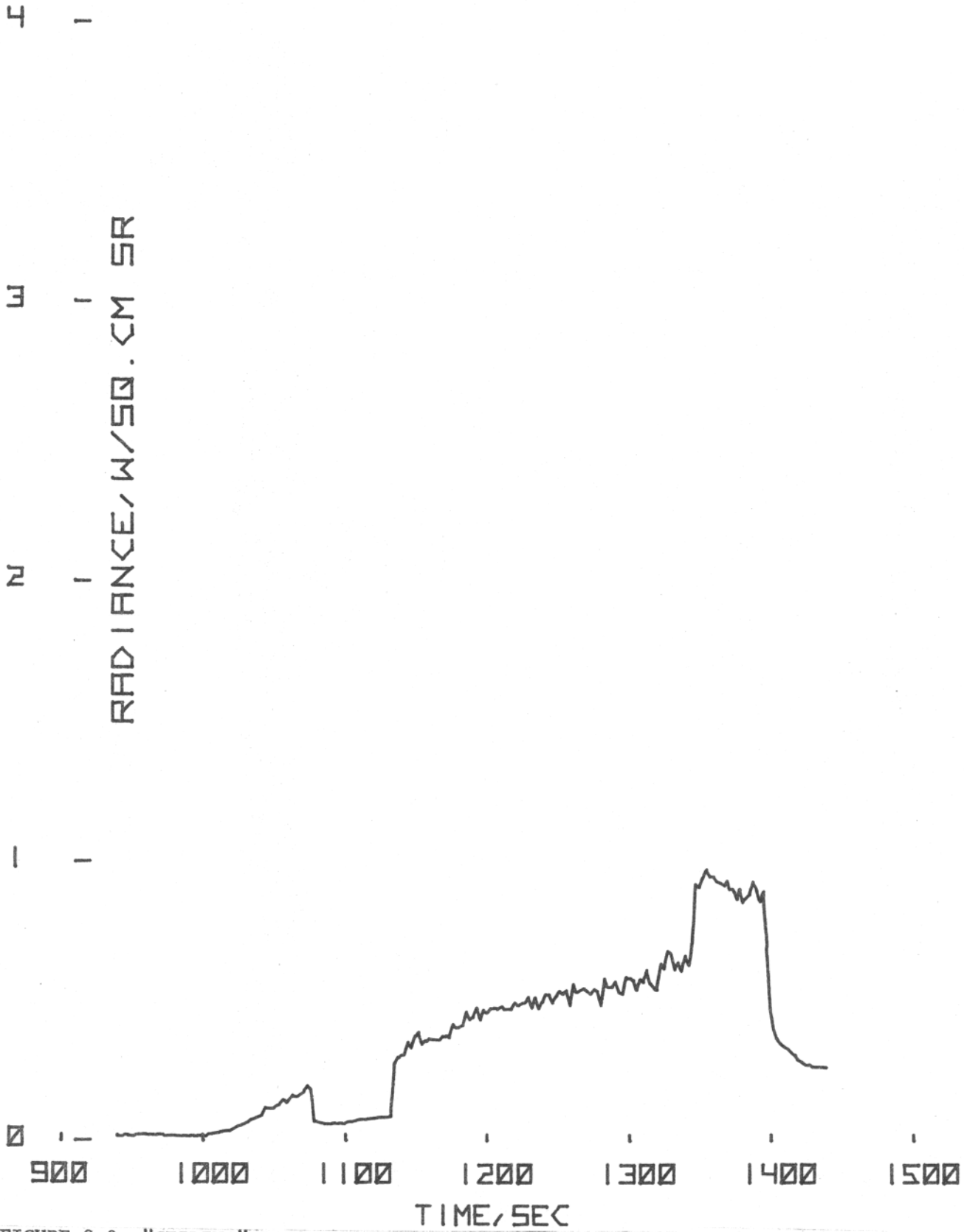

FIGURE 8.9 "CEILING" RADIANCE VERSUS TIME AFTER IGNITION FOR THE PAN FIRE

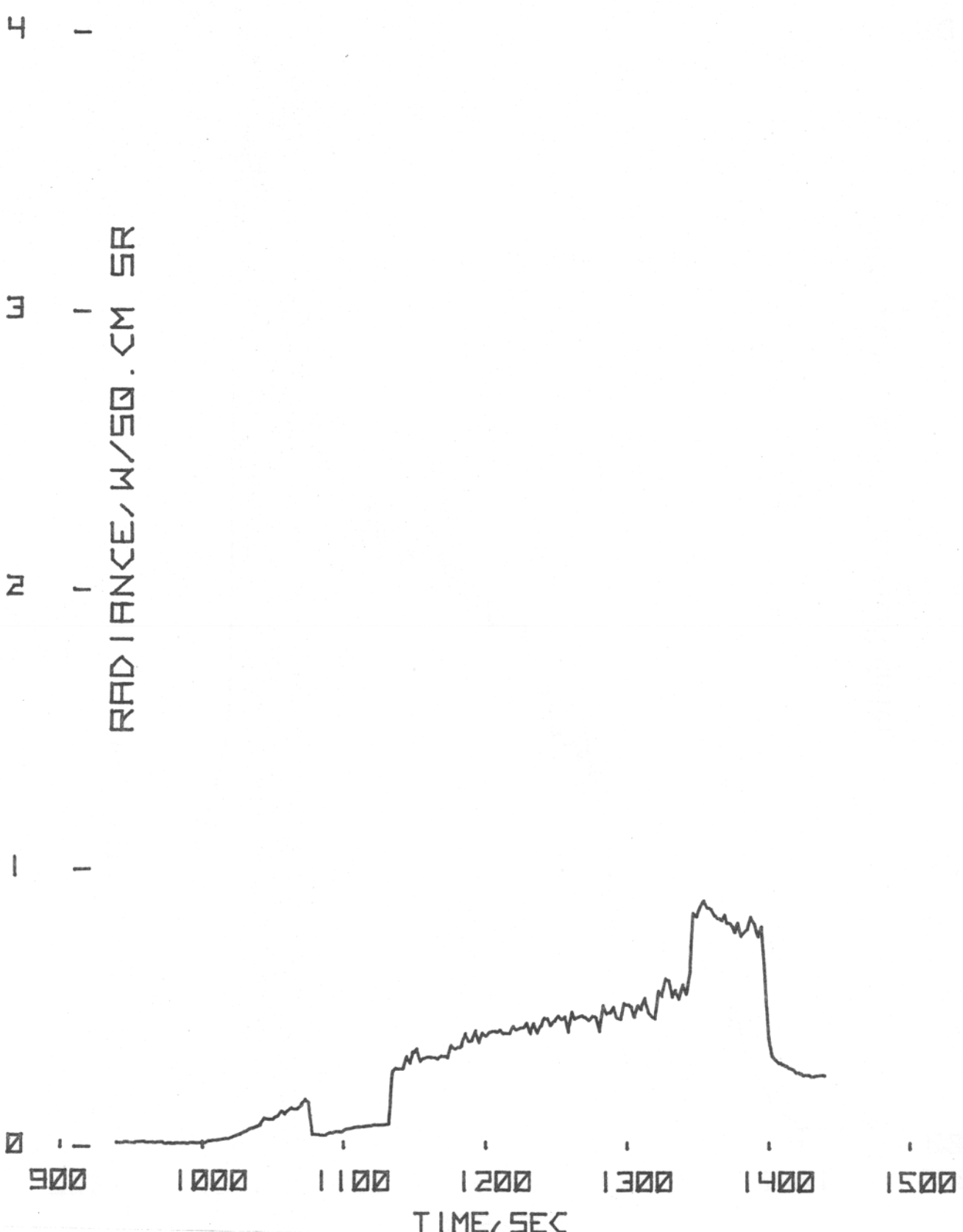

FIGURE 8.10 "COLD-PLATE" RADIANCE VERSUS TIME AFTER IGNITION FOR THE PAN FIRE

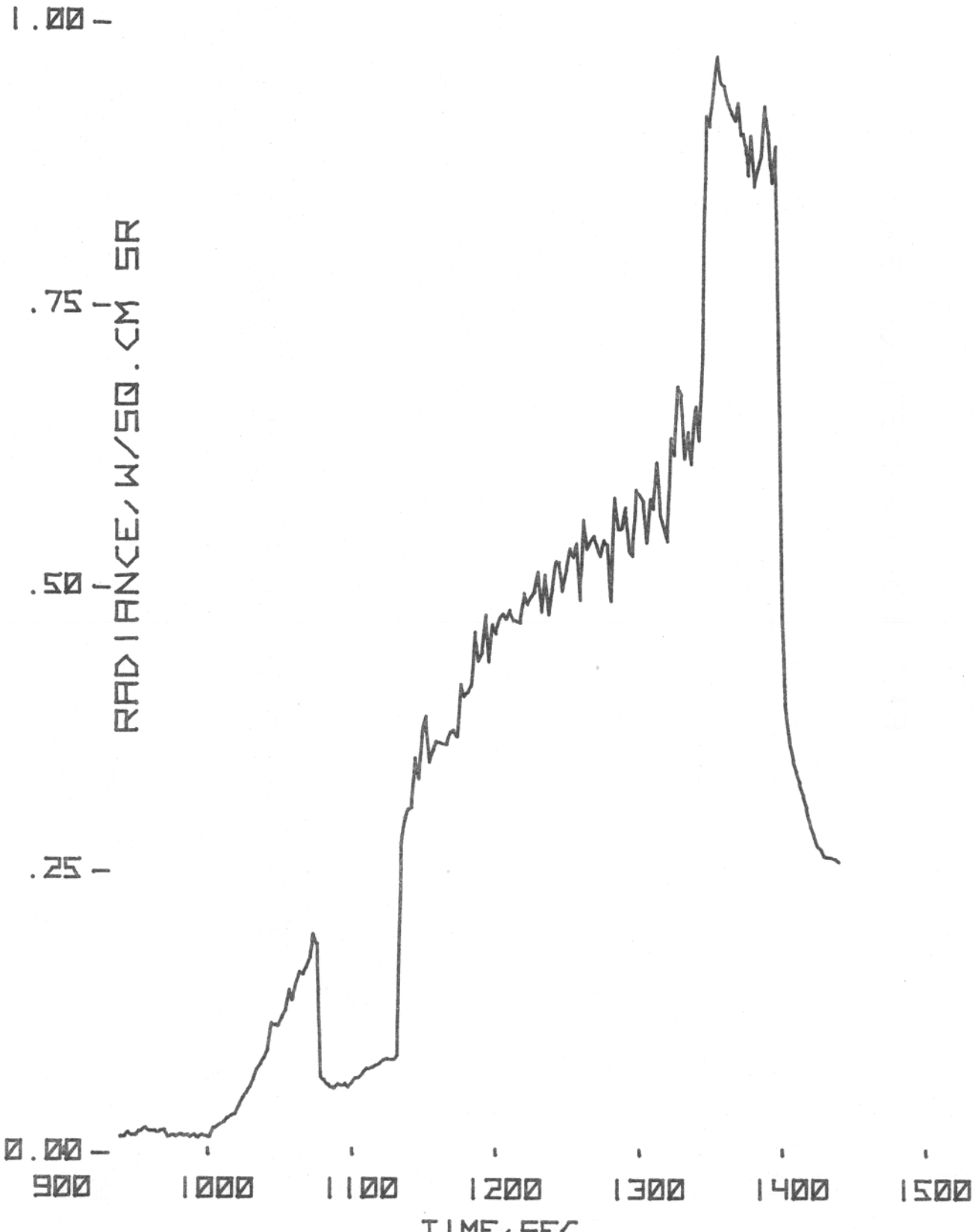

FIGURE 8.11 "CEILING" RADIANCE ON EXPANDED SCALE VERSUS TIME AFTER IGNITION FOR THE PAN FIRE

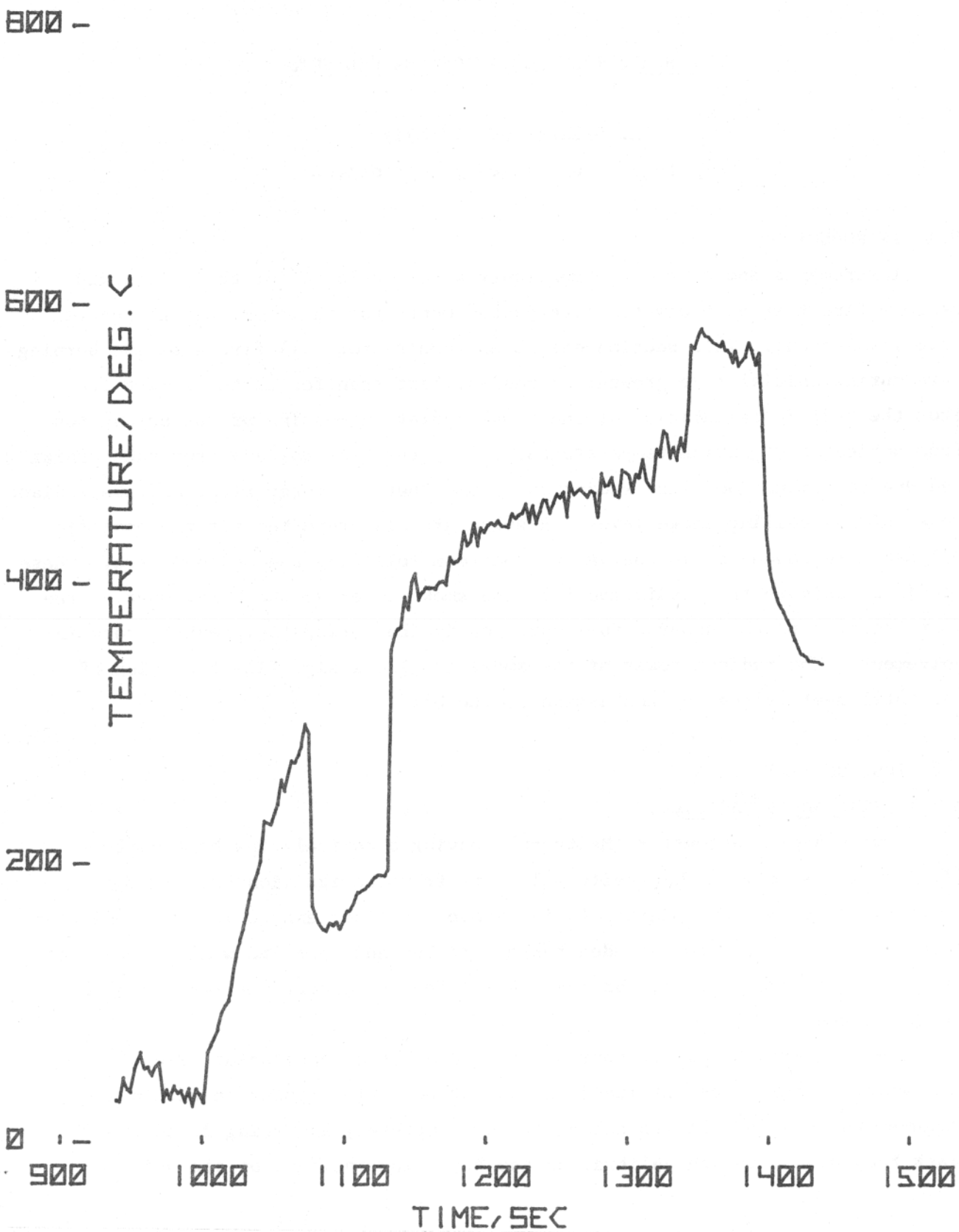

FIGURE 8.12 TEMPERATURE BASED UPON "CEILING" RADIANCE VERSUS TIME AFTER IGNITION FOR THE PAN FIRE

IX

FULL SCALE TEST RADIATION MEASUREMENTS

L. Orloff and J. deRis
Factory Mutual Research Corporation

9.1 INTRODUCTION

Instruments and measuring techniques were developed for the full-scale bedroom fire test to study the fire development from ignition through general room involvement. This section discusses results for: 1) fire size and burning rate during initial fire growth; 2) radiant heat transfer to the wall 6 ft from the bed; 3) calculation of the smoke radiation heating of the bureau top from ambient to ignition temperatures; and 4) the heat release from the burning bed due to combustion, fire radiation, plume thermal energy flux, and the radiant power of the ceiling smoke layer. Results are also reported for the paraffin oil pan fire conducted in the vacated bedroom following the bedroom fire. These findings indicate that radiation from the smoke layer accounts for most of the heat transfer to the unburnt fuel surfaces in the period incipient to room involvement. The radiant power of the smoke is also a significant portion of the total heat release by combustion of the bed.

9.2 INSTRUMENTATION

9.2.1 Wide Angle Radiometer

A wide angle radiometer (Medtherm), having a conical-view half-angle = 57.5°, was placed in the opposite wall 6 ft from the ignition point, I, as shown in Figure 9.1 by point A, 45 in. above the floor and 20 in. from the rear wall. Its field of view included the entire bed and opposite wall, as well as most of the floor, ceiling, and rear wall. The radiometer was water-cooled and N_2 purged.

The Medtherm radiometer consists of a black flat constantan disc of fixed area which measured the net incident radiant heat flux coming in within its measured half-angle. It was calibrated by completely inserting it into a black body oven. During calibration the heat flux incident on the shielded

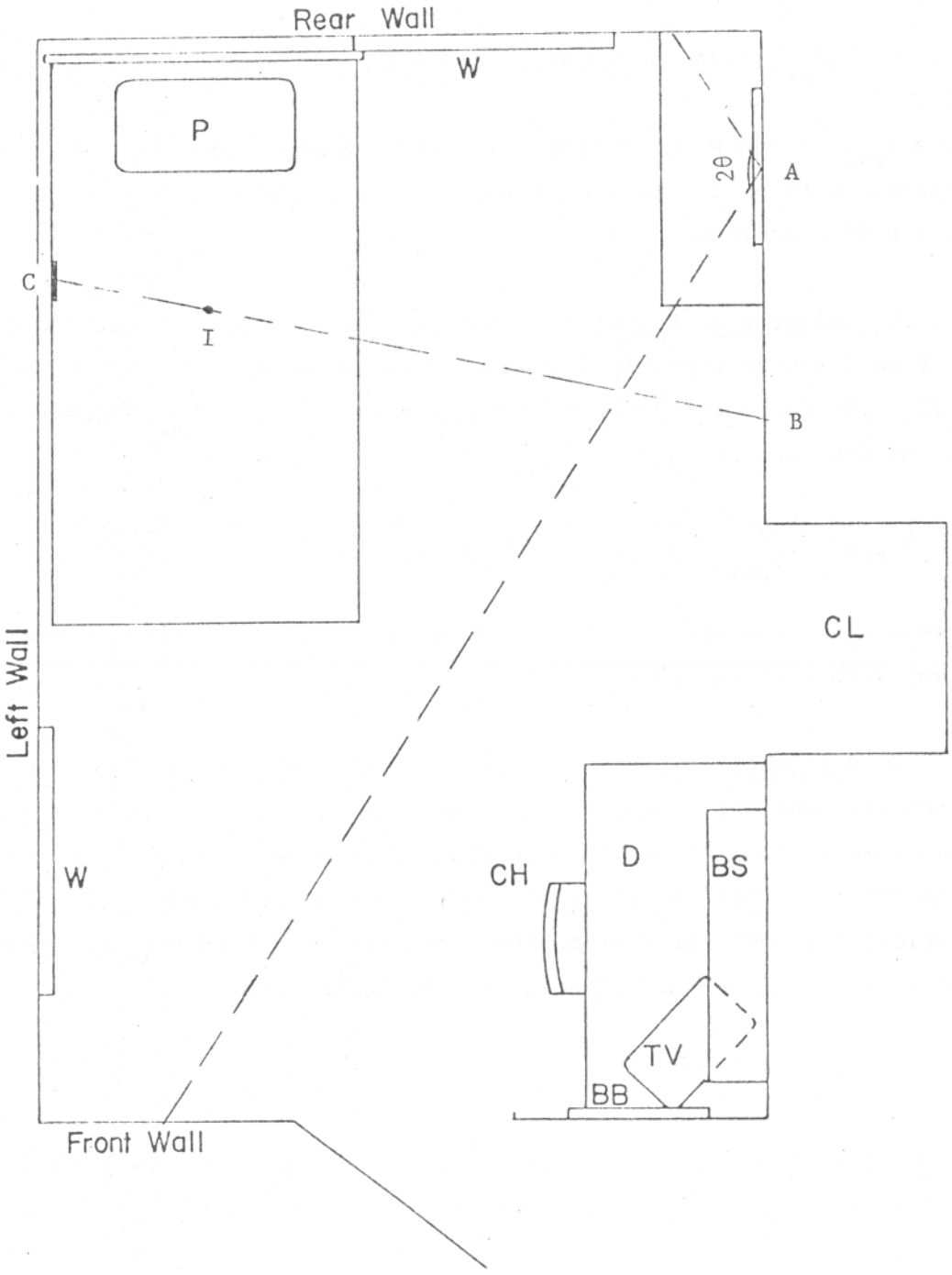

FIGURE 9.1 BEDROOM LAYOUT SHOWING VIEW ANGLE OF WIDE ANGLE RADIOMETER AND LINE-OF-SIGHT OF RAY RADIOMETER

disc $\dot{q}''_{cal}$ was[1]:

$$\dot{q}''_{cal} = 2\pi \int_0^{\theta} \cos\phi\sin\phi \left(\frac{\sigma(T^4_{oven}-T^4_{rad})}{\pi}\right)d\phi = \sigma(T^4_{oven}-T^4_{rad})\sin^2\theta$$

where T_{rad} is the water cooled radiometer temperature. This result was in agreement with an independent calibration made with the radiometer viewing the black body oven from outside.

9.2.1.1 Calibration Factor #1: For the case of the incident radiant flux coming from a source entirely within the radiometer field of view (such as, for example, the flame radiation before flashover). Here the radiometer responds to all the incident radiation, $\dot{q}''_{rad}$, so that

$$\dot{q}''_{rad} = \frac{E_{rad}\dot{q}''_{cal}}{E_{cal}} = \frac{E_{rad}\sigma}{E_{cal}} (T^4_{oven}-T^4_{rad}) \sin^2\theta = 0.00256\ E_{rad}\ (watts/cm^2)$$

where E_{rad} is the output voltage in millivolts (mv.) after amplifaction by an op-amp with gain of 978.1.

9.2.1.2 Calibration Factor #2: For the incident radiant flux coming from all angles with uniform intensity (such as occurs during calibration within the oven or when the radiometer is completely immersed in a constant temperature smoke field). Here the attenuation due to the radiometer field of view is identical for both calibration and measurement so that the total heat flux incident to the plane wall adjacent to the radiometer is

$$\dot{q}''_{rad} = \frac{E_{rad}\sigma}{E_{cal}} (T^4_{oven}-T^4_{rad}) = 0.00360\ E_{rad}$$

with E_{rad} being the measured output signal (after op-amp amplification of 978.1) in millivolt units as recorded on the cassette tape (see Appendix to this Section).

9.2.2 Ray Radiometer

The ray-radiometer had a 2-in. dia circular aperture of reflecting telescopic design with a Sensors Inc. C-1 sensor at the focus of an 18-in. f.1 mirror and was N_2 purged. With this telescopic design the radiometer is sensitive only to the radiation parallel to its axis, and its output is independent of the distance from the radiation source, provided the radiation is not attenuated by the intervening gas. Its horizontal line of sight was 28 in. above the bedroom floor going from position B (5 ft from the rear wall) passing 8 in. above the ignition point, to the center of a 6-in.-square, water-cooled copper plate, C, on the left wall (31 in. from the rear wall), as shown in Figure 9.1.

Since the ray radiometer is sensitive only to radiation parallel to its axis within its 2-in. aperture, D_{rad}, it measures the radiance (watts/cm^{2}sr) emitted by the flames along its line of sight. Any effects of wall emission were eliminated by the water-cooled target plate. The ray radiometer calibration was obtained by viewing a black body source of diameter $D_{oven} < D_{rad}$ providing[2]

$$I_{rad} = \frac{\sigma}{\pi} (T^4_{oven} - T^4_{rad}) \left(\frac{D_{oven}}{D_{rad}}\right)^2 \frac{E_T}{E_{cal}} = 0.00196\ E_T \ (\text{watts/cm}^2\text{sr})$$

where E_T is its output signal in mv after amplification by a factor of 1233.

The resulting flame radiance is shown in Figure 9.2. The sharp drop in flame radiance at 312 sec from ignition is thought to result from the flames being drawn toward the headboard and out of the field of view of the radiometer. There was no evidence from the movies of smoke obscuration along the radiometer line of sight during this period.

9.2.3 Video-Tape Flame Area Measurements

The ignition and fire growth were filmed with a video-tape camera through a 4-in.-square Pyrex window 48 in. above the bedroom floor, 20 in. from the rear wall. The field of view in the ignition plane was approximately 4 ft square.

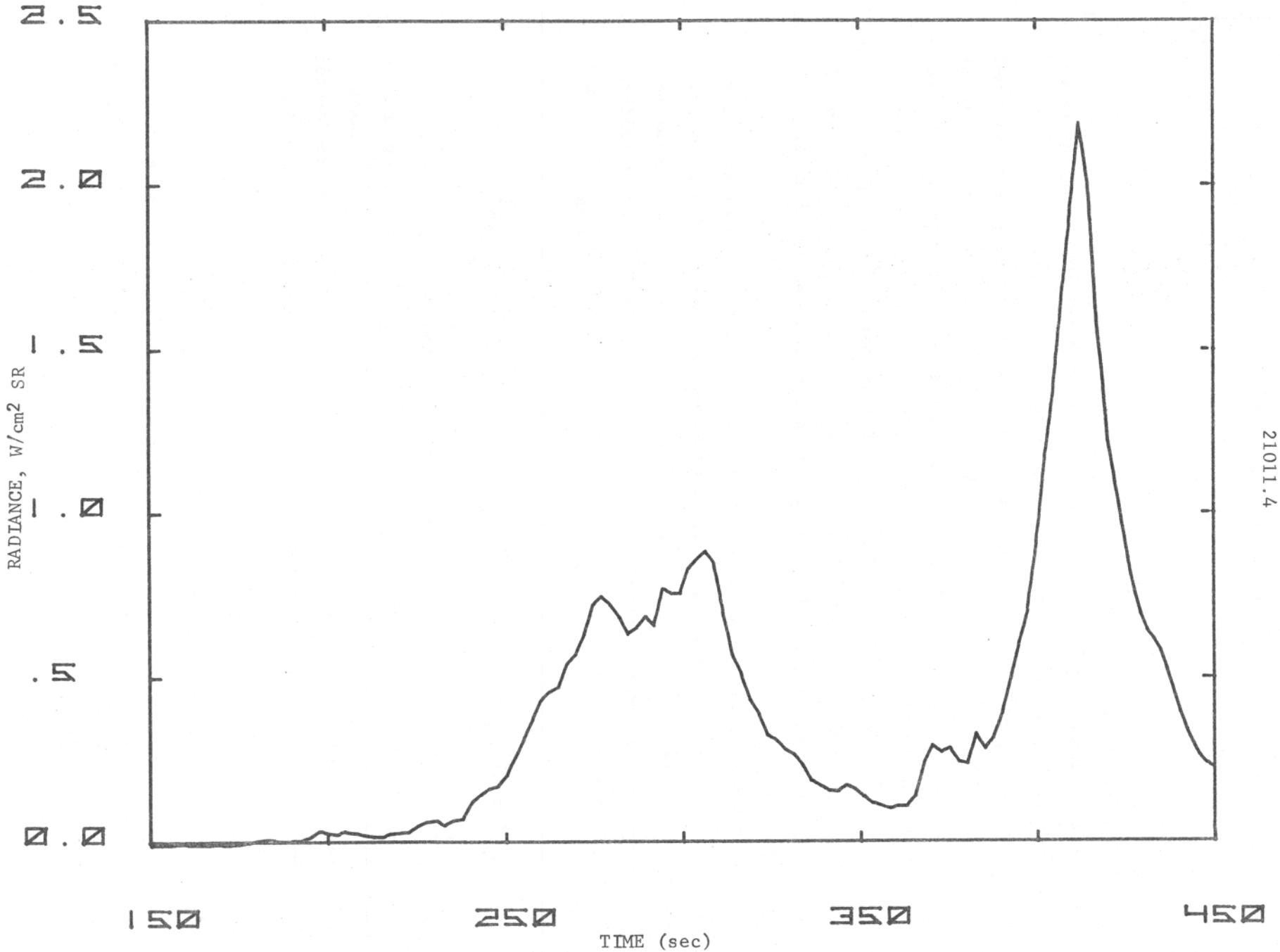

FIGURE 9.2 FLAME RADIANCE VERSUS TIME AFTER IGNITION FOR THE BEDROOM FIRE

The video sound track records time in seconds, initiating (time t=0) 60 sec before the ignition. The flame height and area were measured using 1-ft interval reference marks on the left wall. There was serious smoke obscuration 275 sec after ignition. Figure 9.3 shows the projected flame area versus time from the video tape.

9.2.4 Photographic Flame Area Measurements

1) The flame height and area were also measured from the 35-mm slides #12 through 23, taken by Richard Land at 30-sec intervals. The camera views the flames through the doorway, its optical axis in the plane of the bed covers. The scale at the ignition point was interpolated from reference marks on the door and rear wall. After 6 min the view of the flames was obstructed by the door jamb and smoke. This projected flame area versus time is also shown in Figure 9.3.

2) The third, and best, source of flame height and area measurements was the 16-mm color movie, 12 frames/sec, taken through a window in the front wall left of the door. Ignition is estimated at 11:36:16 on the clock by the bureau. Measurements were averaged from four to five successive frames. In the early stages of the fire, the flame area varied by as much as a factor of 2 within each sequence of frames; thus, the movie is more useful than slides for oscillating flames. This projected flame area versus time is also shown in Figure 9.3. Flame areas and heights measured from this movie are presented in Table 9.1.

9.2.5 Plume Thermal Energy Flux

One can estimate the thermal energy flux of the fire plume from temperature measurements along the axis of the free convective plume above the flames, using the formula given by Alpert[3],

$$Q = .0174 \left[\frac{(T_{max} - T_{room})\, H^{5/3}}{14.9}\right]^{3/2}$$

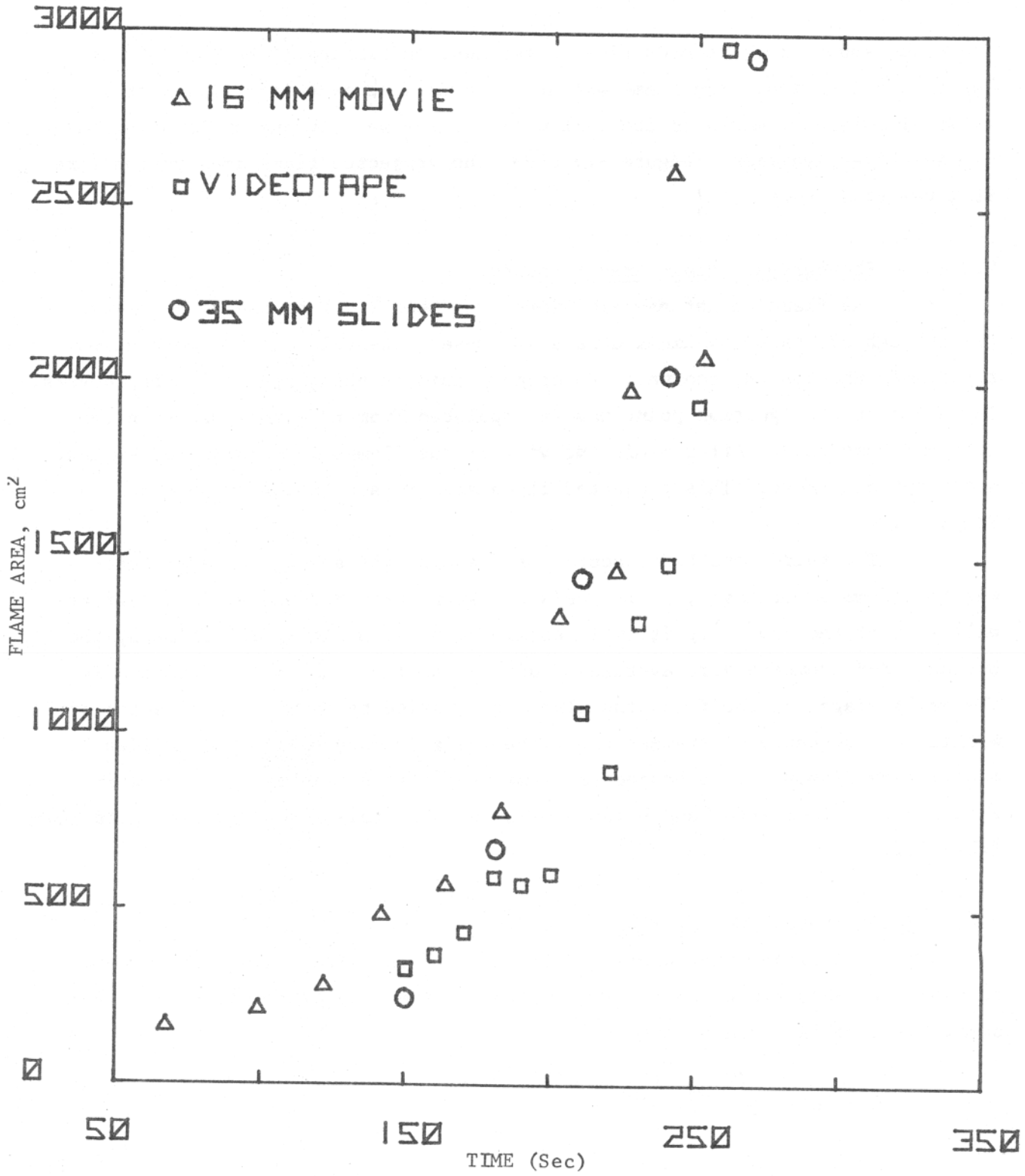

FIGURE 9.3 FLAME AREA VERSUS TIME AFTER IGNITION FOR THE BEDROOM FIRE

TABLE 9.1

MEASUREMENTS OF PROJECTED SURFACE AREA AND FLAME HEIGHT, AND DERIVED BURNING RATES FOR BED FIRE, FROM 16 MM MOVIE

Time (sec)	Flame Area (cm^2)	Flame Height (cm)	Burning Rate (g/sec)
68	62	16	0.079
99	116	24	0.20
122	184	20	0.19
142	386	38	0.72
162	460	37	0.76
182	678	45	1.24
202	1231	51	2.01
222	1359	59	2.63
227	1867	75	4.41
232	2090	63	3.59
242	2490	70	4.59
252	1960	48	2.31

where T_{max} (in °F) is the centerline temperature, H is the height above the fire seat in feet, and Q is the convective power output in kilowatts. T_{max} is obtained from t.c. #119 and #120 respectively, 6.33 ft and 3.83 ft directly above the ignition point. The ambient room temperature is taken from aspirated t.c. #112 (33 in. across from and 7 in. below ignition point). (The results are shown in Figure 9.7.) The temperature data were obtained from Reference 4. After 302 sec the movie shows the flames leaning toward and contacting the rear wall, causing the fire plume center to miss the two thermocouples above the ignition point, so that for the most interesting part of the fire, after 302 sec, this method is invalid.

9.2.6 Smoke Radiation

The wide angle radiometer receives substantial radiant flux from the ceiling smoke layer. The contribution from this source is assessed here.

Consider a surface element of temperature T_s receiving radiation uniformly through a full hemispherical field of view from an optically thick smoke cloud of temperature T_c. The radiance of the smoke is I (watts/cm^{2}sr) = $\sigma(T_c^4 - T_s^4)/(\pi)$.

The irradiance of the surface element is:

$$\dot{q}''(\text{watts/cm}^2) = 2\pi \int_0^{\pi/2} \cos\theta \sin\theta \, I \, d\theta = \pi I.$$

A wall surface element immediately below the smoke layer received smoke radiation from approximately the upper half of its hemispherical field in view, i.e., $\dot{q}''(\text{watts/cm}^2) = (\pi/2)I$. This approximates the physical situation, in which the Medtherm radiometer is a short distance below the smoke layer. The smoke radiance measurements were made by G.H. Markstein using a scanning radiometer (Section VIII) viewing the smoke layer from the floor.

9.2.7 Combustion Heat Release

The heat liberated by combustion of the bed materials was calculated from 1) burning rate measurements (g/sec) obtained from the strip chart record of bed weight loss versus time; and 2) the measured heat of combustion (H_c = 6600 cal/g) for the polyurethane mattress. The pan fire heat liberation rate was similarly found, using H_c = 9800 cal/g for paraffin oil.

The burning rate, $\dot{m}$ (g/sec) can also be estimated from the flame height and area measurements discussed previously, using Emmons' relation,[5]

$$\frac{h}{d} = 3\left[10^6 \frac{\dot{m}^2}{d^5}\right]^{.25}.$$

Assuming a conical fire shape (A = 1/2 dh), $\dot{m} = \frac{A\,h^3}{40.5} \times 10^{-3}$, where A is the area in cm^2, d is the diameter at the base in cm, and h is flame height in cm. The burning rate versus time is plotted in Figure 9.4 and is shown in the fourth column of Table 9.1.

9.3 SMOKE AND FIRE CONTRIBUTIONS TO WALL IRRADIATIONS

Medtherm calibration formulas were given earlier for the situation in which 1) the source is entirely within the field of view of the Medtherm (type I) and 2) the radiometer receives radiation uniformly throughout all angles (type II). The bed fire is a type I source, while the irradiation ($watt/cm^2$) of the wall adjacent the Medtherm by the hot smoke cloud approximates the type II situation with correction for the smoke layer filling only half of the radiometer field of view. Since explicit discrimination of the contributions from the respective source types producing the resultant radiometer signal cannot be accomplished without making very casual ex post facto assumptions, the irradiation of the Medtherm is expressed here in units of millivolts (mv) of Medtherm output signal. The irradiation ($watt/cm^2$) at the wall adjacent to the Medtherm, produced solely by the bed fire is calculated from the radiance measurement ($watt/cm^2 sr$) made with the ray radiometer. The effective Medtherm voltage signal, $E_{eff\text{-}medF}$(mv), produced by Medtherm exposure to the fire is found using Medtherm calibration formula #1, given

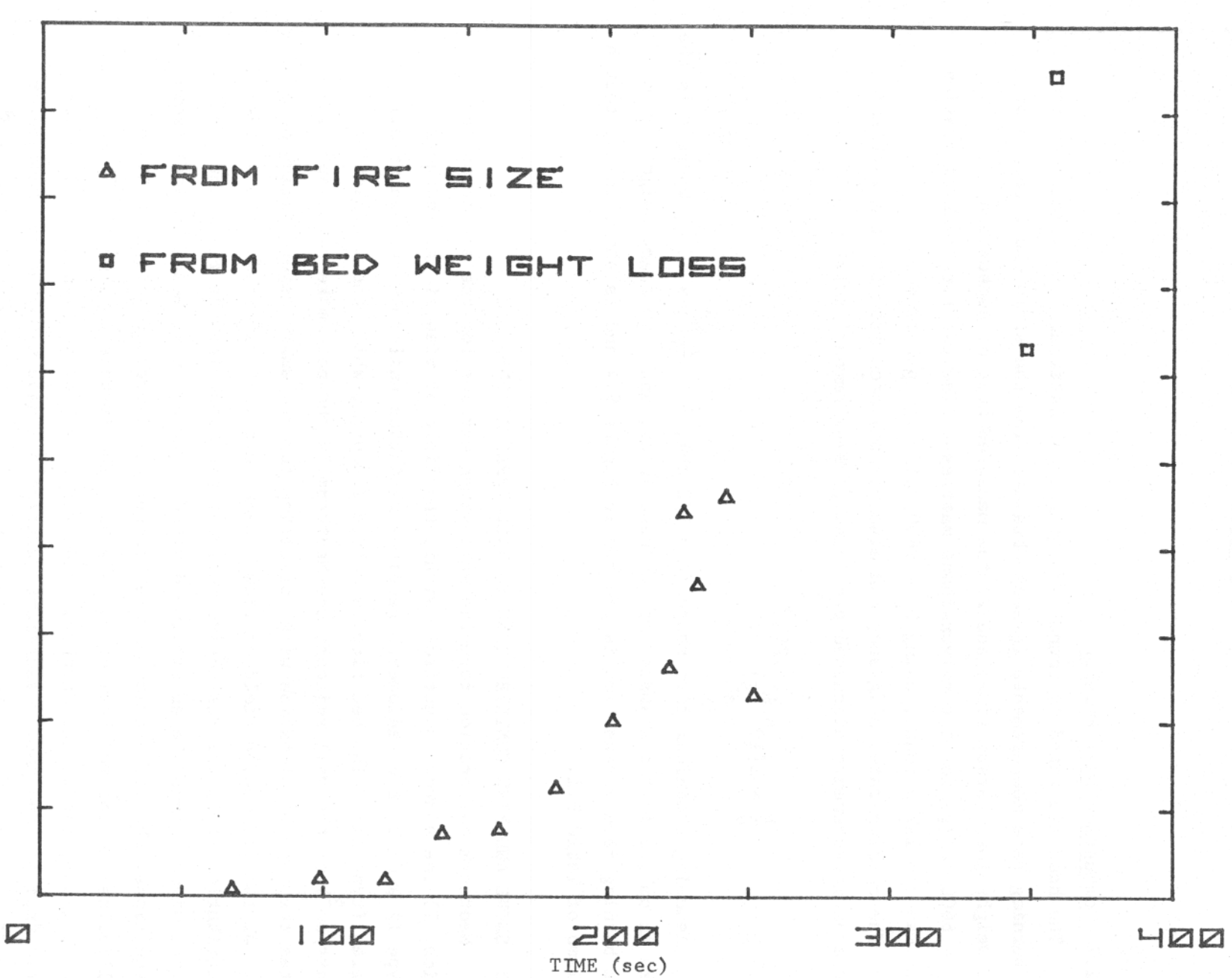

FIGURE 9.4 EARLY BURNING RATE VERSUS TIME AFTER IGNITION FOR THE BEDROOM FIRE

this calculated irradiation due to the fire. This procedure permits comparison of the actual Medtherm output (mv) (i.e., the voltage response to all radiation directed at the instrument) to the derived Medtherm voltage response (mv) to the fire alone. Similarly, the irradiation (watt/cm^2) on the vertical wall by the smoke cloud is calculated from the smoke radiance (watt/cm^{2}sr) measurement. Since the smoke cloud resembles a type II source, Medtherm calibration factor #2 is used to find the derived Medtherm voltage response, $E_{\text{eff-med}_S}$ (mv), due to the smoke radiation.

Figure 9.5 shows the wall irradiance for the bedroom fire in terms of:

1) The actual Medtherm voltage output in mv; and

2) The derived Medtherm response to the smoke radiation, in mv. This is calculated as follows: the irradiance of the wall adjacent the Medtherm by the hot smoke cloud is found from smoke radiance (watt/cm^{2}sr) given in Section VIII. As shown in Section 9.2.6, the irradiance received by the wall when the smoke layer is above the Medtherm is

$$\dot{q}_{\text{smoke}(w/cm^2)} = \pi/2\ [I_{\text{smoke}(w/cm^2 sr)}].$$

The Medtherm output in mv from exposure to this smoke irradiation, $E_{\text{eff-med}_S}$ (mv)

$$E_{\text{eff-med}_S}\ (\text{mv}) = \frac{\dot{q}''_{\text{smoke}}}{\sigma(T^4_{\text{oven}} - T^4_{\text{rad}})/E_{\text{med-cal}}} = \frac{\pi/2\ I_{\text{smoke}}}{.0036}$$

The right-hand ordinate expresses the wall irradiance due to the smoke in watts/cm^2.

After 427 sec the smoke layer descends over the Medtherm, filling its field of view. The irradiance then becomes $q = \pi\ I_{\text{smoke}}$, and the smoke curve in Figure 9.5 after 427 sec is found as $E_{\text{eff-med}_S} = \pi\ I_{\text{smoke}}/.0036$. The smoke and Medtherm output curves are strikingly similar after 427 sec, with smoke radiation accounting for 80-90 percent of the total output of the Medtherm (see Section X). This shows good agreement between the independently measured smoke

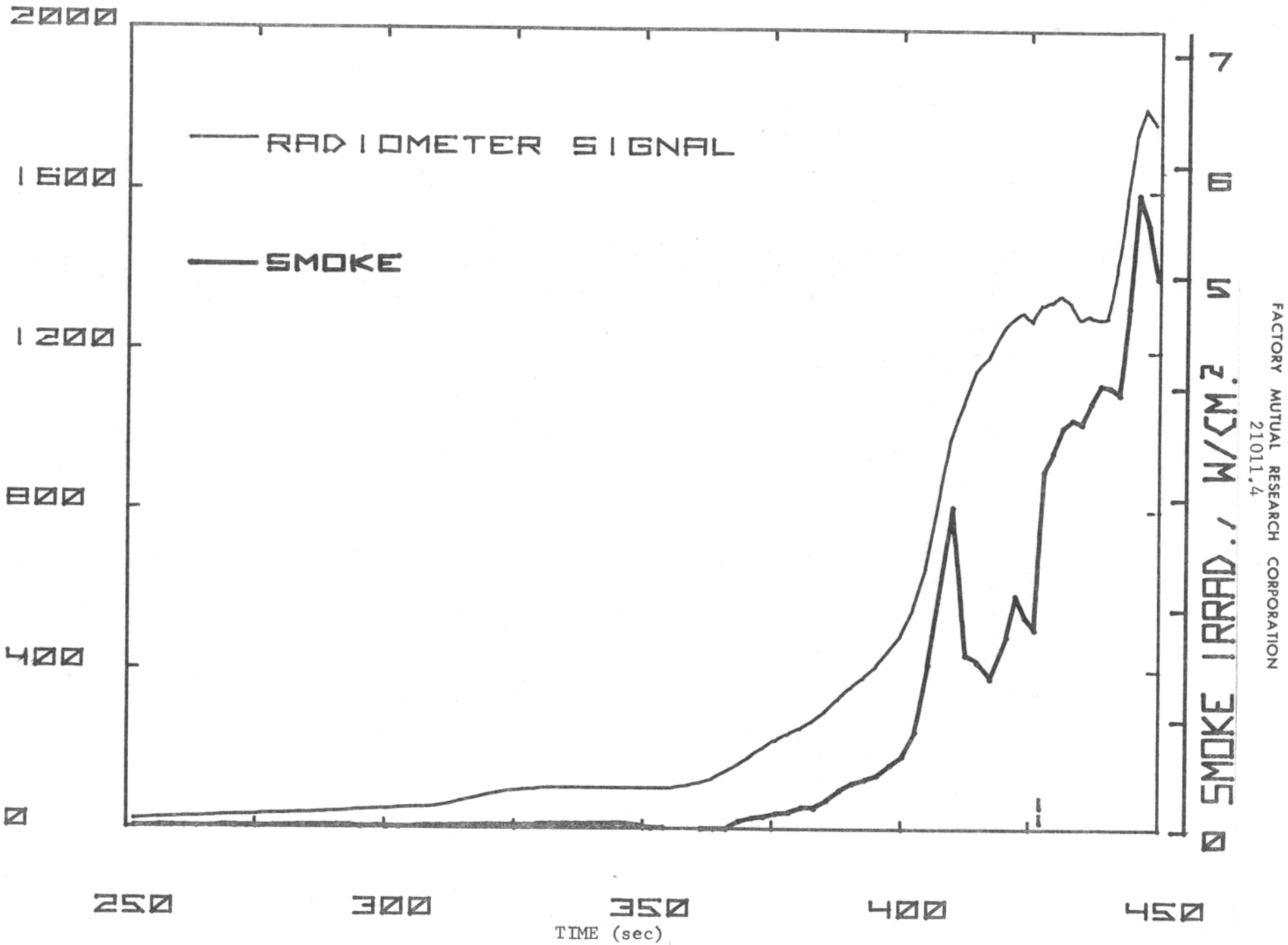

FIGURE 9.5 RADIOMETRIC SIGNAL VERSUS TIME AFTER IGNITION FOR THE BEDROOM FIRE

radiance and the Medtherm measurement at a different location.

The derived Medtherm voltage response to the bed fire radiation is not shown due to the lack of valid flame radiance measurements with the ray radiometer and flame areas after 275 sec.

Figure 9.6 shows similar measurements for the pan fire. The three curves show, respectively:

1) The actual Medtherm voltage in mv;

2) $E_{eff-med}(mv) = \pi/2\ I_{smoke}/.0036$. The extreme right-hand ordinate shows wall irradiance due to smoke in w/cm^2;

3) The derived Medtherm voltage response, $E_{eff-med_F}$, to the pan fire radiation, in mv. This is found by first calculating the irradiance, q (W/cm^2), of the wall adjacent the Medtherm and a) radiance, I_{rad} ($W/cm^2 sr$), measurements made with the ray radiometer, and b) the projected flame surface area, which is assumed that of an isosceles triangle of base equal to the pan diameter and height equal to the pan-to-ceiling distance:

$$\dot{q}''_{rad} = \frac{\text{flame area}}{R^2}\ (\text{sr.}) \quad I_{rad}\ (w/cm^2 sr)$$

where R is the flame-to-Medtherm distance. $I_{rad} = 0.00196\ E_T$ (mv) from Section 9.2.2 above. Thus,

$$\dot{q}''_{rad}(w/cm^2) = \frac{9755\ cm^2}{33445\ cm^2} \times 0.00196\ E_T\ (mv) = .000572\ E_T(mv).$$

We see that this derived Medtherm response (top curve) due to direct pan fire radiation apparently accounts for all the observed Medtherm response with the smoke radiation being less important for the pan fire.

The right-hand ordinate in Figure 9.6 gives the calculated direct fire irradiance $\dot{q}_{rad}(W/cm^2)$.

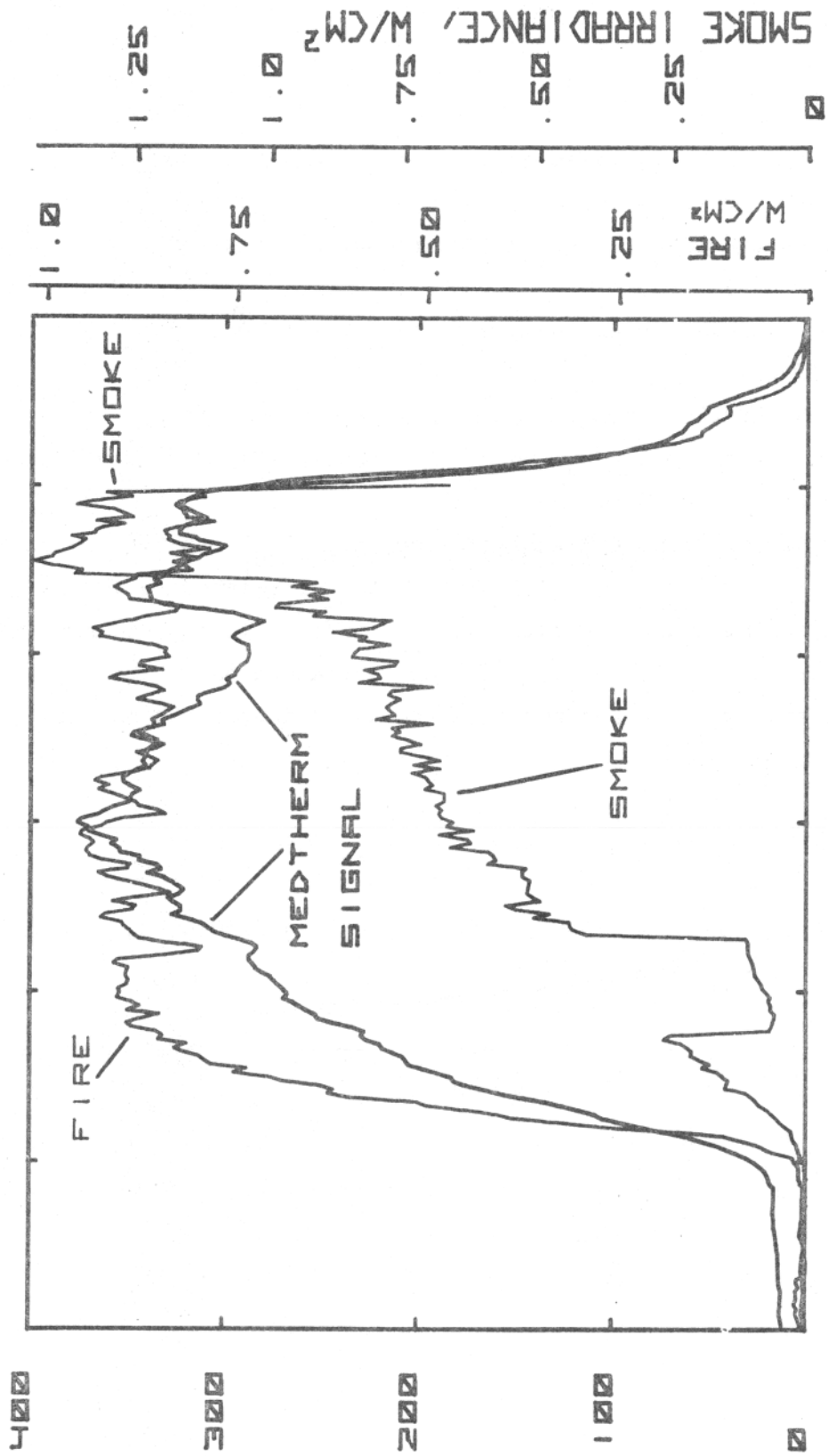

FIGURE 9.6 RADIOMETRIC SIGNAL VERSUS TIME AFTER IGNITION FOR THE PAN FIRE

9.4 RATE OF HEAT RELEASE BY COMBUSTION, BY CONVECTION, AND BY RADIATION FROM THE CEILING SMOKE

Figure 9.7 shows:

1) the combustion heat release from the burning mattress, from Section 9.2.7 above, using bed weight-loss data;

2) the plume thermal energy flux from thermocouple data, (recalling its unreliability) as discussed in Section 9.2.5; and

3) the radiant power from the hot smoke cloud,

$$\dot{Q}_{rad} = [\pi I_{smoke}(w/cm^2 sr)][\text{ceiling area}].$$

We note that near the time of room involvement the ceiling smoke layer radiatively loses about one sixth of the combustion heat release.

Figure 9.8 shows:

1) the combustion heat release from the pan fire, from Section 9.2.7:

$$\dot{Q}_{combustion}(kw) = \dot{m}\ \text{fuel}\ H_c\ \text{paraffin oil}$$
$$= 41023\ \dot{m}(kg/sec) \quad ;$$

2) The radiant power of the pan fire, $\dot{Q}_F$ (kw) from radiance measurements made with the ray radiometer and the assumed flame projected surface area

$$\dot{Q}''_F\ (kw) = 4\pi(\text{area})\ (I_{rad}\ w/cm^2 sr)$$

$$= 4\pi(9755\ cm^2)(0.00196\ E_{Tel})x\ 10^{-3} = 0.240\ E_{Tel};\ \text{and}$$

3) The radiant power of the hot smoke cloud, calculated as for Figure 9.4.

We note that the heat loss from the ceiling smoke layer is significant.

Figure 9.9 shows the plume thermal energy flux from thermocouple data in the pan fire. The lower t.c. at approximately 117 cm over the fuel bed, being only half-way up to the flame height gives a poor measurement of the heat release, while the upper t.c. measurements result in higher than expected convective heat release, probably due to restricted entrainment as the flame and

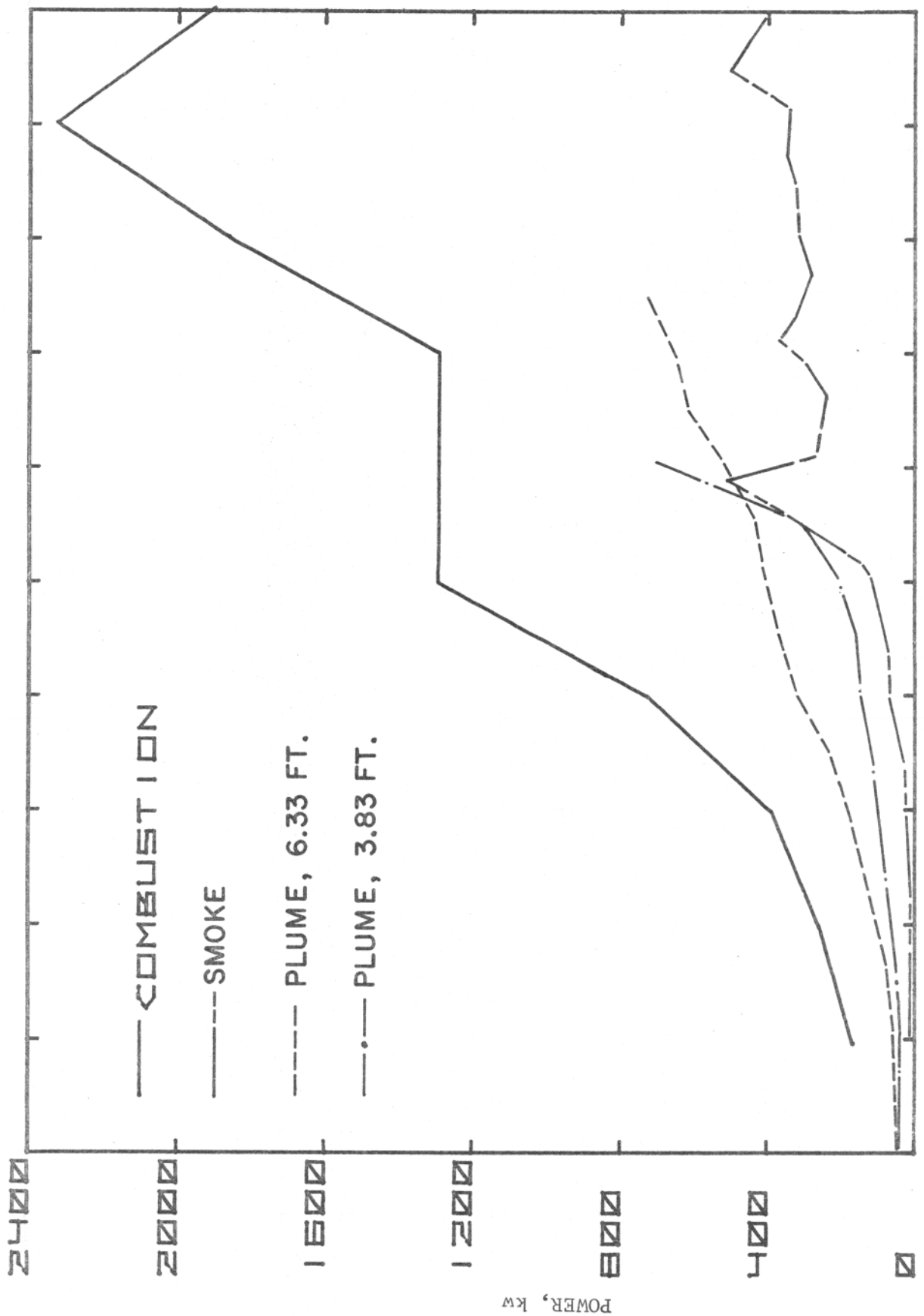

FIGURE 9.7 COMBUSTION HEAT RELEASE, CONVECTIVE POWER OUTPUT AND RADIANT POWER OUTPUT VERSUS TIME AFTER IGNITION FOR THE BEDROOM FIRE

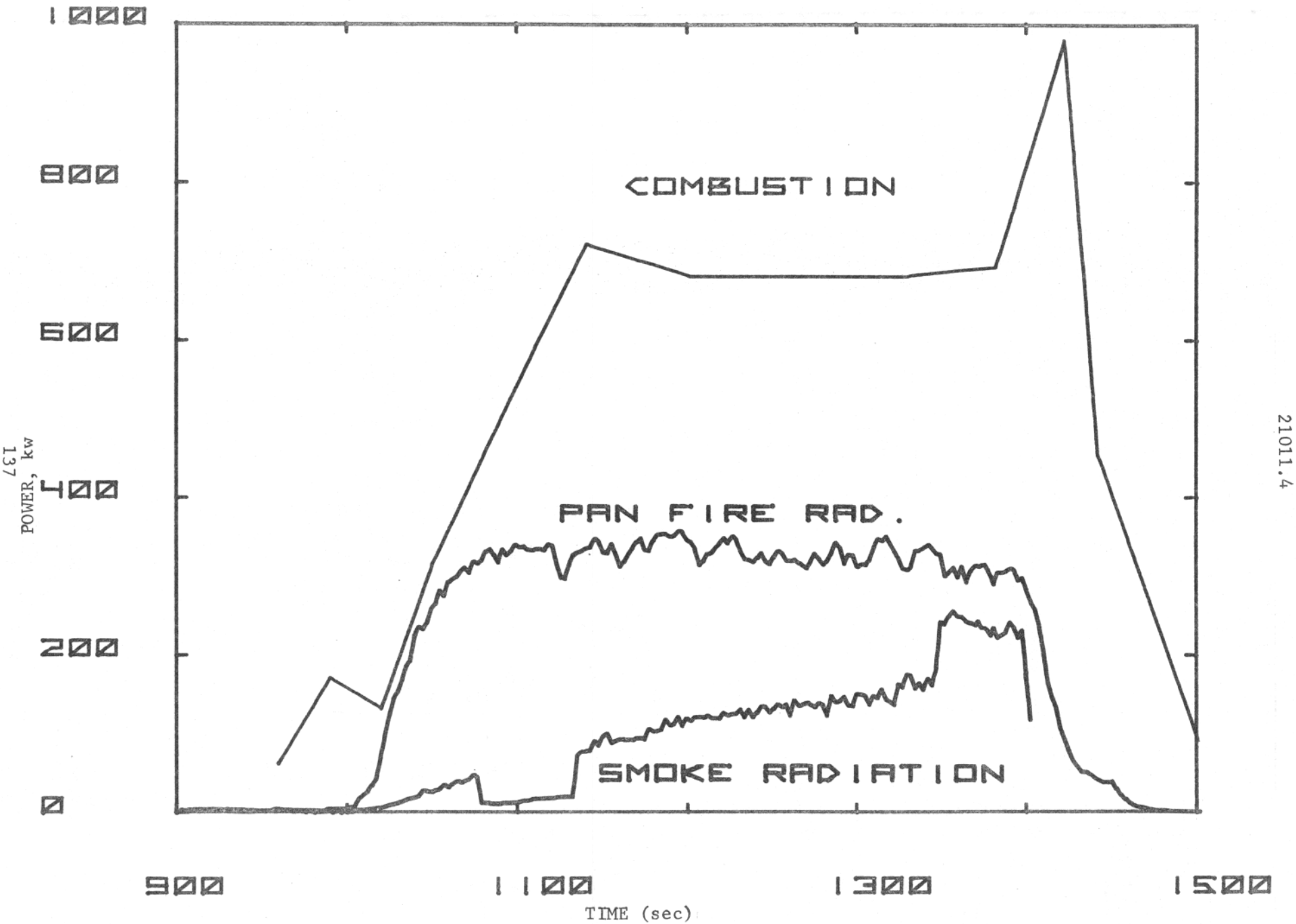

FIGURE 9.8 COMBUSTION HEAT RELEASE, FLAME RADIATION AND SMOKE RADIATION VERSUS TIME AFTER IGNITION FOR THE PAN FIRE

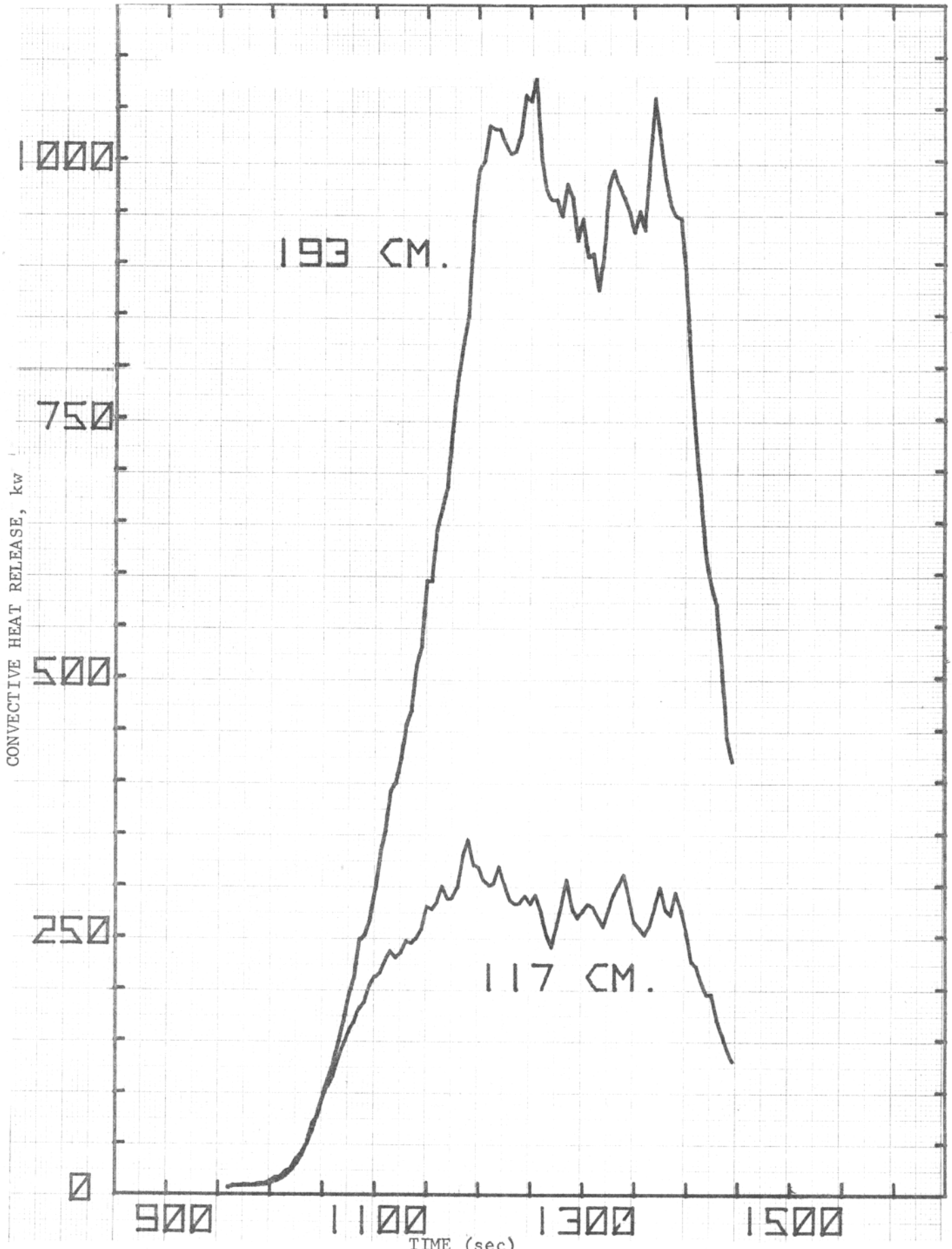

FIGURE 9.9 CONVECTIVE HEAT RELEASE VERSUS TIME AFTER IGNITION FOR THE PAN FIRE

plume are drawn into the room corner. It appears that the thermocouple method of measuring the plume thermal energy flux is not as reliable in this configuration as would be hoped.

9.5 RADIANT IGNITION OF THE BUREAU TOP

We consider the temperature rise of the bureau top surface due to irradiation $\dot{q}''(\tau)$ (watts/cm^2) by the smoke layer. The irradiation is derived from radiance, I (watts/cm^{2}sr) measurements made with the scanning radiometer,

$$\dot{q}''(\tau) \text{ (watts/cm}^2\text{)} = \pi\, I(\tau) \text{(watts/cm}^2\text{sr)},$$

where the bureau top is assumed to receive uniform radiation throughout a hemispherical field of view.

The surface temperature, T(t) of a body exposed to a quasi-steady heat flux $\dot{q}''(\tau)$ from $\tau=t_o$ to $\tau=t$ is given by:[6]

$$T(t) - T(0) = \int_{t_o}^{t} \frac{\dot{q}(\tau)d\tau}{\sqrt{\pi\, \rho_s C_{p_s} \lambda_s (t-\tau)}} ,$$

where ρ, C_{ps}, and λ_s are the density, specific heat, and thermal conductivity of the body respectively. The integral,

$\int_{t_o}^{t} \frac{\dot{q}''(\tau)d\tau}{(t-\tau)^{1/2}}$ is evaluated by approximating $\dot{q}''(\pi)$ with a first order least squares fit to the smoke irradiance data, $\dot{q}''(\tau) = e_n \tau + f_n$ for $t_{n-1} < \tau < t_n$. The constants e_n and f_n are obtained for three sequential least squares fits to the $\dot{q}''(\tau)$ versus t data. The correlation coefficient, R, of each fit is greater than .95, averaging R = .976. The integral is then evaluated for $t_o < t < t_1$ as

$$\int_{t_o}^{t} \frac{\dot{q}''(\tau)d\tau}{(t-\tau)^{1/2}} = \frac{2e_1(2t_1+t_o)}{3}\ (t_1-t_o)^{1/2} + 2f_1(t_1-t_o)^{1/2}.$$

For $t_1 < t < t_2$, the integral can be evaluated from

$$\int_{t_o}^{t} \frac{\dot{q}''(\tau)d\tau}{(t-\tau)^{1/2}} = \int_{t_o}^{t_1} \frac{\dot{q}''(\tau)d\tau}{(t-\tau)^{1/2}} + \int_{t_1}^{t} \frac{\dot{q}''(\tau)d\tau}{(t-\tau)^{1/2}}$$

Similarly, for $t_2 < t < t_3$,

$$\int_{t_o}^{t} \frac{\dot{q}''(\tau)d\tau}{(t-\tau)^{1/2}} = \int_{t_o}^{t_1} \frac{\dot{q}''(\tau)d\tau}{(t-\tau)^{1/2}} + \int_{t_1}^{t_2} \frac{\dot{q}''(\tau)d\tau}{(t-\tau)^{1/2}}$$

$$+ \int_{t_2}^{t} \frac{\dot{q}''(\tau)d\tau}{(t-\tau)^{1/2}}$$

The irradiation by the smoke cloud is negligible prior to 365 sec. First order least squares fits are found for four successive time periods between 365 and 409 sec after ignition. The following thermophysical properties are assumed for the wood surface:

$$\lambda_s = 0.00023 \text{ cal/cm sec°C}$$

$$C_{p_s} = 0.33 \text{ cal/g°C}$$

$$\rho_s = 0.36 \text{ g/cm}^3$$

$1/[4.186\ (\pi\rho_s C_{p_s} \lambda_s)^{1/2}] = 25.79\ \text{cm}^2\text{°C/watt sec}^{1/2}$. At $t_o = 367$ sec. the bureau top temperature, T_o, is assumed 80°C. $T_s(t)$ is then calculated as

$$T_s(t) - 80 = 25.79 \int_{367}^{t} \frac{\dot{q}''(\tau)d}{(t-\tau)^{1/2}}$$

Figure 9.10 shows this calculated T_s versus t.

Murty Kanury[7] gives the critical ignition temperature for cellulosic solid fuels as 300-410°C for piloted and at 600°C for spontaneous ignition by irradiation. A burst of flames appears first on the bureau top at 407 sec in the 16-mm movie. The above calculated surface temperature rises rapidly from 320°C at 397 sec, passing 600°C at 404 sec. The calculation predicts ignition between 401 and 406 sec, where 406°C < T < 600°C. This treatment does not consider 1) reradiant heat loss from the bureau top, which would be significant after 388 sec, or 2) convective cooling (t.c. #99 near the bureau top records 58°C at 400 sec). Further, the smoke passing over the scanning radiometer between the bed and doorway may be hotter than the smoke over the bureau, which would result in over-estimation of the smoke radiant flux. If those considerations were included in this analysis, the T_s versus t curve in Figure 9.10 would rise more slowly after 381 sec, resulting in a later time for the predicted surface ignition.

Finally, it must be recognized that the bureau top was, in fact, covered with assorted magazines. The thermophysical properties used here are for wood, and the consequences of this approximation have not been assessed.

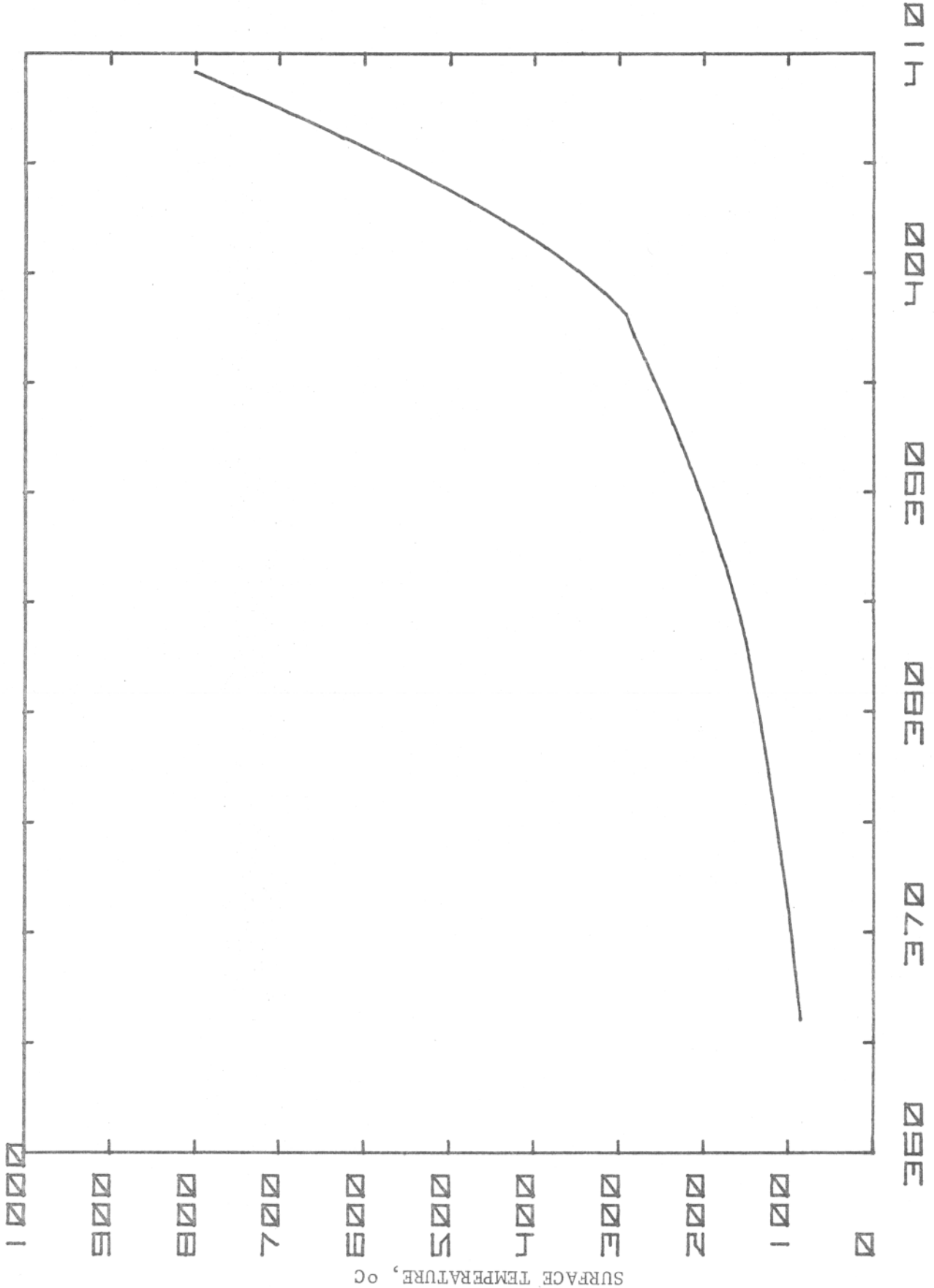

FIGURE 9.10 BUREAU TOP SURFACE TEMPERATURE VERSUS TIME AFTER IGNITION FOR THE BEDROOM FIRE

9.6 CONCLUSIONS

1) Flame areas and heights can best be determined from movie film, which allows averaging of measurements over short time intervals.

2) Movement of the bed fire towards the wall poses difficulties in measuring flame radiance with a ray radiometer and the plume thermal energy flux with thermocouples. It may be helpful to scan the flame area with the ray radiometer. Thermocouples may not be useful for measuring the plume thermal energy flux due to the fire interaction with the room walls.

3) Comparison of Markstein's smoke radiation measurements and the irradiance of the wall measured with a wide-angle radiometer shows that smoke accounts for most of the radiant heat transfer just prior to and following room involvement. Further insight could be gained by placing additional radiometers at various positions to determine the relative contributions of smoke and fire radiation.

4) Calculation of the temperature rise of the bureau top from ambient to ignition temperature, assuming heating solely by smoke radiation, yields a predicted time of ignition in reasonable agreement with observation.

5) The total radiant power lost by the ceiling smoke layer is approximately 20 percent of the combustion heat release of the fire for both the bed and pan fires. The combustion heat release of the pan fire was about a third of that of the bed at its maximum.

REFERENCES

1. deRis, J., "Calibration of Wide-Angle Radiometer," FMRC Interoffice Correspondence, November 1, 1973.
2. deRis, J., "Calibration of a Ray Radiometer," FMRC Interoffice Correspondence, September 29, 1972.
3. Alpert, R.L., "Calculation of Response Time of Ceiling-Mounted Fire Detectors," Fire Technology 8, 181, August 1972.
4. Croce, P.A., Volume 1, this report.

5. Emmons, H.W., in "The Large-Scale Bedroom Fire Test, July 11, 1973," FMRC Technical Report RC74-T-31, Serial No. 21011.4, July 1974.

6. Carslaw, H.S. and Jaeger, J.C., Conduction of Heat in Solids, Oxford University Press, Fairlawn, N.J., 1947.

7. Kanury, A.M., "Ignition of Cellulosic Solids - A Review," FMRC Technical Report, Serial No. 19721-7, November 1971.

APPENDIX

PERFORMANCE OF THE CALCULATOR-BASED DATA ACQUISITION SYSTEM

R.L. Alpert

Factory Mutual Research Corporation

A Hewlett Packard 9821A programmable calculator, with HP 3480/85 (digital voltmeter-50 channel scanner) and digital clock peripherals, were used to obtain the following six channels of information during the fire:

1) Lock-in amplifier output giving radiance of near-ceiling smoke layer alone.
2) Total radiance of ceiling and ceiling smoke layer from narrow-angle radiometer.
3) Irradiance of fire and surroundings from wide-angle radiometer.
4) Radiance of initial fire from narrow-angle radiometer.
5) Total heat flux from Gardon gauge adjacent to bed.
6) Total heat flux from Gardon gauge between wall and bed.

As the fire proceeded, the above information was recorded by the calculator system on a standard audio tape cassette, which was processed just after the test by a second HP calculator with an X-Y plotter peripheral.

The use of a programmable calculator in this manner for data acquisition, reduction and presentation has several advantages over the use of a minicomputer or full-size computer when fewer than ten channels of information are desired. First, the calculator system is highly portable, which means it is available for experiments at widely separated locations. Second, there are no delays due to batch processing or turn-around times of punched cards or tape reels. In fact, almost all data reduction can be done on the same calculator that is initially used to obtain the data. Finally, the most important advantage of the calculator system is that data acquisition (and reduction) programs can be modified and corrected quickly and easily. Such modifications were actually being made until just a few minutes before the

bedroom fire due to changes or irregularities in signals from the various measurement devices. The flexibility of the data acquisition programing will be evident from the following discussion.

Figure 9.11 is a printout of the 9821A program actually used for bedroom fire data acquisition. This program has four main features:

1) The program starts data acquisition when the clock reset button is pressed (line 4). This allows for accurate synchronization with other data recording instruments.

2) The range of the digital voltmeter can be changed after each separate scan of the data channels to allow for changes in the signal voltage level (lines 9-13). It should be noted that each channel can be individually programed to be read with the correct DVM range. In the same instruction that specifies a DVM range, a 1/3-sec true integrating filter built into the DVM can also be specified (line 8) for those signals which are particularly noisy.

3) There are two scan modes in the program: in the "slow" mode (lines 5-19), the time between consecutive scans of the six analog channels is regulated (line 19) to be about 2 sec and a printout of all six channel voltages occurs every 20 scans; in the "fast" mode (lines 21-29), consecutive scans occur as fast as possible (every 1.6 sec) and there are no printouts of the data. Switching from one scan mode to another is accomplished by pressing a special calculator key while the program is running.

4) After each scan, the data are recorded on a separate cassette tape file. While use of such short files is inefficient, it allows for a uniform, short, time between scans, thus eliminating the possibility of missing significant information during rapid bedroom involvement.

```
0:
49→R10;48→R11;48
→R12;48→R13;48→R
14;52→R15⊢
1:
1→B;19→Y⊢
2:
*REW ;*FDF B⊢
3:
DSP "READY?";
STP ⊢
4:
RED 4,X,X;JMP 0+
X≤1000⊢
5:
WTB 1,8⊢
6:
RED 4,X,X;WTB 1,
R10;RED 3,R1,R1;
WTB 1,R11;RED 3,
R2,R2⊢
7:
WTB 1,R12;RED 3,
R3,R3;WTB 1,R13;
RED 3,R4,R4;WTB
1,R14;RED 3,R5,R
5⊢
8:
WTB 1,R15⊢
9:
IF R2>.1;49→R11⊢
10:
IF R3>.1;49→R12⊢
11:
IF R3>1;50→R12⊢
12:
IF R5>.1;49→R14;
IF R5>1;50→R14⊢
13:
IF R4>.1;49→R13;
IF R4>1;50→R13⊢
14:
CLOCK X→R7;DSP ;
RED 3,R6,R6⊢
15:
*RCF B,R1,R7;B+1
→B;Y+1→Y;GTO 16;
IF Y=20;0→Y;GTO
17;IF FLG 0;CFG
0;GTO 21⊢
16:
GTO 19⊢
17:
FXD 0;PRT B-1;
FXD 3;PRT R7⊢
18:
FLT 3;PRT R1,R2,
R3,R4,R5,R6⊢
19:
RED 4,X,X;CLOCK
X→X;JMP 0+(X-R7>
2.2/60)⊢
20:
GTO 5;IF FLG 0;
CFG 0;GTO 21⊢
21:
PRT "FAST";SPC 1
⊢
22:
WTB 1,8;RED 4,X,
X;WTB 1,R10;RED
3,R1,R1;WTB 1,R1
1;RED 3,R2,R2;
WTB 1,R12⊢
23:
RED 3,R3,R3;WTB
1,R13;RED 3,R4,R
4;WTB 1,R14;RED
3,R5,R5;WTB 1,R1
5⊢
24:
IF R2>.1;49→R11⊢
25:
IF R3>.1;49→R12;
IF R3>1;50→R12⊢
26:
IF R5>.1;49→R14;
IF R5>1;50→R14⊢
27:
IF R4>.1;49→R13;
IF R4>1;50→R13⊢
28:
CLOCK X→R7;DSP ;
RED 3,R6,R6⊢
29:
*RCF B,R1,R7;B+1
→B;GTO 22;IF
FLG 0;CFG 0;GTO
5;PRT "SLOW";
SPC 1⊢
30:
END ⊢
```

FIGURE 9.11 DATA ACQUISITION PROGRAM FOR HP 9821A CALCULATOR

X

TEMPERATURES AND RADIATION FROM SOOT LAYER

A.T. Modak

Factory Mutual Research Corporation

Markstein's scanning radiometer data (Section VIII) show that at about 300 sec after ignition, corresponding to a soot layer buildup of approximately 20 cm, the ceiling is obscured from view of the radiometer. From this time onwards, nearly all the signal of the scanning radiometer may be attributed to this 20-cm thick soot layer continuously descending toward the floor. This soot layer increases in thickness and attenuates, successively, the output of the seven optical density meters located at 7.6, 24.1, 40.6, 77.2, 99.1, 121.9 and 167.6 cm from the ceiling in the forward room rack.

10.1 DATA REDUCTION

The optical density meters consist of a light source and a photo-tube detector placed 60.9 cm apart. The photo-detector has a wave length response similar to that of the human eye (range 0.4 μm to 0.7 μm with a peak at 0.55 μm). A characteristic attenuating soot layer of 20 cm corresponds to a photo-detector signal attentuation, over 60.9 cm, of about 95.3 percent (= 100 [1-exp(-60.9/20)]). Unfortunately, the presence of noise in the photo-detector channel, and consequently the poor resolution at low signal, makes the determination of the time corresponding to 95.3 percent obscuration, t_{ob}, somewhat unreliable. In order to circumvent this difficulty, t_{ob} is obtained more reliably from the intersection of the tangent at the 63 percent attenuation point of the photo-detector signal, and the time axis as shown in Figure 10.1. This time is plotted, versus the location of the optical density meters (designated as "soot depth from ceiling"), in Figure 10.2 by the broken line with open circles. The corresponding times at 63-percent attenuation

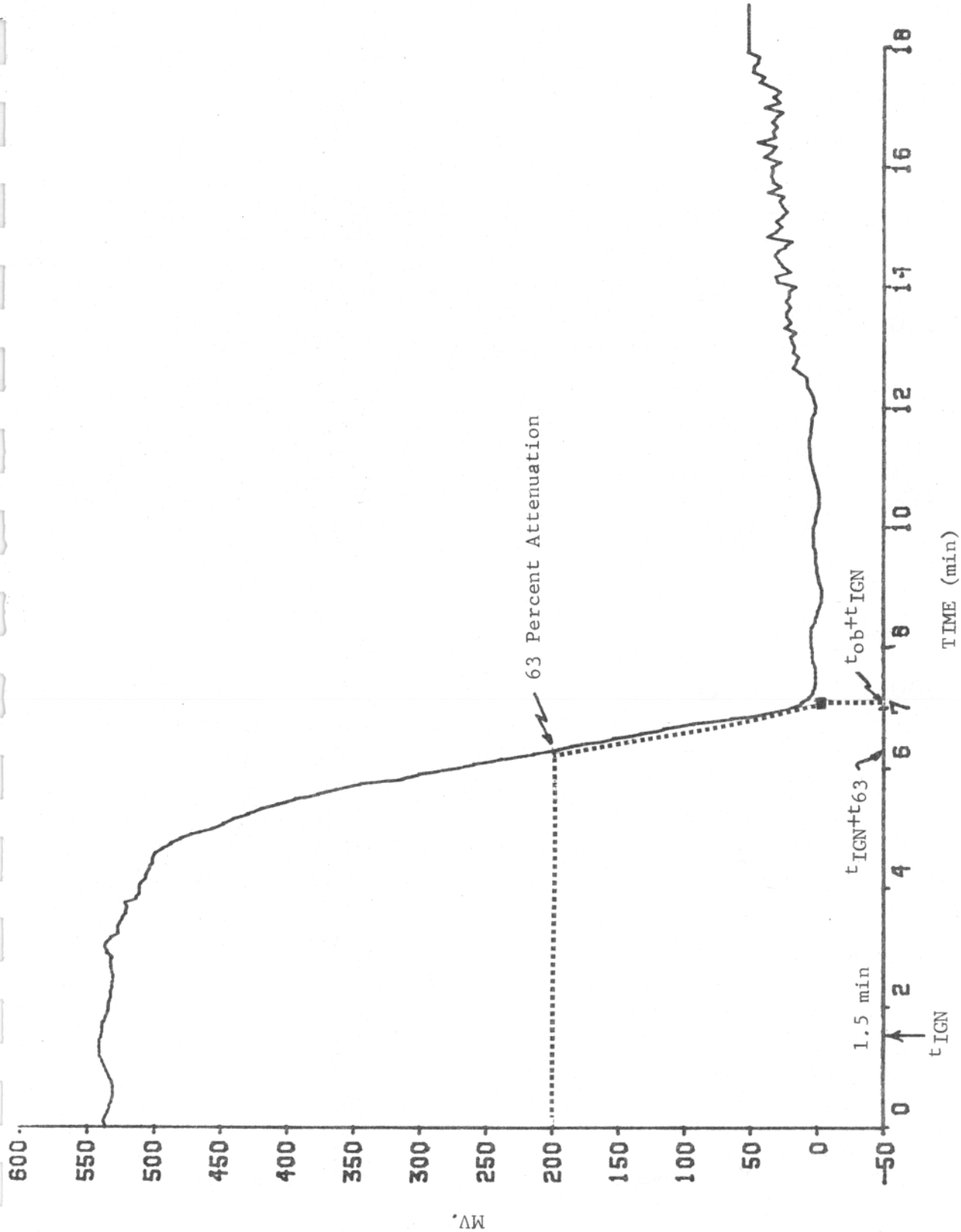

FIGURE 10.1 PHOTO-DETECTOR SIGNAL VERSUS TIME AT A POSITION 77.2 cm BELOW CEILING

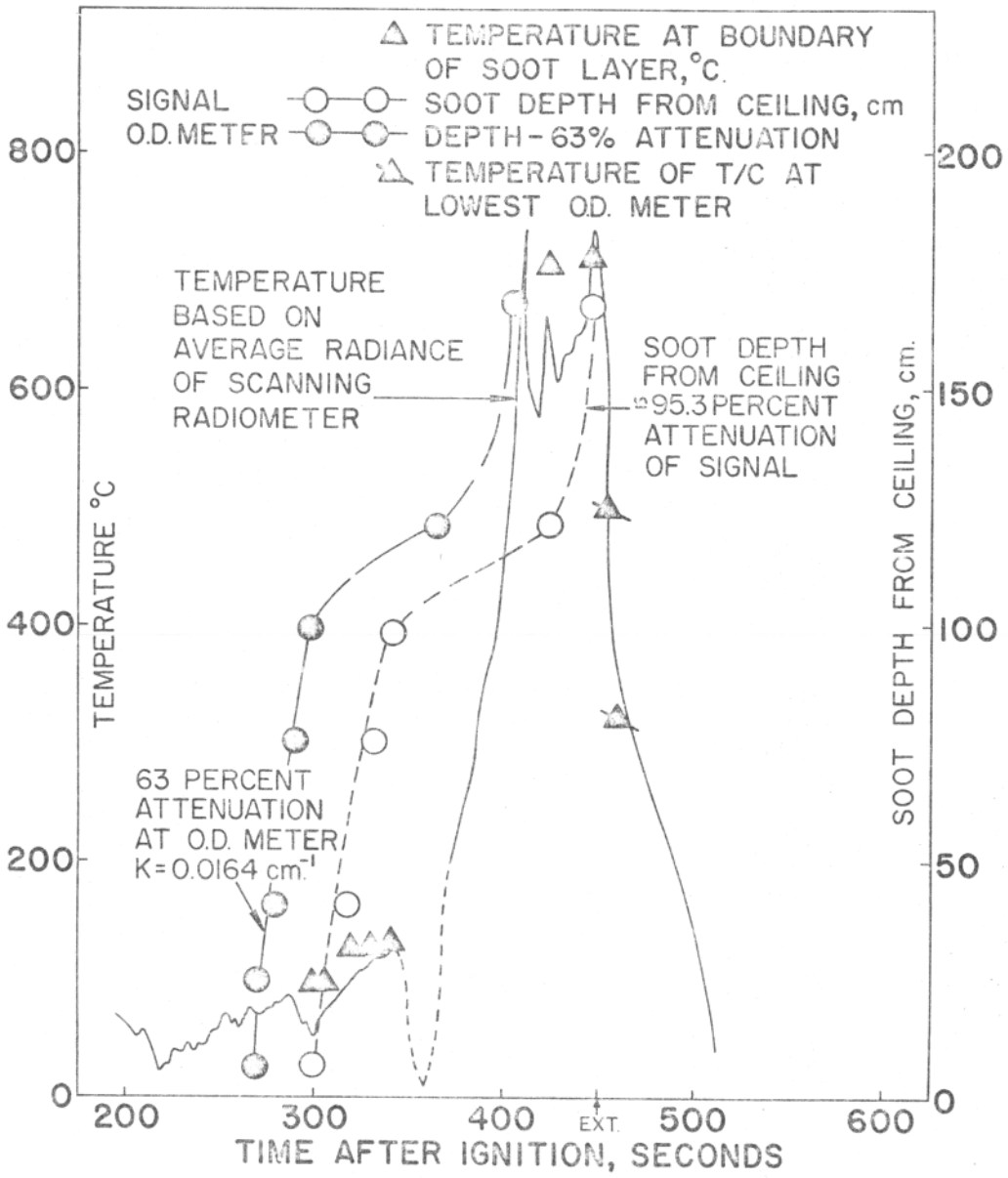

FIGURE 10.2 SMOKE LAYER RADIATION, THICKNESS AND TEMPERATURE VERSUS TIME AFTER IGNITION

are also shown by the broken line with closed circles. As is to be expected, the shapes of the two curves are similar.

The temperatures, T_m, measured by the thermocouples at the location of the optical density meters, at time $t=t_{ob}$, are shown in Figure 10.2 by closed triangles. The solid line corresponds to Markstein's data obtained from a scanning radiometer and converted into an equivalent radiation temperature assuming unit soot emissivity, $T_r = (\pi N_{av}/\sigma)^{0.25}$, where N_{av} W/(cm^2-sr) is the radiance computed from the average d.c. signal of the scanning radiometer and σ is the Stefan-Boltzmann constant. T_m correlates well with T_r indicating that the scanning radiometer sees essentially the descending soot layer. We also note here that a characteristic soot layer path length of 20 cm corresponds to an absorption coefficient of $K = 0.05$ cm^{-1} as compared with $K \simeq 0.03$ cm^{-1} for laminar propane flames.

10.2 WALL HEAT FLUX - WIDE-ANGLE RADIOMETER

The wide-angle radiometer was located at 130 cm below the ceiling. The soot layer obscured the radiometer at ca. 430 sec. This is corroborated by Figure 10.3 which shows that more than 80 percent of the total radiation to the wide angle radiometer (Section IX) is due to the soot layer, and is accounted for by the quantity (πN_{av}). Here N_{av} is the average radiance of the soot layer measured by the scanning radiometer in W/(cm^{2}sr). We note also that in Figure 10.3, the shape of the (πN_{av}) line resembles that of the total radiation line. Since (πN_{av}) is measured by the scanning radiometer located at the floor near the forward room rack, whereas the total radiation line of Figure 10.3 is measured by the wide angle radiometer located on one of the side walls, the close shape resemblance of the two lines provides additional confirmation that a significant fraction of the radiation received by the wide angle radiometer is due to the soot layer. At 450 sec the soot in the room is rapidly cooled by the sprinklers and the fraction of radiation due to the soot layer declines rapidly.

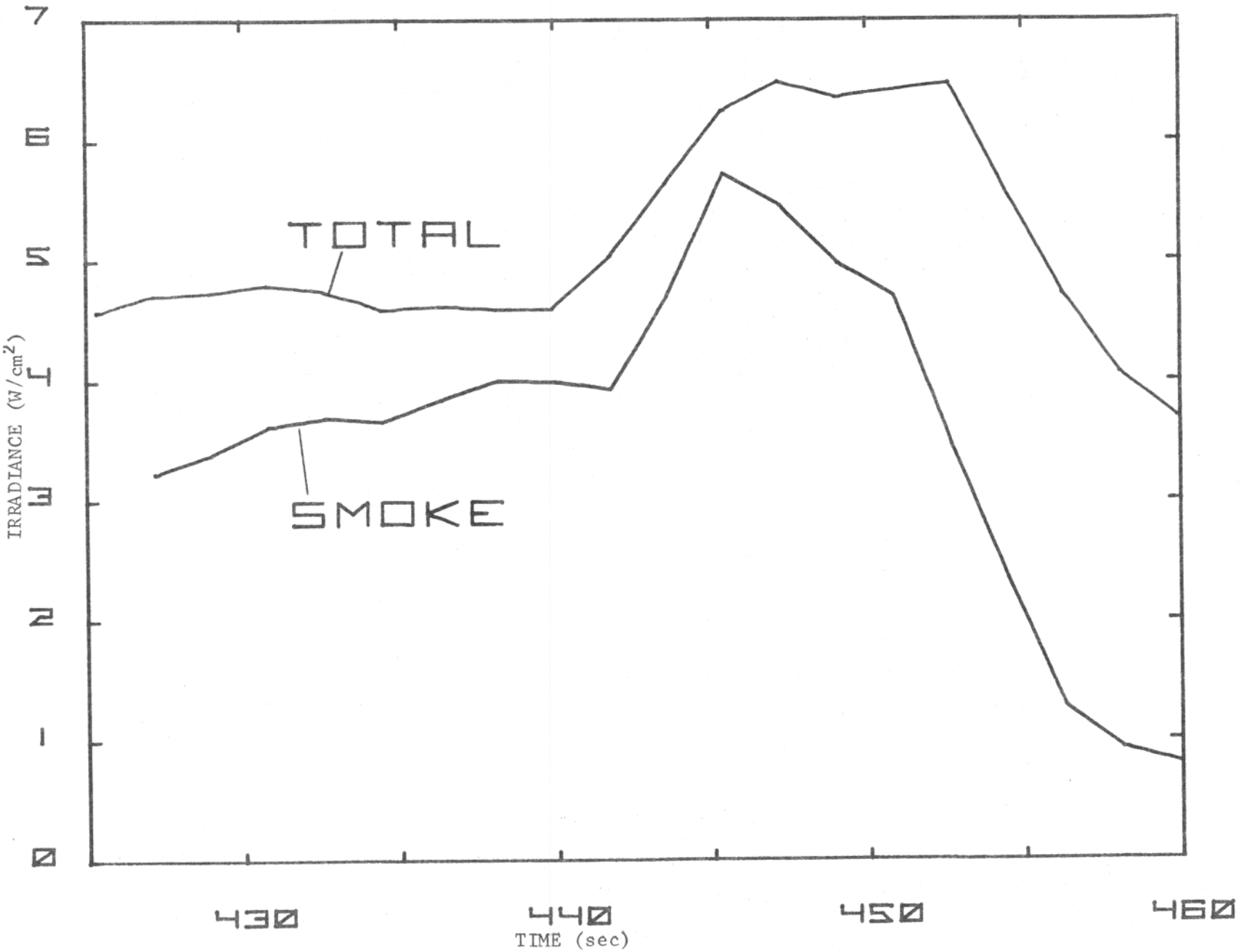

FIGURE 10.3 COMPARISON OF RADIATION MEASURED BY WIDE ANGLE RADIOMETER AND RADIATION DUE TO SMOKE LAYER VERSUS TIME AFTER IGNITION

10.3 CONCLUSIONS

Figure 10.4 shows that after about 400 sec, the hot soot layer descending downward from the ceiling is almost solely responsible for the radiative heating of potentially combustible objects within the room. Combustion processes in the room provide the necessary energy to heat the soot layer, which, in turn, is capable of supplying fluxes as high as 5.5 W/cm^2 to objects within the room. Fluxes of this magnitude are more than adequate to flash ignite all wooden objects in the room.

10.4 RECOMMENDATIONS FOR THE NEXT TEST

Photo-detector noise at low signals makes it difficult to determine t_{ob}, from the signal-time traces of the photo-detectors. Data reduction could be facilitated by either reducing the noise levels or by designing a system in which the signal increases with increasing obscuration. Alternatively, we suggest that two photo-detectors at each location be used, with separation distances of 15.2 cm and 30.5 cm instead of one with a separation distance of 60.9 cm.

Since the wide-angle radiometer was located directly above the bureau, it is subject to serious perturbations when the bureau flashes at ca. 407 sec. A wide-angle radiometer at another location would be more suitable.

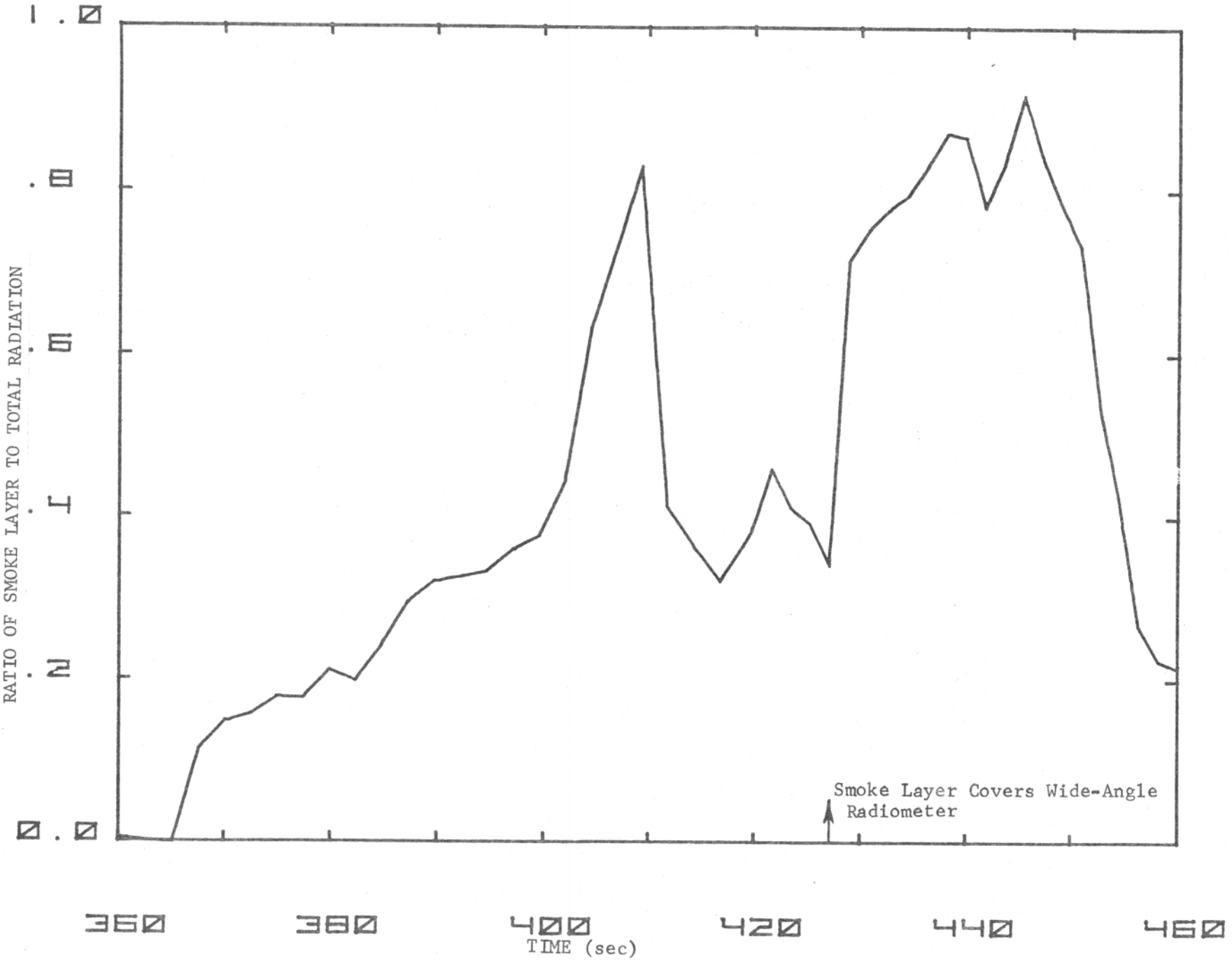

FIGURE 10.4 RATIO OF SMOKE LAYER RADIATION TO TOTAL RADIATION SEEN BY WIDE-ANGLE RADIOMETER VERSUS TIME AFTER IGNITION

XI

TOTAL HEAT FLUX MEASUREMENTS BY GARDON-TYPE GAUGES

R.L. Alpert
Factory Mutual Research Corporation

11.1 INTRODUCTION

A fire initiated in a single fuel element in an enclosure will at first grow in the same manner as a fire in the open. At some point, however, the enclosure may begin to influence the fire growth history by changing either the ambient ventilation or the heat flux environment of the fire. It was to investigate the latter possibility that total heat flux measurements were made close to the bed during this full-scale test. These measurements showed that thermal radiation from the ceiling surface or from the hot smoke layer filling the upper portion of the room was nearly always proportional to the total heat flux incident on the bed. However, most (60-70 percent) of the heat flux "seen" by the bed before and after general room involvement was probably due to flame zones quite close to the bed. Values of heat flux incident on the bed were rising to more than 16 watts/cm^2 five seconds before the test was terminated by sprinkler actuation.

11.2 HEAT FLUX GAUGE DESCRIPTION

To obtain accurate measurements of total heat flux, water-cooled Gardon-type gauges (Medtherm Model 64) with output voltage directly proportional to net absorbed flux were used. The flat sensor face was exposed and sufficiently black to have an absorptance greater than 0.9 for wavelengths from 0.6 to 15 microns.

Both before and after the bedroom fire, two gauges were calibrated with a blackbody oven having a 2.54-cm aperture. The net oven heat flux, $\dot{q}''_{cal}$,

absorbed by the gauge was:

$$\dot{q}''_{cal} = \left(\frac{D}{2d}\right)^2 \sigma(T^4_{Oven} - T^4_g) \cos\theta \qquad (11.1)$$

where σ is the Stefan-Boltzmann constant, θ is the angle of incidence of the oven radiation, T_g is the water-cooled gauge temperature, D is the oven aperture and d is the effective distance between the sensor face and the oven aperture. With a fixed value of d, the sensor was rotated to determine the angular sensitivity of the gauge. This measurement showed that the gauge has a total viewing angle of at least 160 degrees and very likely a full 180 degrees.

The gauge output, E_g, was obtained for several separation distances between the sensing face and the oven (136 to 267 mm). A plot of $E_g^{-1/2}$ versus separation distance yielded a straight line, which means that E_g is proportional to $\dot{q}''_{cal}$. The straight line intercept with $E_g^{-1/2} = 0$ then allowed the absolute magnitude of "d" in eq 11.1 to be obtained. Before the bedroom fire, the two gauge calibration factors, $\dot{q}''_{cal}/E_g$, were 1.18 and 0.0108 W/cm^{2}mv, the latter value resulting from use of an operational amplifier with a gain of roughly 1000. Recalibration after the bedroom fire gave respective factors of 1.2 and 0.012 W/cm^{2}mv, thus showing a negligible effect of the fire environment on both gauges.

11.3 LOCATION OF GAUGES

Both gauges were placed as close as possible to the bed mattress (polyurethane) near the point of ignition in order to obtain some measure of the radiative and convective heat flux from the environment to the initial fire. Each gauge was very nearly flush with the top surface of the mattress and 0.915 m (3 ft) from the rear bedroom wall, as was the ignition point. One gauge was located on the wall side of the bed 3.18 cm from the mattress while the second gauge was on the opposite side of the bed 6.36 cm from the mattress.

Until the fire diameter approximately equaled the total mattress width, the gauges were mainly measuring the radiant flux from the mattress flames.

Since these flames initially spread toward the wall, the gauge on the wall side of the bed should respond to the fire well ahead of the other gauge.

Gardon gauges consist of a thin "constantan" metal disc surrounded by and joined to a massive copper body, which in this case is water cooled. The temperature of the copper body was monitored by a chromel-alumel thermocouple bead while the gauge output was generated by the EMF across two copper wires joined respectively to the copper body and the center of the constantan disc. Thus, the temperature of the center of the constantan sensing surface of the heat flux gauge could be derived from the gauge output voltage and the known, approximately linear, temperature-EMF relation of the copper-constantan system.

The gauge on the wall side of the bed had the 1.2 W/cm^2mv calibration factor and a sensing surface, center temperature increase (above that of the copper body) of 20 degrees $C/W/cm^2$. On the opposite side of the bed was the gauge with the 0.011 W/cm^2mv calibration factor and a surface temperature increase of 2 degrees $C/W/cm^2$. The ability of the former gauge to measure large incident heat fluxes was effectively limited by the maximum allowable temperature of the gauge sensing surface, about 500°C.

11.4 BEDROOM FIRE RESULTS

Figure 11.1 contains plots of the heat flux absorbed by each gauge and data on the total burning rate of the bed as a function of time after ignition. One obvious feature of the plots is the difference between the heat flux measurements of the two gauges. Prior to 435 sec after ignition, the two gauges had very similar outputs but the wall gauge responded to the fire about 10-20 sec before the right-side gauge. As noted earlier, this behavior was expected since a slightly unsymmetrical fire spread, favoring the wall direction, was evident from photographs beginning around t=300 sec.

It was not obvious, however, why the wall gauge measured a decreasing flux at t=435 sec while the other gauge registered a flux sharply increasing to 16 W/cm^2. One possible explanation for this behavior is the difference

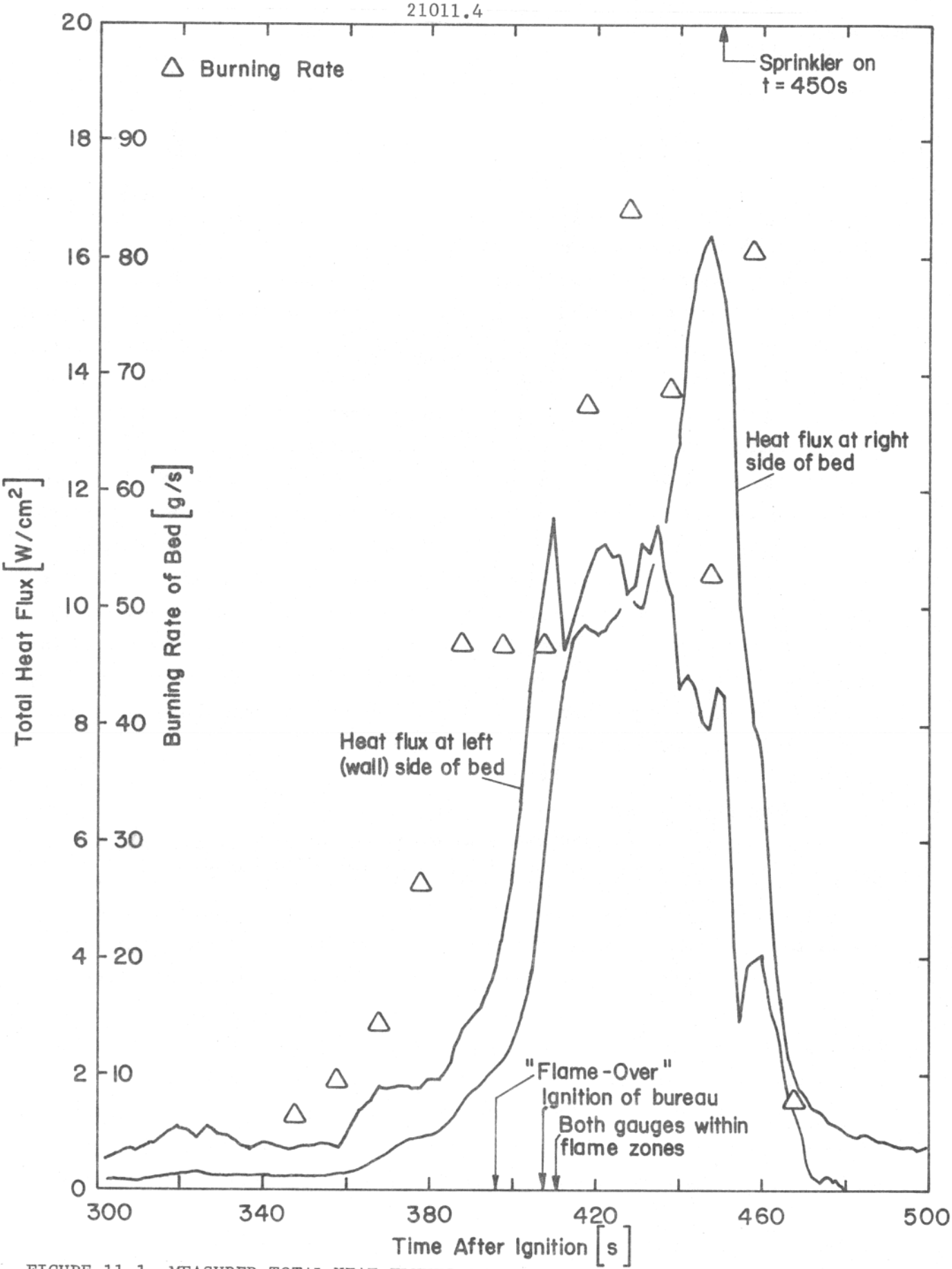

FIGURE 11.1 MEASURED TOTAL HEAT FLUXES AND BURNING RATE VERSUS TIME AFTER IGNITION

in the condition of the two sensing surfaces just after the bedroom fire. The wall gauge was covered with a substantial amount of charred paper which fell from the burning wall surface while the second gauge was quite clean and free of dust. It is possible that the material covering the face of the wall sensor was generated just before t=435 sec, when there was general room involvement, and that at subsequent times until sprinkler actuation at t-450 sec, the material insulated the sensor face from radiant and convective heat flux.

Both gauges showed a rapid increase in heat flux just after the appearance of flame in parts of the thickening smoke layer within the bedroom. Thereafter, the bureau opposite the bed ignited when a heat flux near the bed of 5-10 W/cm^2 was measured. A nearly constant heat flux of 10 W/cm^2 was measured during general room involvement when both gauges were surrounded by flame but most of the carpet was not yet burning. When the carpet did become involved, the peak heat flux was measured. Both gauge outputs finally dropped to zero when the sprinkler was actuated.

The calibration factors given in Section 11.2 allowed the net heat flux absorbed by each gauge to be obtained from the output signal. The heat flux incident on the gauge was somewhat larger than the net absorbed value due to re-radiation from the sensing surface and convective cooling from the surroundings. However, the net and incident heat fluxes were probably about equal since the maximum temperature of the center of each constantan disc was less than 100°C until 400 sec after ignition. Peak sensing-surface temperature was 291°C for the wall gauge and 137°C for the right-side gauge. In any case, the vaporization temperature of the burning mattress was 343°C (see Reference 1) so that the heat flux absorbed by the mattress was also somewhat less than the incident flux.

11.5 DISCUSSION OF RESULTS

11.5.1 Heat Flux To Bed

Data on the overall burning rate of the bed[1] show a very close resemblance, in Figure 11.1, to the time history of the total heat flux signal.

If the heat flux measured by the two gauges was characteristic of that absorbed by the burning bed, the ratio of this heat flux to the fuel (mattress, etc.) mass flux should be the effective heat of vaporization of the fuel. Fuel mass flux can be obtained from the bed weight-loss measurement and the surface area of vaporizing material on the bed. The similar behavior of the weight-loss and heat flux data would thus be expected if the vaporizing fuel surface area did not vary appreciably.

Estimates of the fire base dimensions obtained from slides and a video recording were used to calculate the surface area of vaporizing fuel on the bed alone as a function of time during the test. These calculations yielded surface areas of 0.5 to 1.0 square meter between t=300 and t=380 sec and an area of about 3 m^2 after t=400 sec. While it is assumed that, at most, only the top surface of the mattress and one side of the headboard can contribute fuel, much more fuel surface is available. Studies[2] have shown, for instance, that the fire first spreads down into the mattress, then outward to form an expanding cylinder of burning urethane foam. This effect is ignored.

Table 11.1 gives the ratio, $\dot{q}''/\dot{m}''$, of measured heat flux to calculated mass flux as a function of time after ignition, based on information from the two gauge locations. The value of $\dot{q}''/\dot{m}''$ should be close to L_g, the heat of gasification of the fuel. For the urethane foam, measurements[1] show L_g to be about 279 cal/gm.

It can be seen from Table 11.1 that $\dot{q}''/\dot{m}''$ for the wall gauge was comparable to L_g until general room involvement at 400-410 sec after ignition. Thereafter, $\dot{q}''/\dot{m}''$ was much greater than L_g, possibly because enough urethane was consumed by t=410 sec to decrease the actual surface area (but not the overall burning rate, $\dot{m}$) of vaporizing fuel on the bed itself, thus substantially increasing $\dot{m}''$. If the remaining fuel contributing to the fire was mostly wood, the fuel surface temperature may be much greater than the temperature of the gauge sensing surface.

For the right side gauge, $\dot{q}''/\dot{m}''$ was somewhat less than L_g prior to t=410 sec, probably due to the proximity of the fire to the wall during this time.

radiation was obscured by the smoke layer, but it is not known if such obscuration continues after t=410 sec. The irradiance of the floor, and presumably the bed, by the combination of ceiling surface and smoke is π times the radiance values given in SectionVIII.Figure 11.2 (triangle symbols) shows how this computed radiant flux from the ceiling varied in comparison with the Gardon gauge measurements of incident flux.

Although the smoke radiation obviously did not account for most of the heat flux incident on the bed, the time variation of the smoke radiant flux was nearly coincident with that of the total flux measured by the Gardon gauges. The smoke layer radiation was thus a nearly constant fraction, about 25-32 percent of the heat flux incident on the bed. An exception to this did occur for a few seconds during the sharp rise in smoke radiation up to about 50 percent of the Gardon-measured flux at t=410 sec, when general room involvement began due to remote ignition of fuel. Both Orloff and de Ris (Section IX) and Modak (Section X) clearly show the smoke radiation to be directly responsible for this fire spread behavior.

Between 410 and 450 sec after ignition, there is a possibility that the smoke layer became more transparent to radiation from the solid surface of the ceiling. The maximum radiant flux from this ceiling surface would be simply the blackbody emissive power, σT_s^4, based on the ceiling temperature, T_s. By interpolation from existing thermocouple data[1], the values of T_s can be determined at the same location where the smoke layer radiance measurements were made. The resultant calculations of radiant flux incident on the floor are shown (circle symbols) in Figure 11.2.

It can be seen that this calculated ceiling surface flux did not have the same time variation as either the measured ceiling flux or the measured total flux at the bed. Furthermore, the maximum possible ceiling surface emission was still somewhat less than the measured radiant flux from the ceiling. Radiation incident on the end of the bed from the hot gases was thus probably much more important than ceiling surface radiation even after t=410 sec. This conclusion is generally applicable to all but one

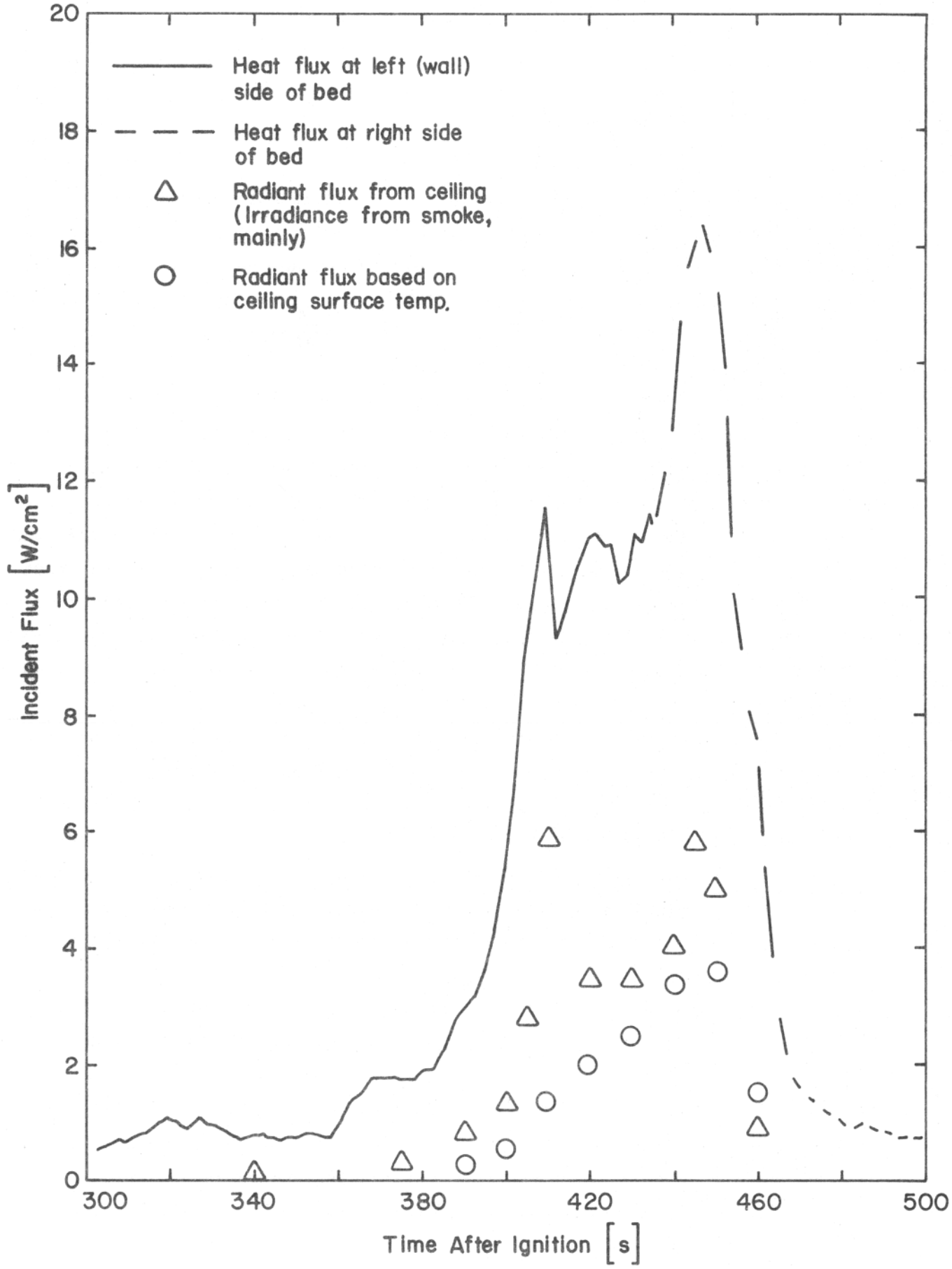

FIGURE 11.2 INCIDENT HEAT FLUXES DUE TO SMOKE LAYER AND CEILING COMPARED WITH MEASURED TOTAL HEAT FLUX VERSUS TIME AFTER IGNITION

area of the bedroom since peak ceiling temperatures were less than 600-700°C everywhere except in the corner of the room over the bed. Temperatures of 850°C were achieved at the latter location, resulting in an emissive power from the ceiling of up to 9 W/cm^2 when t=435 sec after ignition. The very limited area of such high ceiling surface temperature would result in a much smaller flux (perhaps 2-4 W/cm^2) actually incident on the bed.

The preceding discussion seems to show that the heat flux environment of the initial bed fire was significantly enhanced by smoke and/or ceiling surface radiation, but that most of the heat flux incident on the bed was apparently from convective and radiative transfer within the bed-fire flame zone. However, for a few seconds during the remote ignition of the bureau (top of bureau at t=407 sec, drawers at t=413 sec), radiation from the smoke layer accounted for all of the heat flux measured on the right side of the bed (compare Figures 11.1 and 11.2). This brief "pulse" of radiation from the "smoke" may, thus, have ultimately been responsible for general room involvement.

REFERENCES

1. Volume I, this report.
2. Pagni, P., Appendix to Section III of this Volume.

XII

PERFORMANCE OF THE FAN ANEMOMETERS

R. Land

Harvard University

Two fan anemometers were tested by locating one in the top of the doorway and the other near the center of the room just below the ceiling. The doorway fan was 20 cm in from the door jamb and 6.3 cm down from the top doorsill with the plane of the fan about 5 cm back from the room wall face. The ceiling fan was located 30 cm from the room center toward the bedside wall, and suspended 8.3 cm down from the ceiling surface. Both anemometers had independent power sources and output signal conditioners. These boxes were within 5 ft of the probes and contained the lamp power, detector power, and electronic amplifiers with frequency-to-voltage converters. The output signals were conducted in shielded cables to both strip chart recorders and the 2114 data acquisition system[1]. The thermocouples integral with the fan probes were connected to the 9601A system instrumentation panel in the control room. Both of the anemometers were calibrated in low velocity facilities at Harvard before being installed in the test room.

Installation of the probes required careful sealing of the holes in ceiling and door jamb for both support and nondisturbance of the flow to be measured. Pretest operation of the units indicated great sensitivity to electrical noise. It was thought that the appropriate grounds had been selected before the test to insure minimal signal interference with the automatic gain features in the amplifiers.

The data show two problems, electrical noise throughout the test period, and no usable readings from about 6 min on into the test. The strip chart data for the ceiling probe show spikes from the moment it was turned on and indicate values much greater than anticipated. The strip chart for the doorway probe shows noise, but after 1 or 2 min into the burn, the fan signal

apparently overcame the noise, and readings are clear until 6 min when for no apparent reason the signal drops to zero. The voltages read simultaneously by the data acquisition system from the same terminals give an apparently much more satisfactory situation. One may refer to Volume I of this report for the complete set of data, both temperature and velocity, during all but the time following 6 min when the flow data failed. The conversion of the data into velocities did not use a temperature correction since neither anemometer was heated above 300°C before 6 min and temperature corrections appear necessary only above such temperatures.

Following the room fire and extinguishment, both probes looked in reasonable working order although both readout systems were not producing useful data. The light pipes were unaffected, the mirrors looked shiny enough, and the fans were turning. On the day following the pan fire test, the probes, without having been moved, still looked all right although the doorway fan was now unable to turn. The ceiling fan had been subject to temperatures of over 500°C for more than 5 min in the second test, having been briefly subject to nearly 900°C in the first test. Both anemometers were reasonably carefully removed from the test facility and recalibrated at the Harvard facilities. The ceiling fan needed no adjustment although one of the light pipes had softened somewhat and was useless. The doorway fan only needed simple bearing adjustment and then was completely operable for calibration. Calibration of rotation versus velocity was obtained using a Strobotac (GR Company). Both fans were found to be within 5 percent of the original calibration.

While the ceiling flow data may be suspect, the doorway data during the first 6 min demonstrates rather impressively the capabilities of these probes. Actually, the trend of the computer stored data for the ceiling flow corresponds roughly to the data obtained during the first 6 min in the test of 1973. A bidirectional flow probe using a sensitive pressure transducer was located 12.6 cm down in the doorway on the opposite jamb[2]. Data from this probe have been compared with that from the fan in Figure 12.1 during the period when the fan was functional.

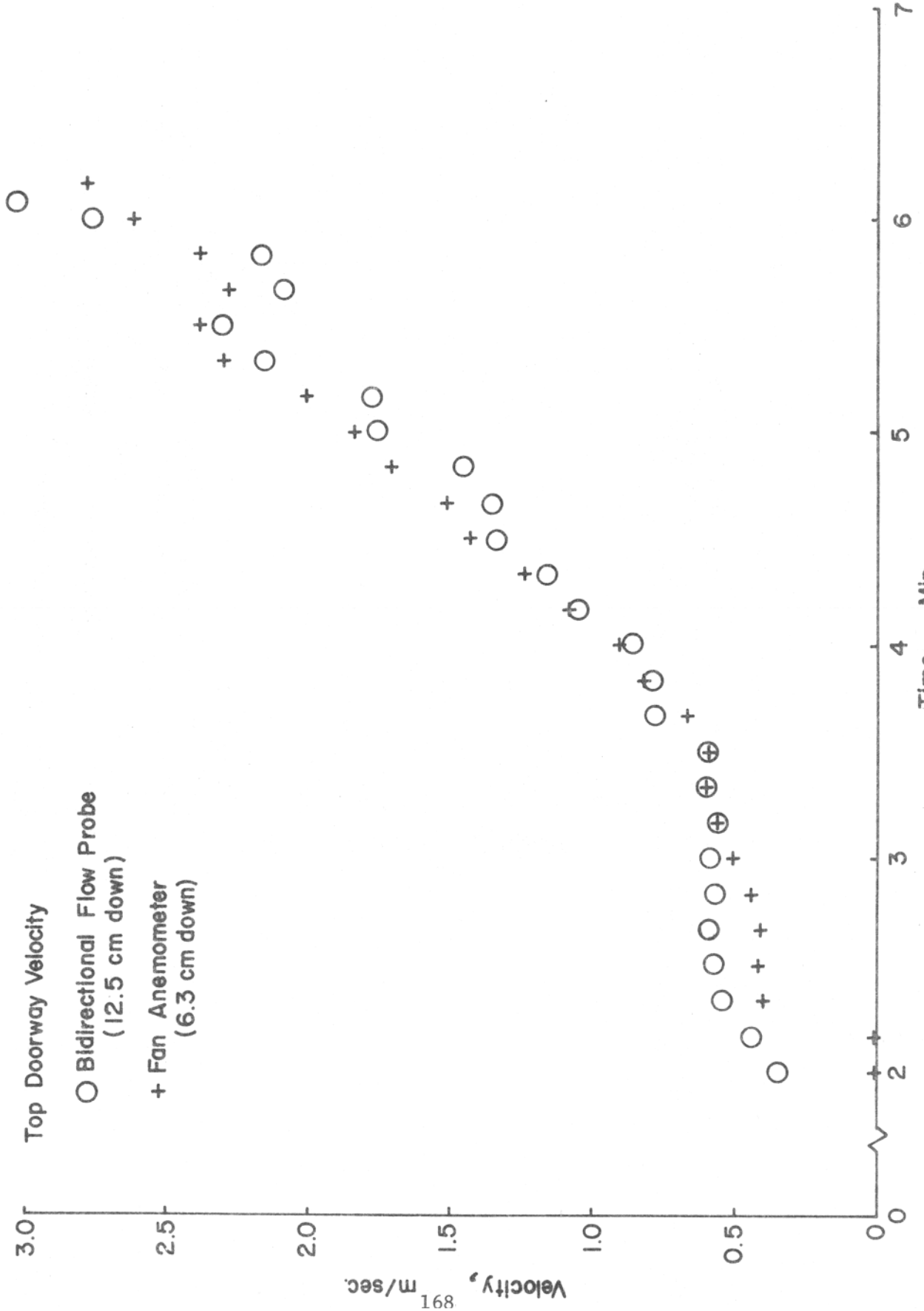

FIGURE 12.1 MEASURED VELOCITIES FROM DOORWAY FAN ANEMOMETER AND HIGHEST BIDIRECTIONAL FLOW TUBE VERSUS TIME AFTER IGNITION

Again the fan anemometers in a full-scale test demonstrated their survival and potential to give useful data. The primary hazard this time seemed to be sensitivity to electrical noise, although no really satisfactory explanation has been found for the loss of data after 6 min for both units. Clearly, the fan as an element to sense the flow works perfectly throughout the tested range of parameters. The light pipes seem to survive in all but the most extreme temperature cases. The electronic circuits seem to need improvement.

Further testing of an improved mechanical, optical, and electrical design for the fan anemometers is proposed for the 1975 full-scale test.

REFERENCES

1. Volume I, this report.
2. Heskestad, G., Appendix K in "The Large-Scale Bedroom Fire Test, July 11, 1973," FMRC Technical Report No. RC74-T-31, Serial No. 21011.4, July 1974.

XIII

MEASUREMENT OF GAS TEMPERATURES IN A ROOM FIRE ENVIRONMENT BY MEANS OF A SIMPLE ASPIRATED THERMOCOUPLE

J.S. Newman and P.A. Croce
Factory Mutual Research Corporation

13.1 INTRODUCTION

The measurement of gas temperature by a thermocouple, particularly in a fire environment, is subject to several sources of error[1]. Under steady conditions, two sources for error must generally be considered - conduction heat transfer along the lead wires and radiation heat transfer to or from the bead. Moreover, errors associated with the time response, i.e., heat capacity, of the bead may also arise in unsteady conditions.

Conduction errors may be minimized rather simply by running thermocouple lead wires along expected isotherms. Radiation errors may be reduced by using a thermocouple with low surface emissivity or by shielding the thermocouple, preferably with a material of low emissivity. In a fire environment, surface emissivities are difficult to control; and, under extreme conditions, shielding is not sufficient to reduce all radiation errors and may even introduce additional errors related to slower response times.

Errors due to radiation or heat capacity may be minimized to a considerable extent by enhancing the convective heat transfer to the bead, e.g., through decreasing the diameter of the bead or by artificially increasing the gas velocity over the bead. This can be achieved by the use of a high velocity, aspirated thermocouple probe.[1] In such a probe, a stream of gas is aspirated at high velocity past a thermocouple junction located inside a sheath, which additionally serves as a radiation shield.

The purpose for using aspirated thermocouples in the second bedroom fire test was to minimize errors in the measurement of gas temperatures in a room fire environment. The objective was to develop a reliable aspirated probe that is economical for full-scale fire test applications.

Figure 13.1 illustrates the aspirated thermocouple assembly which was employed at nine locations in the bedroom (nominal sizes in English units are used in the figure). A commercially available (Omega Engineering), inconel-sheathed thermocouple was simply mounted inside a 6.4mm OD stainless steel tube that was connected to a suction pump. The total fabrication cost was about $50.00 per probe (compared with several hundred dollars for the least expensive, commercially available, sophisticated unit).

In order to determine the effectiveness of the prototype probe in measuring true gas temperature, a series of laboratory experiments was performed, followed by an analysis of the bedroom fire test data from the three doorway aspirated thermocouples.

13.2 LABORATORY EXPERIMENTS

A set of experiments was conducted using acetone pan fires to evaluate the effect of aspirating velocity on the measured temperature. A 230-mm dia, 38-mm high, circular aluminum pan charged with 300 ml of acetone was used. The aspirated probe and a reference bare-bead thermocouple (both of 24-gauge wire) were located 50 mm apart in a horizontal plane and the same distance from the center of the pan. The thermocouple pair was tested at two positions as shown in Figure 13.2, one on the fire axis above the pan and one in the entrainment flow near the base of the fire.

Figure 13.3 presents the temperature measured by aspirated and bare-bead thermocouples as a function of the aspirating velocity. In this diagram the solid points correspond to a position on the pan centerline 300 mm above the pan, while the unfilled points correspond to a location 50 mm beside the top edge of the pan. Each point represents an average value over the same 1-min, steady interval for at least two acetone fire tests. The standard condition indicated is 7.65 m/sec (25 fps) and represents the aspirating velocity used in the bedroom fire test. In particular, the large difference between the aspirated and bare-bead temperatures should be noted. Above the pan, the aspirated temperature is approximately 900°C while the bare bead reads 720°C;

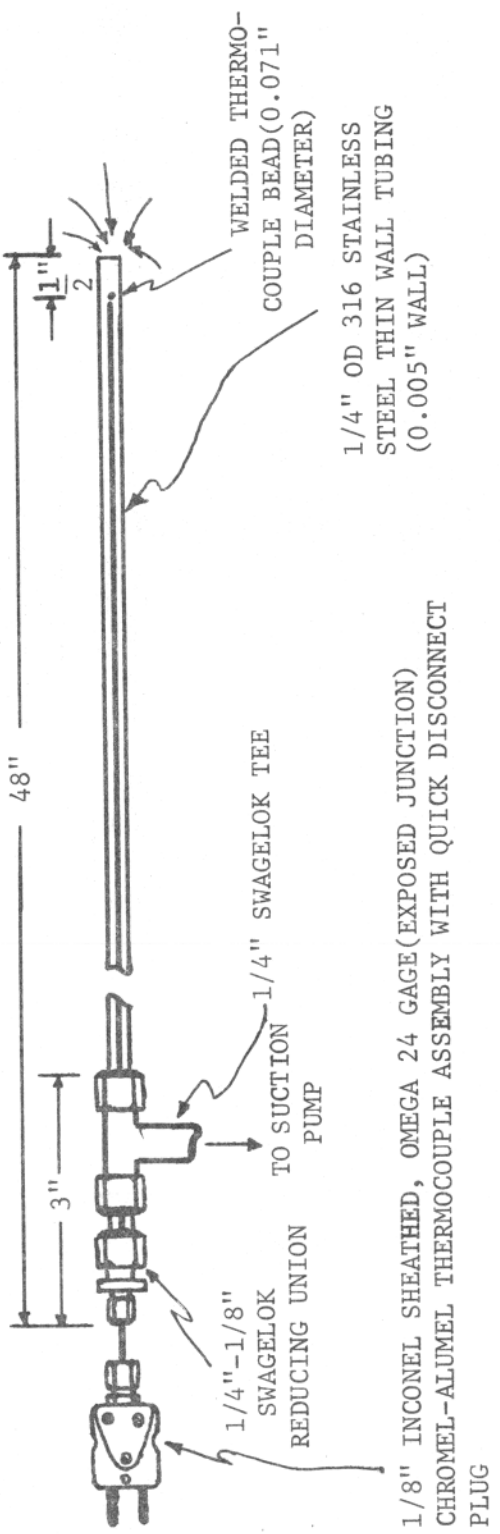

FIGURE 13.1 ASPIRATED THERMOCOUPLE ASSEMBLY

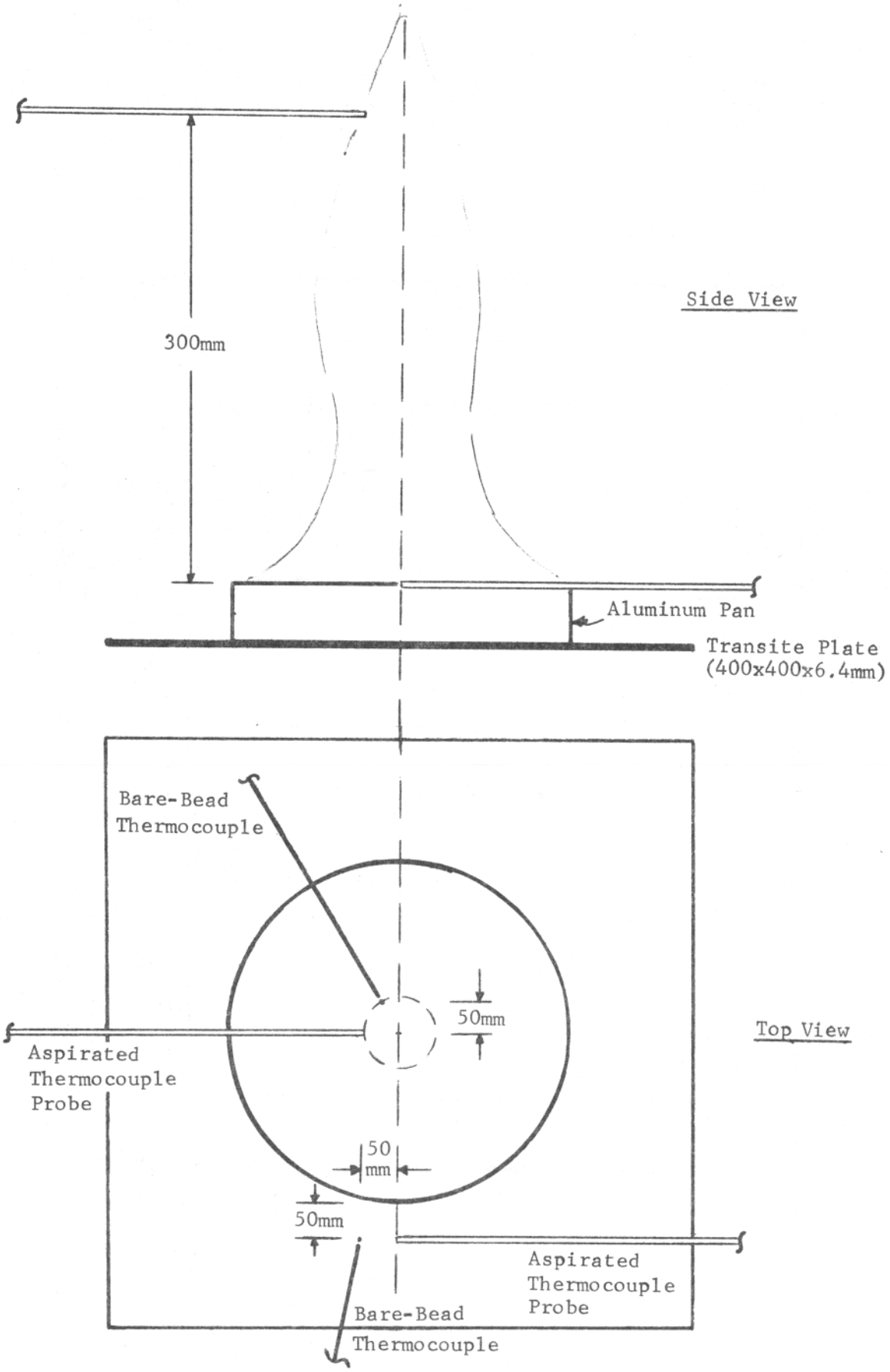

FIGURE 13.2 SETUP FOR LABORATORY PAN FIRE TESTS

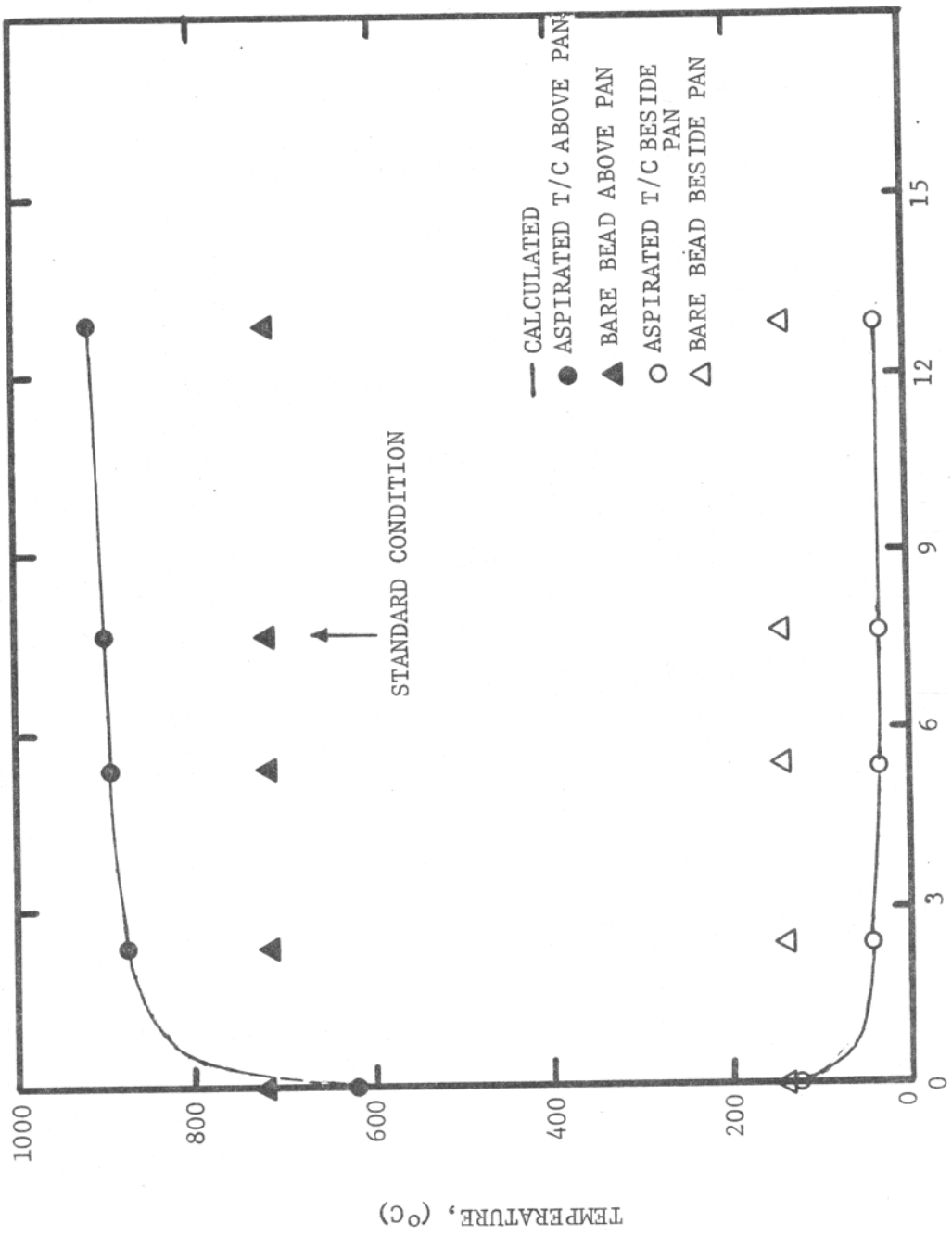

FIGURE 13.3 TEMPERATURE VERSUS ASPIRATING VELOCITY FOR ACETONE PAN FIRE TESTS

beside the pan, the respective values are 37°C and 140°C. The aspirated temperature also appears to approach asymptotically a value which should correspond to the true gas temperature.

In order to determine the asymptotic value and explain the large discrepancy between aspirated and bare-bead values, the following steady heat balance equations for both types of thermocouples were utilized (See Section 13.5 for definition of symbols):

1) for the bare-bead thermocouple,

$$h_B A_B (T_G - T_B) = q_{rB} = \overline{F}_{BE}\, A_B\, \sigma\, (T_B^4 - T_E^4), \tag{13.1}$$

2) for the aspirated thermocouple bead,

$$h_A A_A (T_G - T_A) = \overline{F}_{AS}\, A_A\, \sigma\, (T_A^4 - T_S^4), \tag{13.2}$$

3) for the aspirated probe shield,

$$h_{Si} A_{Si} (T_G - T_S) + h_{So} A_{So} (T_G - T_S) + \overline{F}_{AS} A_A\, \sigma\, (T_A^4 - T_S^4)$$

$$= q_{rS} = \overline{F}_{SE}\, A_{So}\, \sigma\, (T_S^4 - T_E^4). \tag{13.3}$$

No conduction terms are included; for all cases to be considered - both in the laboratory and during the bedroom fire test - thermocouple leads and shields were nearly isothermal over a sufficient length to assume conduction errors negligible. The above set of three equations contains 16 quantities, six of which are known directly (T_A, T_B, A_A, A_B, A_{Si} and A_{So}), and four of which (h_B, h_A, h_{Si} and h_{So}) can be obtained from empirical correlations for flow over single spheres[2], developing flow in the entry region of a tube[3], and cross flow over cylinders[4]. The remaining six quantities (T_G, T_S, T_E, $\overline{F}_{BE}$, $\overline{F}_{AS}$ and $\overline{F}_{SE}$) are considered separately for each experimental condition.

13.2.1 Experiments Above Pan Fire

For the case when the thermocouples are positioned above the pan, the flames are assumed to be optically thin*. Hence, $\overline{F}_{BE} = \varepsilon_B$, $\overline{F}_{SE} = \varepsilon_S$, $\overline{F}_{AS} = \varepsilon_A F_{AS}$ and T_E = ambient temperature (25°C). The unknowns are T_G, T_S, ε_B and ε_S+. The solution is obtained from the three heat balance equations and the dependence of T_A upon aspirating velocity. The solution is by trial and error: A value of T_G is selected; ε_B is calculated from the bare-bead heat balance, eq 13.1; T_S is calculated from the aspirated-bead heat balance, eq 13.2; and ε_S is calculated from the aspirated probe shield heat balance, eq 13.3. This procedure is repeated for each set of data corresponding to each aspirating velocity. The initially assumed value of T_G is adjusted as necessary until a discrete T_G is obtained over the entire velocity range. The gas temperature obtained by this method is 922°C§.

In order to corroborate the calculated value of gas temperature, a second series of laboratory tests was conducted using a similar acetone pan fire and bare-bead thermocouples of varying diameter. Such a test permits extrapolation to zero bead diameter to obtain true gas temperature. The results of these tests are shown in Figure 13.4, which presents both calculated and measured values. The measured quantity for the largest bead diameter was first used to calculate the "true gas temperature" (the calculated point shown for $D_B = 0$) from the heat balance equation. With this true gas temperature value, thermocouple bead temperatures were calculated for the other two bead sizes. The good agreement with measured values in Figure 13.4 supports the adequacy of the heat-balance equation set (with assumptions) for describing the performance of the aspirated probes under these test conditions.

*This assumption is supported by a calculated estimate of the radiative input to a bare bead from the flames (an order of magnitude less than either the convective input or the reradiative loss to ambient walls), and by the measured data points in Figure 13.4 (strong dependence of measured temperature on bead size).

+F_{AS} is calculated from the internal geometry of the probe, and $\varepsilon_A = \varepsilon_B$.

§Other quantities obtained in this computation were $T_S = 835$°C, $\varepsilon_B = 0.67$ and $\varepsilon_S = 0.17$.

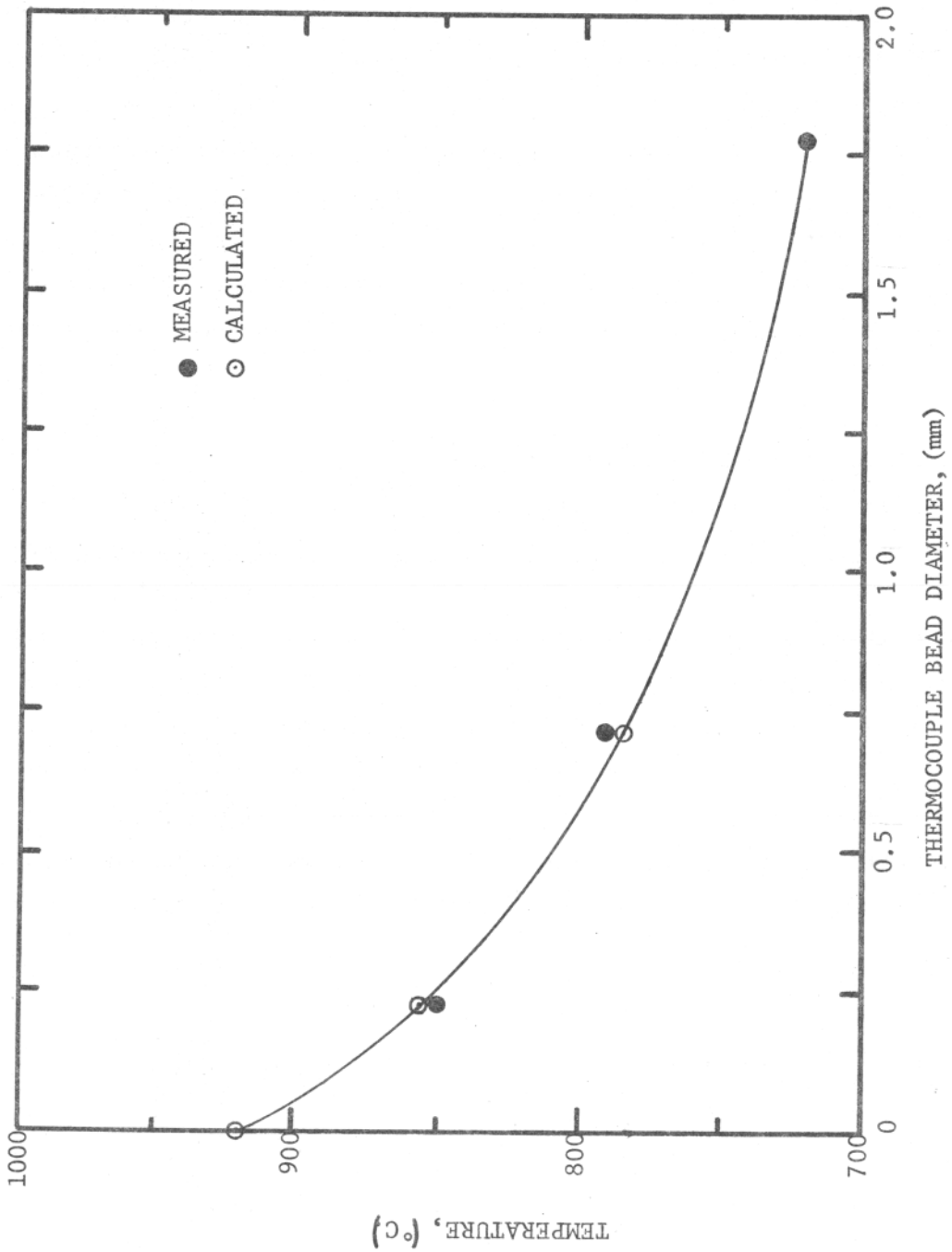

FIGURE 13.4 TEMPERATURE VERSUS BARE-BEAD DIAMETER FOR ACETONE PAN FIRE TESTS

13.2.2 Experiments Beside Pan Fire

The performance of the aspirated thermocouple at low gas temperatures (but with radiation present) was studied in a series of tests in which the aspirated and reference bare-bead thermocouples were located beside the acetone pan fire 50 mm radially outward from the top edge of the pan. For this set of conditions, the right-hand sides of eq 13.1 and 13.3 are taken as q_{rB} and q_{rS} respectively, where q_{rB} and q_{rS} are radiative inputs from the flames. The unknowns are T_G, T_S, q_{rB} and q_{rS}, and q_{rB} and q_{rS} are required to differ only by a geometric factor. Calculated values were found to be: T_G= 33°C and T_S= 184°C, while T_A= 36°C and T_B= 141°C (See Figure 13.3)*. It should be noted that, during a pan fire experiment, the ambient temperature in the closed laboratory rose from 25°C to 38°C.

13.2.3 Effect Of Bead Location Inside Tube

In additional laboratory tests both above and beside an acetone pan fire as shown in Figure 13.2, the effect of the placement of the thermocouple bead inside the shield was studied. Figure 13.5 presents measured temperature plotted against the normalized distance from the end of the shield for the standard aspirating velocity. The aspirated temperature is relatively insensitive to location inside the shield; even with the bead placed at the end of the shield, T_A was 880°C compared to 895°C at distances of two, three and four shield diameters. (The standard condition shown in Figure 13.5 is at 13 mm, or two shield diameters, and corresponds to what was used in the bedroom fire). At low gas temperatures, T_A varied only 2°C over a range of zero to four shield diameters.

*In a single test, in which the aspirated probe was positioned radially with the open end facing the base of the fire, no significant difference was observed (T_A= 35°C).

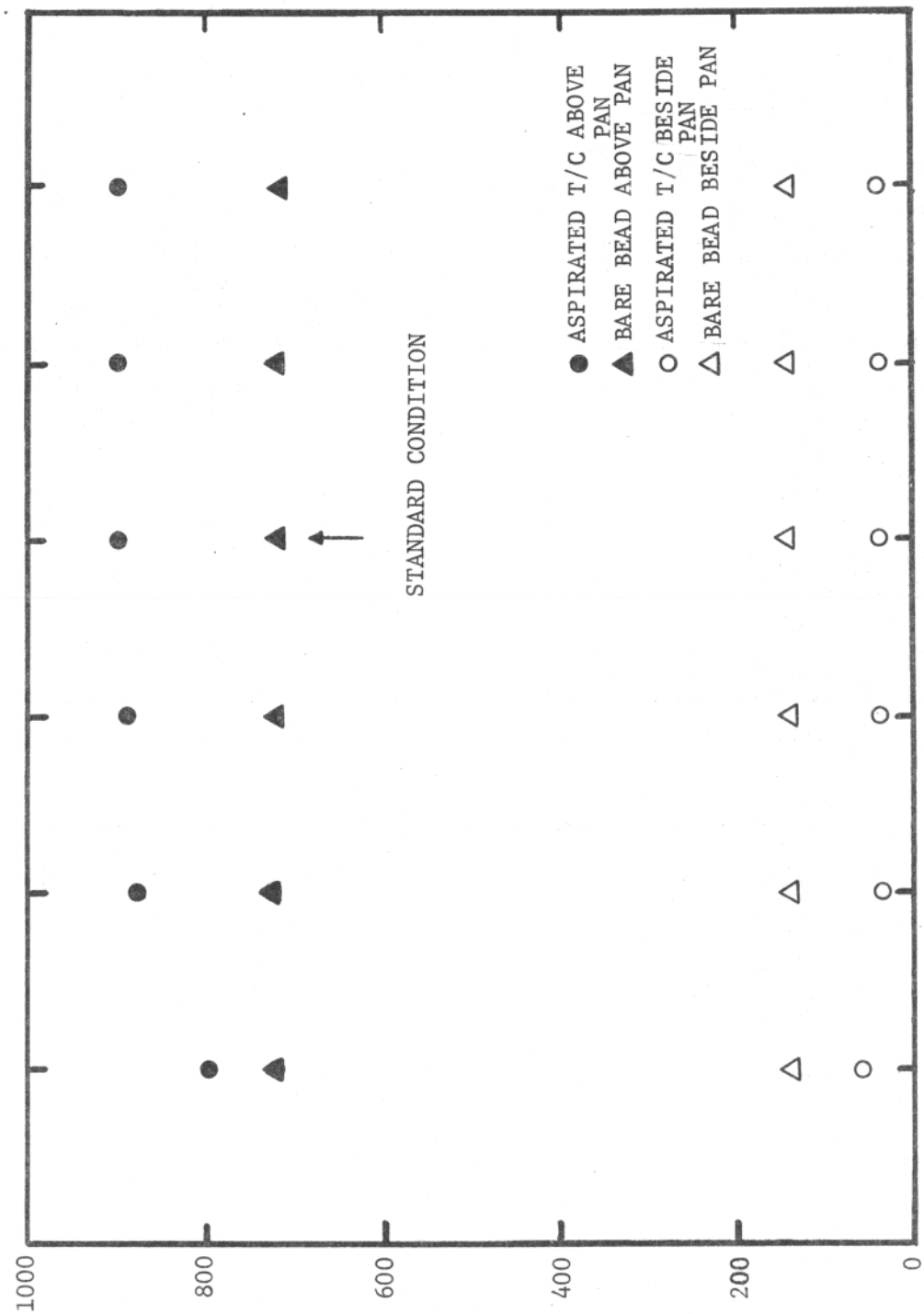

FIGURE 13.5 TEMPERATURE VERSUS NORMALIZED DISTANCE FROM END OF SHIELD FOR ACETONE PAN FIRE TESTS

13.2.4 Response Time

A final series of laboratory tests measured the relative response time* as a function of aspirating velocity. A hot air blower was used. Relative response times were determined for heating in the high-velocity (approx 18 m/sec), hot air stream followed by cooling of the thermocouples in the cool, still room air; results are shown in Figure 13.6. With no aspiration, the bare bead responded more rapidly than the aspirated probe both in the high velocity stream and in still air, as anticipated. As the aspirating velocity is increased, the aspirated thermocouple responds equally as fast as the bare bead in the high velocity stream and significantly faster than the bare bead in still air (three times faster at standard condition). Thus, at the standard condition of 7.65 m/sec, the aspirated thermocouple responds as quickly as, or faster than, the bare-bead thermocouple over a range of ambient velocities comparable to those in the bedroom fire test.

13.3 BEDROOM TEST RESULTS

Since the performance of the aspirated thermocouples in the laboratory experiments seemed to be well described by the heat balance equations, a similar approach was taken to evaluate their performance in the bedroom fire test. The three doorway probes[5] were selected not only because they are significant in characterizing the heat and mass flow into and out of the bedroom, but also because local velocity measurements, important in the analysis for each probe, were available. The probes were located along the vertical centerline and in the plane of the doorway at distances of .076 m, 1.02 m and 1.63 m down from the top jamb.

Since the heat balance eq 13.1-13.3 are written for steady conditions, the interval 7-7 1/2 min after ignition, a relatively steady period, was initially selected for analysis. Consider the uppermost aspirated thermocouple.

*defined as the ratio of the aspirated to bare-bead thermocouple time constants τ_{asp}/τ_{bead}

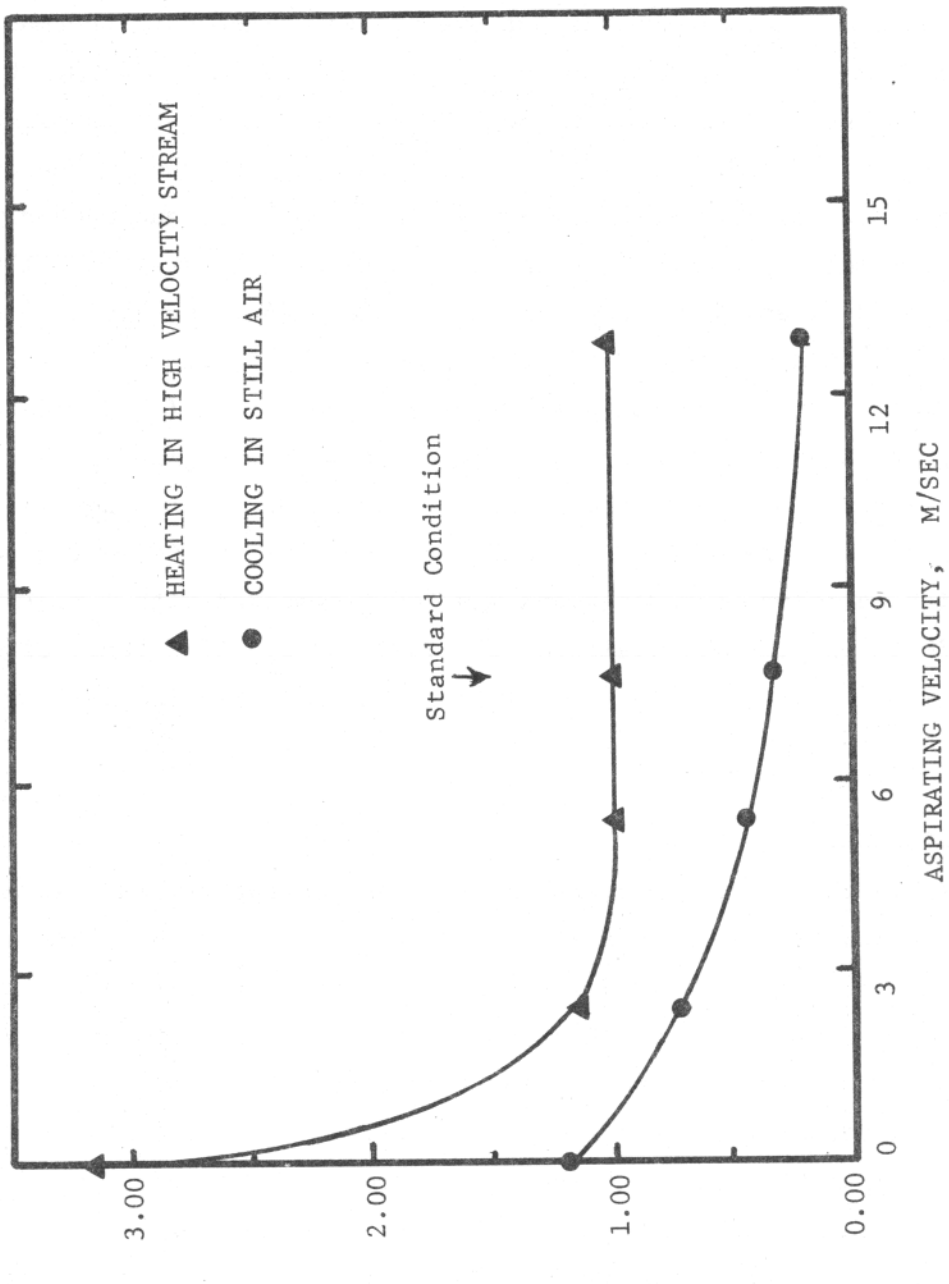

FIGURE 13.6 RELATIVE RESPONSE TIME VERSUS ASPIRATING VELOCITY FOR HOT-AIR GUN TESTS

The heat balance equations were solved for the three unknowns, T_G, T_S and T_E, with $\overline{F}_{BE} = \varepsilon_B$, and $\overline{F}_{SE} = \varepsilon_S$. (The emissivities for the shield and thermocouple were assumed to be the same as those calculated for the acetone pan fires.) The solution yields $T_G = 800°C$ and $T_S = 796°C$ compared with $T_A = 799°C$, $T_B = 803°C$ and $T_E = 807°C$. The close agreement between the aspirated, bare-bead and calculated values is not unexpected, since both thermocouples were totally immersed in a hot, optically thick smoke layer during this time in the test (see Sections VIII and X). For the mid and low thermocouple pairs, T_E was taken as 807°C, and F_{BE} and F_{SE} were considered unknowns. The solution was obtained by solving the three heat balance equations and requiring F_{BE} and F_{SE} to differ only by a geometric factor. The results were $T_G = 531°C$ and $T_S = 477°C$ with $T_A = 524°C$ and $T_B = 613°C$ for the mid location, and $T_G = 35°C$ and $T_S = 54°C$ with $T_A = 35°C$ and $T_B = 81°C$ for the low position.

Lastly, a time was selected in the bedroom fire (6 1/3 min after ignition) during which the temperatures in the doorway were beginning to rise dramatically. The same computational procedures that were used for the near-steady bedroom fire interval were applied in this case and gave the following results: For the high position, $T_G = 315°C$ and $T_S = 280°C$ compared with $T_A = 313°C$ and $T_B = 370°C$; for the mid position, $T_G = 25°C$ and $T_S = 27°C$ compared with $T_A = 25°C$ and $T_B = 31°C$; and for the low position, $T_G = 25°C$ and $T_S = 27°C$ compared with $T_A = 25°C$ and $T_B = 31°C$.

13.4 DISCUSSION

Table 13.1 gives a summary of results for the various cases examined in terms of the difference between the calculated gas temperature and measured values. These results indicate that the simple, aspirated thermocouple probe measures gas temperature better than a bare-bead thermocouple by approximately an order of magnitude under fire conditions where bare beads register serious errors. These results are supported by an independent determination of gas temperature with different size thermocouple beads in a laboratory test. It is concluded that this prototype probe is sufficiently reliable to be utilized in future full-scale tests, but should perhaps be additionally supported

TABLE 13.1

SUMMARY OF TEST RESULTS WITH ASPIRATED THERMOCOUPLES

	Calculated T_G (°C)	$(T_G - T_A)$ (°C)	$(T_G - T_B)$ (°C)
ACETONE PAN FIRE			
Above	922	+27	+202
Beside	33	- 3	-108
BEDROOM FIRE (7:00 - 7:30 min)			
High	800	+ 1	- 3
Mid	531	+ 7	- 82
Low	35	0	- 46
BEDROOM FIRE (6:20 min)			
High	315	+ 2	- 55
Mid	25	0	- 6
Low	25	0	- 6

with independent determinations under fire test conditions to establish its accuracy. This can be done easily with thermocouple beads of different size and/or the use of a more sophisticated, commercially available probe.

13.5 NOMENCLATURE

A	Surface area
D	Diameter
F	Geometric view factor
$\overline{F}$	Radiation "view" factor for gray bodies
h	Average convective heat transfer coefficient
q_r	Radiative heat transfer
T	Temperature
ε	Emissivity, gray
σ	Stefan-Boltzmann constant

Subscripts

A	Aspirated thermocouple
B	Bare bead thermocouple
E	Environment
G	Gas
i	Inner
o	Outer
S	Aspirated probe shield

REFERENCES

1. Herzfeld, C.M., ed., Temperature: Its Measurement and Control in Science and Industry, Vol. 3, Part 2, Rheinhold Publishing Corp., New York, 1962, and earlier editions.
2. Rowe, Claxton, and Lewis, Transactions of the Institute of Chemical Engineers, Vol. 43, 1965.
3. Rohsenow, W.M. and Choi, H.Y., Heat, Mass and Momentum Transfer, Prentice-Hall, Inc., Englewood Cliffs, N.J., 1961.
4. Kreith, F., Principles of Heat Transfer, 2nd Edition, International Textbook Co., Scranton, Pa., 1967.
5. Volume I, this report.